OPTIMIZATION AND EVALUATION OF RHEIN-RICH *SENNA ALATA* LEAF
EXTRACT INCORPORATED SHELLAC ELECTROSPUN NANOFIBERS USING
DESIGN OF EXPERIMENTS

By

Miss Wah Wah AUNG

A Thesis Submitted in Partial Fulfillment of the Requirements
for Doctor of Philosophy PHARMACEUTICAL ENGINEERING
(INTERNATIONAL PROGRAM)
Silpakorn University
Academic Year 2023
Copyright of Silpakorn University

-

โดย
MissWah Wah AUNG

วิทยานิพนธ์นี้เป็นส่วนหนึ่งของการศึกษาตามหลักสูตรปรัชญาดุษฎีบัณฑิต
วิศวเภสัชกรรม แบบ 1.1 ปริญญาปรัชญาดุษฎีบัณฑิต (หลักสูตรนานาชาติ)
มหาวิทยาลัยศิลปากร
ปีการศึกษา 2566

OPTIMIZATION AND EVALUATION OF RHEIN-RICH *SENNA ALATA* LEAF EXTRACT INCORPORATED SHELLAC ELECTROSPUN NANOFIBERS USING DESIGN OF EXPERIMENTS

By

Miss Wah Wah AUNG

A Thesis Submitted in Partial Fulfillment of the Requirements
for Doctor of Philosophy PHARMACEUTICAL ENGINEERING
(INTERNATIONAL PROGRAM)
Academic Year 2023
Copyright of Silpakorn University

Title	Optimization and evaluation of rhein-rich *Senna alata* leaf extract incorporated shellac electrospun nanofibers using design of experiments
By	Miss Wah Wah AUNG
Field of Study	PHARMACEUTICAL ENGINEERING (INTERNATIONAL PROGRAM)
Advisor	Associate Professor Chutima Limmatvapirat, Ph.D.
Co advisor	Professor Sontaya Limmatvapirat, Ph.D.

Faculty of Pharmacy, Silpakorn University in Partial Fulfillment of the Requirements for the Doctor of Philosophy

.... Dean of Faculty of Pharmacy
(Professor Pornsak Sriamornsak, Ph.D.)

Approved by

.... Chair person
(Associate Professor Srisagul Sungthongjeen, Ph.D.)

.... Advisor
(Associate Professor Chutima Limmatvapirat, Ph.D.)

.... Co advisor
(Professor Sontaya Limmatvapirat, Ph.D.)

.... Committee
(Professor Thawatchai Phaechamud, Ph.D.)

.... Committee
(Assistant Professor Vipaluk Patomchaiviwat, Ph.D.)

630830003 : Major PHARMACEUTICAL ENGINEERING (INTERNATIONAL PROGRAM)
Keyword : Senna alata, rhein, ultrasound-assisted extraction, Box–Behnken design, electrospun fibers, fractional factorial design, shellac, antimicrobial activity

Miss Wah Wah AUNG : Optimization and evaluation of rhein-rich *Senna alata* leaf extract incorporated shellac electrospun nanofibers using design of experiments Thesis advisor : Associate Professor Chutima Limmatvapirat, Ph.D.

Rhein, a key component of anthraquinones, is a crucial active compound in *Senna alata* leaves with a variety of pharmacological effects. Achieving high-quality herbal extracts necessitates selecting suitable extraction methods for each plant. In this study, a systematic approach involving single-factor analysis and Box-Behnken design was used to optimize ultrasound-assisted extraction (UAE) conditions for rhein-rich extracts. The rhein content was quantitatively determined using a validated high-performance liquid chromatography–diode array detection (HPLC–DAD) method. The optimal extraction conditions were identified as 95% v/v aqueous ethanol used as solvent, 59.52 ºC, and 18.4 min, with a solvent-to-solid ratio of 25.48:1 mL/g, yielding a predicted rhein content of 10.44 mg/g extract. The research aimed to incorporate these extracts into shellac electrospun fibers. Through fractional factorial design and Box–Behnken design, optimal electrospinning conditions was established as a voltage of 24 kV, a solution feed rate of 0.8 mL/h, and a shellac–extract ratio of 38.5:3.8 (% w/w) resulting in nanofibers with a diameter of 306 nm, low bead-to-fiber ratio (0.29), and 96% extract entrapment efficiency within nanofibers. The results revealed that the concentration of shellac significantly influenced both the diameter of the fibers and the formation of beads. *In vitro* release studies revealed a biphasic profile with an initial rapid release of 88% within the first hour, followed by a sustained release pattern exceeding 90% over the subsequent 12 hours, as anticipated based on zero-order release kinetics.The fiber mats incorporated with the extract remained stable for 60 days when subjected to 40°C temperature and 75% relative humidity during stability testing. The optimized extract and nanofibers displayed antimicrobial efficacy against various pathogens. These findings indicate that rhein-rich extracts and their incorporation into shellac electrospun fibers exhibit significant biological activities for potential therapeutic and cosmetic applications.

ACKNOWLEDGEMENTS

F

This thesis is partially supported by the Faculty of Pharmacy, Silpakorn University.

Wah Wah AUNG

TABLE OF CONTENTS

Page

List of tables

List of figures

List of Abbreviations

%	Percent
% w/w	Percent weight by weight
°C/min	Degree Celsius per minute
°C	Degree Celsius
cm^{-1}	Per centimeter
µg	Microgram(s)
µL	Microliter(s)
µg/mL	Microgram per milliliter
µm	Micrometer(s)
µS	Microsiemens
nm	Nanometer(s)
k	Release rate
n	Release exponent value
λ	Wavelength
2θ	Two theta
ABTS	2,2′-azino-bis-(3-ethylbenzothiazoline-6-sulfonic) acid
AC	Alternating current
Adj R^2	Adjusted coefficient of determination
AIC	Akaike information criterion
ANOVA	Analysis of variance
AOAC	Association of Official Agricultural Chemists
ASEAN	Association of Southeast Asian Nations
ATCC	American Type Culture Collection
atm	Atmosphere
BBD	Box-Behnken design
C. albicans	*Candida albicans*
CCD	Central composite design
CFU/mL	Colony forming unit per milliliter
CLSI	Clinical Laboratory Standards Institute
cm	Centimeter(s)

DC	Direct current
DMSO	Dimethyl sulfoxide
DMST	Department of Medical Sciences, Thailand
DOE	Designs of experiment
DPPH	1,1-diphenyl-2-picrylhydrazyl
DSC	Differential scanning calorimetry
E. coli	*Escherichia coli*
et al.	and others
FFD	Fractional factorial design
FRAP	Ferric-reducing antioxidant power
FTIR	Fourier-transform infrared
g	Gram (s)
g/kg	Gram per kilogram
G	Gauge (needle)
h	Hour (s)
HPLC-DAD	High performance liquid chromatography with diode array detection
HPLC–UV	High performance liquid chromatography with ultraviolet detection
HorRat	Horwitz ratio
IC_{50}	Half-maximal inhibitory concentration
ICH	International Conference on Harmonization
KBr	Potassium bromide
kHz	Kilohertz
kV	Kilovolt
L	Liter (s)
LD_{50}	Median lethal dose
LOD	Limit of detection
LOQ	Limit of quantitation
MAE	Microwave-assisted extraction
MBC	Minimum bactericidal concentration
ME	Maceration extraction
mg	Milligram (s)
mg/g	Milligram per gram

mg/kg	Milligram per kilogram
mg/mL	Milligram per milliliter
MIC	Minimum inhibitory concentration
min	Minute (s)
mL	Milliliter (s)
mL/g	Milliliter per gram
mL/h	Milliliter per hour
mm	Millimeter
mN/m	Millinewton per meter
mPa. S	Millipascal-second
MRSA	Methicillin-resistant *Staphylococcus aureus*
MSC	Model selection criterion
NF	National Formulary
No.	Number
P. aeruginosa	*Pseudomonas aeruginosa*
PBS	Phosphate buffer solution
Pred R^2	Predicted coefficient of determination
PXRD	Powder X-ray diffraction
R^2	Coefficient of determination
RH	Relative humidity
RSD	Relative standard deviation
RSM	Response surface methodology
SA	*Senna alata*
S. aureus	*Staphylococcus aureus*
SD	Standard deviation
SEM	Scanning electron microscopy
SFE	Supercritical fluid extraction
TFC	Total flavonoid content
TPC	Total phenolic content
TSA	Tryptic Soy Agar
TSB	Tryptic Soy Broth
UAE	Ultrasound assisted extraction

UK	United Kingdom
USA	United States of America
USP	United States Pharmacopeia
UV-vis	Ultraviolet-visible
v/v	Volume by volume
w/v	Weight by volume

Chapter 1
Introduction

1.1. Statement and significance of the problem

Senna alata (L.) Roxb. or *Cassia alata* L., (Family- Fabaceae) a perennial shrub has been considered of high value due to its ethnomedicinal uses in multiple health disorders (1). *S. alata* (SA) leaf extract has been documented to exhibit various biological properties, including analgesic, laxative, anti-inflammatory, antioxidant, anthelminthic, and antimicrobial activities (2-6). The evidence from the toxicity studies provides support for considering the extracts yielded from SA leaves as safer herbal remedies. In the previous acute and sub-acute toxicity study of 90 % ethanolic SA leaf extracts, the results showed the absence of obvious toxicity without mortality or changes in the general behavior in Swiss albino mice, even with the highest administered doses of 3,000 mg/kg of body weight (7). Acute and subacute toxicity of watery extract were investigated in Wistar rats and mice. They revealed the lethal dose 50 (LD_{50}) of aqueous extract is more than 2000 mg/kg in acute toxicity, indicating that the extract could be practically non-toxic with this dose. In subacute toxicity, there was no major lesion after histological examination of the liver and kidneys (8, 9). Consequently, SA leaf extract could be affirmed for the safety of oral administration for short period of time within a specified administered dose.

Furthermore, numerous research studies have investigated the use of SA leaf extract, either as a standalone ingredient or in combination with other herbs, in the formulation development of herbal ointment, antiseptic soap, and herbal gel. These studies observed that SA leaf extract exhibits remarkable antibacterial, antifungal, and anti-inflammatory properties (10-14). As a consequence, it has been established that the incorporation of this extract into topical formulations holds great promise for the effective remedy of common infections on skin.

The leaf extract contains flavonoids, terpenoids, tannins, phlobatannins, saponins, cardiac glycosides, anthraquinones, carbohydrates, and proteins in major proportions (15). In recent times, a significant challenge in the herbal medicine formulated with SA has been the substandard quality of SA leaves extract containing lower anthraquinone content below the specified standard value in the monograph (16).

In order to effectively mitigate this concern, it is imperative to implement a systematic approach for the acquisition of high-quality extracts. Choosing the most suitable extraction method for each plant is vital in achieving the preferred quantity and quality of herbal extracts, encompassing active components and bioactivities. Due to the ability of ultrasound-assisted extraction (UAE) method to extract bioactive components in a short period of time, at a reduced temperature, and with minimal energy and solvent consumption (17), it was accepted for SA leaf extraction. UAE involves the use of high frequency ultrasound waves to form cavitation effects in the solvent, which penetrate plant cell walls and facilitate the release of target compounds (18).

Rhein, a primary constituent of anthraquinones, stands out as one of the prominent active compounds found in SA leaves. It has exhibited a diverse range of pharmacological effects, including antioxidant, nephroprotective, anti-inflammatory, anticancer, antimicrobial, and anti-influenza A virus (19). Rhein has demonstrated favorable characteristics regarding its absorption when administered orally or applied topically in comparison to other anthraquinones like emodin, aloe-emodin, chrysophanol, and physcion (20-22). According to previous research, it is suggested that the antibacterial efficacy of rhein, could be associated with its hydroxyanthraquinone nucleus (Figure 1) comprising two carbonyl groups at C9 and C10 as well as two hydroxyl groups at C1 and C8. Furthermore, rhein possess a substituted polar carboxylic group at C3, which has the potential to improve its antibacterial activity (23). The previous report also demonstrated that rhein exhibits higher potency as an antibacterial compound when compared to other anthraquinones (24).
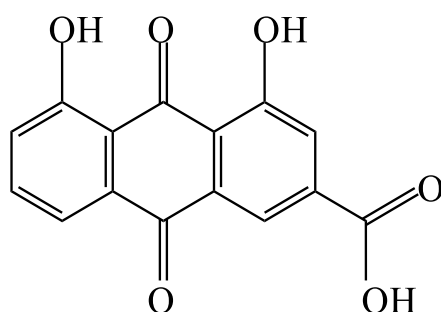
Figure 1. Chemical Structure of Rhein ($C_{15}H_8O_6$)

Due to the intriguing biological activities of rhein, particularly its antibacterial and anti-inflammatory effects, SA leaf extract containing rhein can be developed into a wound healing product. As a result, rhein emerges as a viable candidate for serving as a quality control marker for SA extracts and their associated pharmaceutical products. Hence, it is prioritized to meticulously examine the extraction parameters aimed at attaining a SA leaf extract enriched with a high rhein content. Due to the fact that the aromatic chromophore of rhein absorbs ultraviolet light at a λ 254 nm (25), rhein contents can be determined using a high-performance liquid chromatography with diode array detector (HPLC-DAD). This study intended to collect data on the optimal extraction parameters for the UAE method employing a response surface methodology (RSM), specifically a Box-Behnken design (BBD) to obtain rhein-rich extract.

Another objective of this research was to explore the integration of SA leaf extract into electrospun nanofibers, utilizing bleached shellac as the polymer matrix. Shellac, derived from lac insects (*Laccifer lacca*) claims a range of desirable properties, making it a versatile material for application in food and pharmaceutical technology. Shellac presents numerous advantages over synthetic polymers, including biodegradability, non-toxicity, renewable and sustainable sourcing, biocompatibility, and low cost. Shellac is a natural biodegradable material that can break down over time whereas synthetic polymers can persist in the environment for long periods. Shellac is generally regarded as a safe option for human health and environmental considerations due to its non-emission of harmful chemicals or toxins during degradation, making it a suitable choice for applications in which contact with humans, or the environment is a concern. Shellac is biocompatible, meaning that it is well-tolerated by the human body. This property makes it appropriate for use in biomedical applications. Shellac can be cost-effective material due to its availability and natural sourcing (26, 27).

In general, due to the nature of polymer matrices or molten state and the particular circumstances involved necessary to create and sustain solutions while in a liquid form, electrospinning is not an easy task for natural polymers. However, electrospinning of shellac offers a unique opportunity due to its solubility in anhydrous ethanol and low molecular weight (28, 29). Moreover, although numerous research have explored the utilization of bleached shellac for various applications, as evidenced by the literature (30-32), its specific application in the fabrication of electrospun

nanofibers remains unexplored. Consequently, this study employed bleached shellac as a crucial component in the production of electrospun fibers, incorporating SA leaf extract.

Electrospun nanofibers, in particular, hold promise in pharmaceutical applications, including tissue engineering scaffolds, wound dressings, and drug delivery system owing to its distinguished features like a significant specific surface area, good porous structure, excellent biocompatibility, and degradability (33). The electrospinning process is also capable of incorporating drugs and other bioactive molecules, enhancing their therapeutic potential (34).

The morphological character of electrospun nanofibers significantly influences their properties. In the electrospinning process, the morphology of resulting fibers can be controlled by strategically adjusting various influential factors that affect fiber morphology. This study used systematically approaches for screening of electrospinning parameters to fabricate SA leaf extract-incorporated shellac fibers using fractional factorial design (FFD). Subsequently, BBD was employed to optimize electrospinning conditions.

With antibiotic resistance becoming a global health challenge, there is an increasing effort to search for novel antimicrobial agents derived from natural origin. Several microbial pathogens are linked to a range of skin infections. *Streptococci* and *Staphylococci* are recognized as common culprits for wound infections. In immunosuppressed individuals, these microorganisms can cause opportunistic skin infections. *Escherichia coli* is typically a component of the natural intestinal flora, but when found outside the intestines, it can give rise to wound infections and sepsis. *Pseudomonas aeruginosa*, a common pathogen in burn patients, has the capacity to infect various regions of the human body (35). Numerous previously published studies (36-39) have suggested that SA leaf extract exhibits great potential as an antimicrobial agent against a wide spectrum of bacterial and fungal strains.

Nonetheless, due to the limited duration of bacterial inhibition, the development of antibacterial agents designed to ensure prolonged antibacterial effect is pivotal. The application of polymers as a drug carrier facilitates the sustained and controlled release of antibiotics, offering a potential solution for prevention of infections. SA leaf extract has been successfully encapsulated in niosomes, subsequently incorporated into an

alginate-pectin film for controlled drug release in the context of wound dressing (40). In numerous research studies, the bioactive properties of natural herbal extracts have proven to be highly effective when incorporated into a polymeric nanoscale matrix. As a consequent, the incorporation of SA leaf extract into electrospun fibers is a feasible approach, offering the ability to control the release of extract for enhancing its effectiveness in various applications. Moreover, electrospun nanofibers incorporated with SA leaf extract would be developed as a promising material for pharmaceutical application aimed at combatting bacterial infections.

1.2. Aim and objectives

1.2.1. Aim:

The primary aim of this research was to develop shellac electrospun fibers incorporated with an extract obtained from SA leaves.

1.2.2. Objectives:

(1) To optimize conditions in UAE for enhancing the rhein content in SA leaf extract

(2) To investigate the influential parameters governing the electrospinning procedure in order to achieve the desired characteristics of nanofibers loaded with the aforementioned extract

(3) To fabricate shellac electrospun fibers incorporated with rhein-rich SA leaf extract under the identified optimal conditions

(4) To evaluate both the SA leaf extract and electrospun fibers produced using the optimal conditions, with a focus on their properties, characteristics, and suitability for the potential applications

1.3. Hypothesis to be tested

(1) The optimal UAE conditions leading to the production of a rhein-rich extract can be determined through a combination of single factor analysis and BBD experiments.

(2) The independent factors and their interactions influencing the electrospinning process can be systematically identified to achieve the desired outcomes in the fabrication of nanofibers.

(3) The properties of both SA leaf extract and the resulting electrospun fibers hold significant potential for pharmaceutical applications, based on their specific characteristics and attributes.

1.4. Scope of the research work

This research emphasized the development of shellac electrospun fibers incorporating SA leaf extract including three phases. The initial phase was optimization of extraction conditions and evaluation of rhein-rich SA leaf extract. The second phase was fabrication and optimization of SA leaf extract-loaded shellac electrospun nanofibers and the final phase was characterization and evaluation of optimized nanofibers.
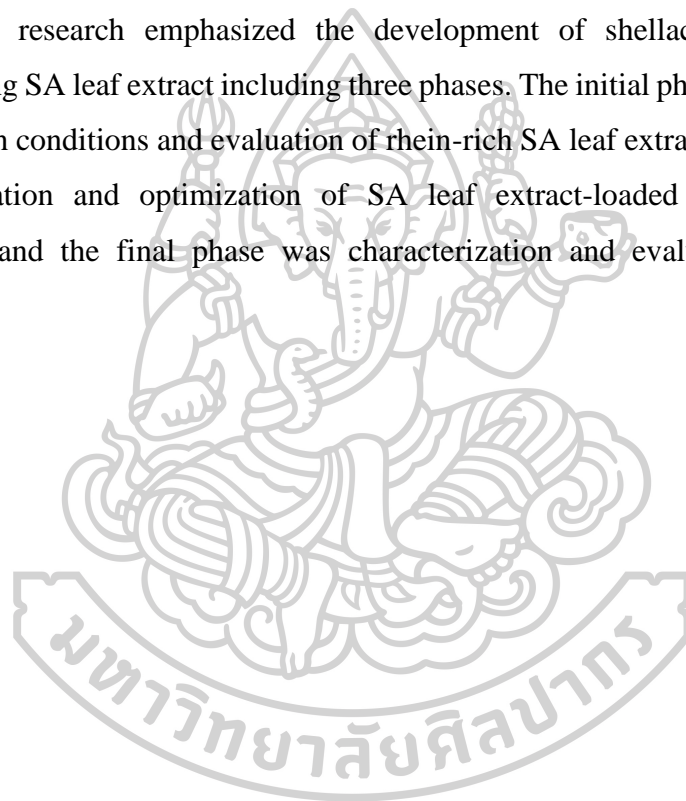
Chapter 2
Literature review

2.1. *Senna alata* **(L.) Roxb. (***Cassia alata* **L.)**

    Senna alata (L.) Roxb. (*Cassia alata* L.) is a plant classified within the Fabaceae family. SA is commonly referred to as the "candle bush" because of the shape of its inflorescences (Figure 2), or it is also known as the "ringworm tree" due to its fungicidal properties. It is an ornamental plant that is indigenous to the Amazon rainforest. It is abundantly available in Asia and all over Africa. This shrub is widely distributed and cultivated in the Philippines, Thailand, and Indonesia for medicinal purposes. SA leaves (Figure 3) have been deemed valuable due to its ethnomedicinal uses in the treatment of numerous health conditions.

Figure 2. *S. alata* Plant.
Source: http://aceprd.unijos.edu.ng/plant-info

Figure 3. Dried Leaves of *S. alata*.

SA leaves are utilized more frequently than the roots, flowers, and stembark due to the contribution of more active compounds in the leaves (1). Its fresh or dried leaves have been used as household medicines in various countries to alleviate constipation, stomachache, ringworm diseases, and cutaneous infections (41). The extract of SA leaves has been demonstrated to have numerous pharmacological properties. These pharmacological activities are correlated with the contribution of active components in the extract. According to the Indian Medicinal Plants textbook, the antibacterial activity of SA leaves is attributed to the presence of rhein, an anthraquinone compound (42). SA leaf extract with a high yield of anthraquinones containing aloe-emodin, emodin, and rhein has been reported as the active antifungal agents (43).

2.2. Phytochemical constituents and biological activities

Several studies have been demonstrated that SA plant composed of phytochemical constituents such as alkaloids, glycosides, steroids, flavonoids, anthraquinones, tannin, phlobatannins, phenolic compounds, carbohydrates, proteins and free amino acids, volatile oils, reducing sugars, coumarins, saponins, triterpenoids, resins, cyanophore, cardiac glycosides, polyuronides, fixed oils and fats (15, 37, 44).

Akporhuarho et al. studied the antioxidant and bioactive constituents of the ethanolic SA leaf extract. They discovered that the ethanolic extract contained high concentrations of phenolic and flavonoid compounds, which are reputed to possess antioxidant properties. The extract was evaluated for 1,1-diphenyl-2-picrylhydrazyl (DPPH) radical scavenging, nitric oxide radical scavenging, and ferric-reducing antioxidant power (FRAP) activities with respective values of 0.65 mg/mL, 0.89 mg/mL, and 2.61 mg/mL (44).

Cavalcante et al. developed an HPLC method for the identification, separation, and quantification of phenolic compounds in the SA leaf extract. Aqueous and hydroalcoholic extracts contained 3-hydroxybenzoic acid, rutin, myricetin, cyanidin, quercetin, and kaempferol, according to their research (45).

Igara et al. evaluated the antioxidant activity of the methanolic extract of SA leaves using FRAP and DPPH assays in a concentration IC_{50} range of 50 ug/mL to 400 ug/mL. They observed that the activity of the extract was concentration-dose

relationship with respect to FRAP and DPPH assays from 4.14 ± 0.00 % to 25.73 ± 0.17 % and 0.00 ± 0.00 % to 11.5 ± 0.34 %, respectively (46).

Saito et al. applied the reverse phase-solid phase extraction to prepare an aqueous extract from SA leaves. The resulting extract showed antimicrobial efficacy against *P. aeruginosa*, *Staphylococcus epidermidis*, *Staphylococcus aureus*, and *Bacillus subtilis*. It also prevents biofilm forming in *Staphylococcus epidermidis* and *P. aeruginosa*. They identified four flavonoid compounds, kaempferol, kaempferol-*O*-diglucoside, quercetin-*O*-glucoside, kaempferol-*O*-glucoside, and two anthraquinones, rhein and danthron, as the primary components of SA leaf extract by high-resolution mass spectrometry (47).

Damodaran and Venkataraman investigated the therapeutic efficacy of SA leaves against *Pityriasis versicolor* in humans. The research was performed among 200 volunteer (ages between 16 to 60) from Tamil Nadu state in India within 10 years. A 100-g of green, developed, and healthful leaflets was thoroughly squashed and squeezed by hand with 50 mL of distilled water (in a stainless-steel vessel). The obtained solution was filtered and was determined to be a 100% concentrated solution. The 100% concentrated solution was mixed with distilled water to obtain 80% v/v and 90% v/v solutions. Various concentrations of plant extract (80% v/v, 90% v/v, and 100% v/v) were applied to the affected areas of the body (the neck, trunk, face, and hands). The findings suggested that SA leaf extract could be applied as a herbal medication with no side effects for *Pityriasis versicolor* infections (48).

Villasenor et al. studied SA leaf extracts prepared with different solvents; hexane, chloroform, and ethyl acetate; to examine anti-mutagenic, anti-inflammatory, antifungal, analgesic, and anti-hyperglycemic activities. The chloroform-extracted compound demonstrated anti-mutagenic activity at a dosage of 2 mg/20 g mouse weight, resulting in a 65.8% inhibition of tetracycline mutagenicity. It exhibited the highest activity against *Trichophyton mentagrophytes*, with an effective dose of 50 mg/mL, but it could not active against *Candida albicans*. The hexane extract exhibited the highest analgesic property, resulting in a 59.9% reduction in the number of squirms induced by acetic acid at a dosage of 5 mg/20 g mouse weight. Both the hexane and ethyl acetate extracts, at a dose of 5 mg/20 g mouse weight, demonstrated inhibition of carrageenan-induced inflammation, with 65.5% and 68.2% inhibition, respectively.

Additionally, the ethyl acetate extracts, at a dose of 5 mg/20 g mouse weight, displayed antihyperglycemic properties, reducing blood glucose levels by 58.3% (49).

It is evident from the preceding that the leaves of SA contain numerous active phytochemicals with biological activities. Therefore, it is of interest to develop extracts with high biological activity and prepare them as pharmaceuticals. Recent studies reported for phytoconstituents, bioactivities, and extraction methods of SA leaf are listed in Table 1.

Table 1. Extraction Methods, Phytoconstituents and Bioactivities of SA Leaf Extract.

No	Type of solvent	Extraction method	Phytoconstituents	Bioactivities	Model/method used	Reference
1.	Methanol	Maceration	Rhein, Aloe-emodin, Kaempferol	-	-	(50)
2.	Methanol	Maceration	Alkaloids, Saponins, Flavonoids, Phenols	Antioxidant	DPPH radical scavenging assay Hydroxy radical inhibitory assay Hydrogen peroxide scavenging assay FRAP assay	(51)
	Ethyl acetate		Alkaloids, Saponins, Flavonoids, Phenols			
	N-hexane		Alkaloids			
3.	Aqueous	-	Polyphenols (flavonoids, anthocyanins, tannins, leuco anthocyanins, free quinones), Steroids, Terpenoids	Anthelmintic Antioxidant	Harvested ground worms *Benhamia Rosea* genus DPPH radical scavenging assay	(6)

No	Type of solvent	Extraction method	Phytoconstituents	Bioactivities	Model/method used	Reference
4.	Ethanol	Maceration	Alkaloids, Phytosterols, Carbohydrates, Saponins, Phenols, Tannins, Flavonoids	Antibacterial	Agar disc diffusion assay *B. subtilis, Pseudomonas, E. coli*	(52)
	Petroleum ether		Alkaloids, Phytosterols, Flavonoids			
	Acetone		Alkaloids, Phytosterols, Flavonoids			
5.	Aqueous	Maceration, Soxhlet	Saponins, Tannins, Flavonoids, Steroids, Anthraquinone, Terpenoids	Antibacterial	Agar well diffusion Broth dilution *Serratia marcescens, E. coli, Cronobacter* species, *Enterococcus* species, *Klebsiella pneumoniae, Enterobacter clocae, Citrobacter* species, *Pseudomonas* species, *Proteus mirabilis, Coagulase* Negative *Staphylococci* (CoNS)	(53)
	Methanol		Saponins, Tannins, Anthraquinone, Steroids, Flavonoids			
	Ethyl acetate		Saponins, Tannins, Flavonoids, Anthraquinone, Steroids			

No	Type of solvent	Extraction method	Phytoconstituents	Bioactivities	Model/method used	Reference
6.	Aqueous	Maceration	Flavonoids, Alkaloids, Tannins, Anthraquinones	Anticonvulsant, Sedative effect	Swiss albino mice	(54)
7.	Ethanol	Maceration	Kaempferol 3-O-gentiobioside, Phytol, Stigmasterol, Sitosterol, Dimethyl derivatives, Methyl esters, Octanoic acid derivatives	Antidiabetics	Albino Wister rat	(55)
8.	Methanol	Soxhlet	Glycosides, Terpenoids, Steroids, Saponins, Tannins, Flavonoids, Alkaloids, Phenols, Carbohydrates, Anthraquinone, Cardiac glycosides, Phlobatannins	Antifungal	Agar incorporation method, Broth microdilution method, *Trichophyton tonsurans*, *Trichophyton rubrum*, *Trichophyton mentagrophytes*, *Microsporum audouinii*, *Microsporum canis, Microsporum gypseum, Epidermophyton floccosum*	(56)
	Ethanol		Glycosides, Terpenoids, Steroids, Saponins, Tannins, Flavonoids, Alkaloids, Phenols, Carbohydrates			

No	Type of solvent	Extraction method	Phytoconstituents	Bioactivities	Model/method used	Reference
			Anthraquinone, Cardiac glycosides, Phlobatannins			
	N-hexane		Glycosides, Steroids, Saponins, Tannins, Flavonoids, Alkaloids, Phenols, Carbohydrates			
			Essential oils, Anthraquinone, Cardiac glycosides, Phlobatannins			
	Chloroform		Glycosides, Terpenoids, Steroids, Saponins, Tannins, Flavonoids, Alkaloids, Phenols, Carbohydrates, Anthraquinone, Cardiac glycosides, Phlobatannins			
9.	Ethanol	Maceration	Alkaloids, Flavonoids, Triterpenoid, Steroids, Phenols	Antivenom	Swiss albino mice	(57)

No	Type of solvent	Extraction method	Phytoconstituents	Bioactivities	Model/method used	Reference
10.	Methanol	Maceration	1-Butanol-3-methyl, Pentadecane 2, 6, 10, 14-tetramethyl, β-D-Glucopyranose-4-O-β-β-galactopyranosyl, Hexadecenoic acid methyl ester, n-Hexadecenoic acid, 9, 12, 15-Octadecatrienoic acid methyl ester, Phytol, 9, 12, 15-Octadecatrienoic-2-3-dihydroxyl propyl ester, Ethyl -iso-allocholate, Vitamin E	Antioxidant	FRAP assay DPPH radical scavenging assay	(46)
11.	Ethanol	Maceration	-	Inhibitory effects on chondrosarcoma cell metastasis	Human chondrosarcoma cell line, SW1353	(58)

No	Type of solvent	Extraction method	Phytoconstituents	Bioactivities	Model/method used	Reference
12.	Aqueous	Soxhlet	Alkaloids, Phenolic compounds, Tannins, Carbohydrates, Reducing sugar, Polyuronides, Coumarins, Saponins, Steroids, Triterpenoids, Flavonoids, Resins, Cyanophores, Cardiac glycosides, Anthraquinone	Antibacterial	Agar well diffusion Methicillin-resistant *S. aureus* (MRSA)	(37)
13.	Ethanol	Maceration	Phenolics, Flavonoid, Alkaloids, Tannins, Terpenoids, Saponins, Steroids, Cardiac glycosides	Antimalarial Antioxidant	Albino mice *Plasmodium berghei* NK65 DPPH	(59)
14.	Ethanol	Maceration	Alkaloids, Terpenoids, Flavonoids, Phenols, Saponins, Tannins	Antidiabetic	Albino mice	(60)
15.	Ethanol	Maceration	Emodin, Kaempferol, Kaempferol-3,7-diglucoside, Kaempferol-3-O-β-D-glucopyranoside	Antibacterial	Broth microdilution *S. aureus* ATCC 25923 *S. epidermidis* ATCC 12228	(61)

No	Type of solvent	Extraction method	Phytoconstituents	Bioactivities	Model/method used	Reference
					E. coli ATCC 25922	
					B. subtilis ATCC 6633	
16.	Ethanol, Ethyl acetate, N-hexane	Maceration	Alkaloids, Saponins, Tannins, Flavonoids, Triterpenoids, Steroids, Glycosides	Antioxidant Antifungal	DPPH radical scavenging assay Agar diffusion method *C. albicans* *Cryptococcus neoformans*	(62)
17.	Ethanol Aqueous	Percolation	Alkaloid, Phenol, Saponin, Tannin, Phlobatannins Alkaloids, Tannins, Saponins, Phenols, Flavonoids	Antibacterial	Agar well diffusion method *E. coli, Streptococcus pyogene, S. aureus*	(63)
18.	Ethanol, Aqueous	Maceration	Alkaloids, Coumarins, Glycosides, Flavonoids, Phenols, Resins, Saponins, Tannins, Terpenoids	Antioxidant	DPPH free radical scavenging assay Human blood	(64)

No	Type of solvent	Extraction method	Phytoconstituents	Bioactivities	Model/method used	Reference
				In vitro thrombolytic activity	Thromboplastin LI kit with human blood	
				In vitro Anticoagulant activity		
				In vitro anthelmintic activity	Aquarium worm (*Tubifex tubifex*)	
19.	Ethanol	Soxhlet	-	Hepatoprotective activity	Swiss albino mice	(65)
20.	Carbon dioxide (CO$_2$)	Supercritical fluid extraction (SFE)	-	Hyaluronidase inhibition activity	Hyaluronidase assay	(66)

No	Type of solvent	Extraction method	Phytoconstituents	Bioactivities	Model/method used	Reference
21.	Aqueous ethanol	Microwave assisted extraction (MAE)	Tannins, Saponins, Flavonoids	Antimicrobial activity	Paper disc diffusion method *S. aureus, E. coli, Salmonella enteritidis B. subtilis*	(67)
22.	Aqueous ethanol	Ultrasonic assisted extraction (UAE) Microwave assisted extraction (MAE)	Rhein, Kaempferol, Astragalin	-	-	(68)

2.3. Extraction methods

Extraction is a method employed to separate the active pharmaceutical constituents within plant or animal tissues from the inactive or inert components. This is achieved using selective solvents. The established extraction procedures for raw materials are designed to separate the therapeutically beneficial components and remove the undesired materials by treating it with a selective solvent. Either the crude extract can be fractionated to isolate specific chemical components, or it can undergo additional processing to be incorporated into various dosage forms. Hence, the standardization of extraction methods take part in pivotal role to determine the quality of herbal drugs (69). The choice of an effective extraction technique holds substantial responsibility for both the quality and quantity of bioactive components present in plant materials. Throughout the process of extraction, solvents permeate the solid plant materials, dissolving compounds of comparable polarity. The choice of a proper solvent is also crucial, and it adheres to the fundamental principle of "like dissolves like". Moreover, modifications to the methods are continuously developed (70).

Extraction methods can be broadly categorized into two types: conventional and non-conventional (modern techniques). In smaller research settings or at the Small Manufacturing Enterprise level, the most utilized traditional extraction techniques include Soxhlet, maceration, percolation, decoction, and hydro-distillation. Nevertheless, these methods come with several disadvantages, including extended extraction durations, elevated expenses, limited extraction specificity, reduced efficiency, increased solvent usage, and potential degradation of bioactive compounds due to longer exposure to high temperatures.

Therefore, novel extraction techniques such as microwave-assisted extraction (MAE), ultrasound-assisted extraction (UAE), and supercritical fluid extraction (SFE), pressurized liquid extraction, deep eutectic solvent-assisted extraction, cold plasma-assisted extraction, and enzyme-assisted extraction have been introduced to mitigate limitations of conventional extraction methods. Due to the reduced usage of plant raw materials, solvents, and energy, these techniques are also known as green extraction technology. Modern extraction technologies are founded on the discovery and development of the extraction procedure. Benefits of these techniques include improved isolation, decreased energy consumption, the use of alternative solvents, the

ability to extract substances of high quality, increased selectivity, renewable natural products, safe extracts, and minimum adverse effects on the environment. In addition, the utilization of "green" solvents enables to gain the non-toxic substances that are considered as safe and favored by end users (71).

Ling et al. investigated the impact of alternative extraction methods on total phenolic content (TPC), total flavonoid content (TFC), and kaempferol content from SA leaves. MAE yielded the most TPC, TFC, and kaempferol content, followed by UAE and maceration extraction (ME). The analysis of scanning electron microscopy (SEM) revealed extensive contraction of mesophyll and epidermis in the UAE and MAE compared to ME, resulting in approximately 24% to 93% more TPC and TFC than in ME. The effectiveness of polyphenol extraction is dependent on the degree of cell disruption in SA leaves (72).

Gritsanapan and Mangmeesri determined the quantitative analysis of anthraquinone contents in SA leaf extracts obtained from the various extraction methods: maceration, percolation, and Soxhlet extraction. The results found that the maximum total anthraquinones ($2.48 \pm 0.20\%$ w/w) was obtained from the maceration, while the extracts from the percolation and Soxhlet extraction yielded total anthraquinones of 2.46 ± 0.31 and $2.13 \pm 0.29\%$ w/w, respectively (73).

Some typical conventional and non-conventional extraction methods are described below:

2.3.1. Conventional extraction methods

2.3.1.1. Soxhlet Extraction

Soxhlet extraction is considered the optimal method for the simultaneous extraction of solid plant materials treated by a heated solvent. It is a firmly established and widespread used method, exceeding other conventional extraction methods in most cases, except when dealing with thermolabile compounds. The procedure involves placing powdered solid materials within a thimble made of filter paper, which is then positioned inside the Soxhlet apparatus (74) (as depicted in Figure 4). This apparatus is connected to a round-bottom flask containing the solvent and a reflux condenser.

In the process, the solvent within the flask is thoroughly heated, and its vapor rises through the side tube, condenses in the condenser, and drips into the thimble

containing the materials, gradually filling the Soxhlet. After the solvent ascends to the upper part of the linked tube, it returns to the flask, bringing along the portion of the substance that has been extracted. This process is iterated until a full extraction is accomplished (75).
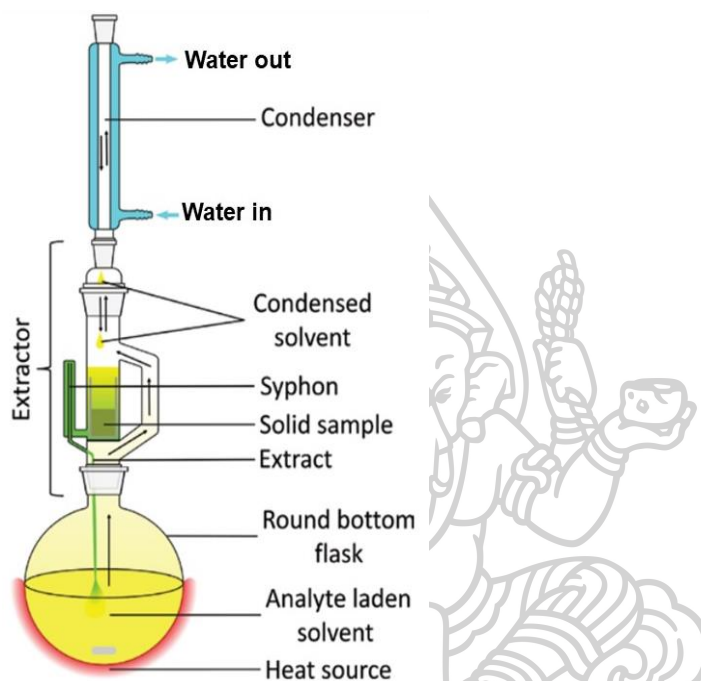
Figure 4. Soxhlet Apparatus (74).

Advantages (69)	**Disadvantages** (76)
- A very simple technique	-Risk of heat related destruction of thermolabile compounds
- Substantial quantity of plants materials can be extracted at one time	
- Reuse the solvent	- Prolong extraction time
- Not require filtering after extraction	- Labor intensive
- Employed as both small scale and large scale	- Allow minimal alteration of variables
	- High solvent consumption

2.3.1.2. Maceration

Maceration is a liquid-solid extraction method. Maceration is traditionally employed to extract bioactive components from plant materials by introducing solvents, with or without the application of heat and mechanical agitation or shaking. These techniques improve the dispersion of substances and mass transfer. The solvent is mixed with powdered solid materials placed in a sealed container (Figure 5) (77). It is allowed to extract over an extended period, ranging from several hours to several days. Adequate time is provided for the solvent to permeate the plant cell wall and dissolve the components found within the plant. This process occurs exclusively via molecular diffusion (76).
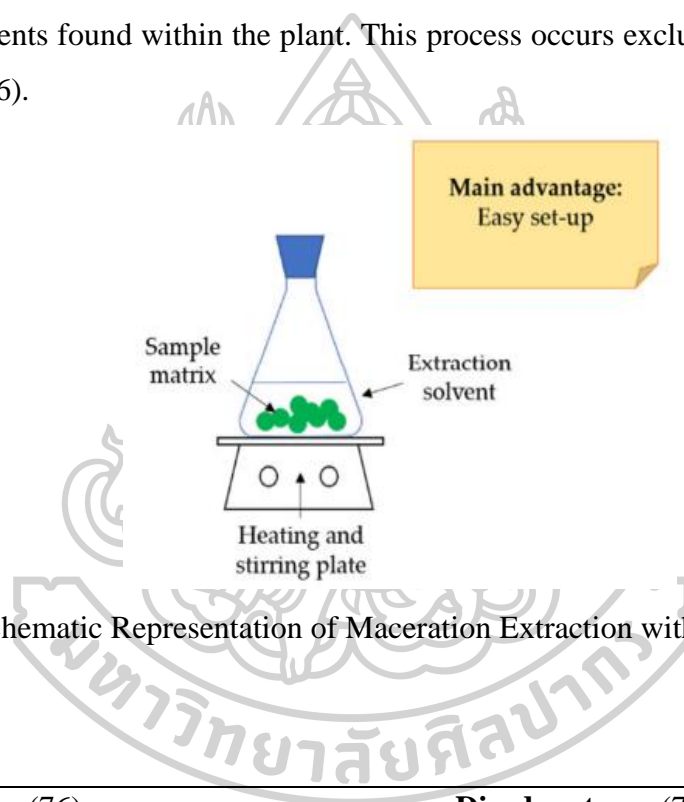
Figure 5. Schematic Representation of Maceration Extraction with a Source of Heat (77).

Advantages (76)	**Disadvantages** (76)
- Utilizes simple tools and equipment	- Long duration of extraction time, which can last up to weeks at times.
- No specific operator expertise needed	
- Energy-efficient procedure	- Not completely extract the compound
- Well-suited for substances with very low solubility, due to extended contact times	- A particularly slow and time-intensive procedure
- An appropriate method for less potent and cost-effective medications	- Necessitating a larger quantity of solvent

2.3.1.3. Percolation

Percolation is a commonly used method for extracting active ingredients, often utilized in the preparation of tinctures and fluid extracts. Typically, a percolator, a narrow, cone-shaped vessel open at both ends, is used. Plant materials are soaked in an appropriate amount of solvent and left to rest for several hours in a securely closed container. Subsequently, the mass is compacted, and the upper part of the percolator is sealed. Additional solvent is poured to create a thin layer above the plant material, and the mixture is allowed to steep within a sealed percolator for an extended duration. The outlet of percolator is then opened, permitting the liquid to gradually drip out. Additional solvent is poured as needed until the percolate reaches approximately 75% of the final required volumes. The resulting extract is subsequently pressed, and the liquid is combined with the percolate. Adequate solvent is added to achieve the necessary volume, and the combined liquid is clarified through filtration or natural settling, followed by decantation (Figure 6) (69, 78).
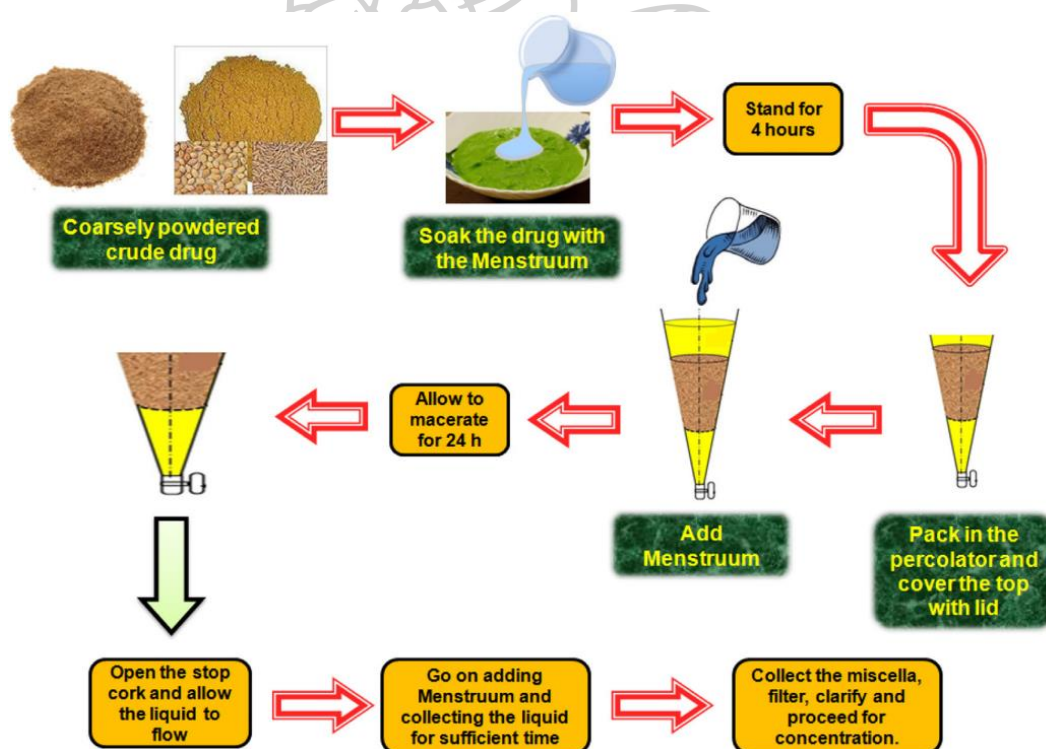
Figure 6. Schematic Representation for the Extraction of Crude Plant Material using the Percolation Procedure (78).

Advantages (76)	**Disadvantages** (76)
- Less time consuming compared with maceration	- A longer extraction period compared to Soxhlet extraction
- Well-suited for extraction of heat-sensitive constituents	- High usage of solvent
- Appropriate method for potent and expensive raw materials	- Need a well-trained person
- Short duration and enhance completely extraction	- Highlight the particle size of the materials throughout the entire process

2.3.1.4. Decoction

Decoction is an aqueous-based method ideal for extracting aqueous-soluble substances from crude plant materials. This involves boiling the plant material with water to create a liquid preparation. Decoction is the preferred technique when dealing with hard and fibre consisting plants, barks, and roots (Figure 7) (79). Decoction involves breaking the plant materials into small pieces or powder. The amount of water used in this method varies based on the hardness of the plant materials (70).
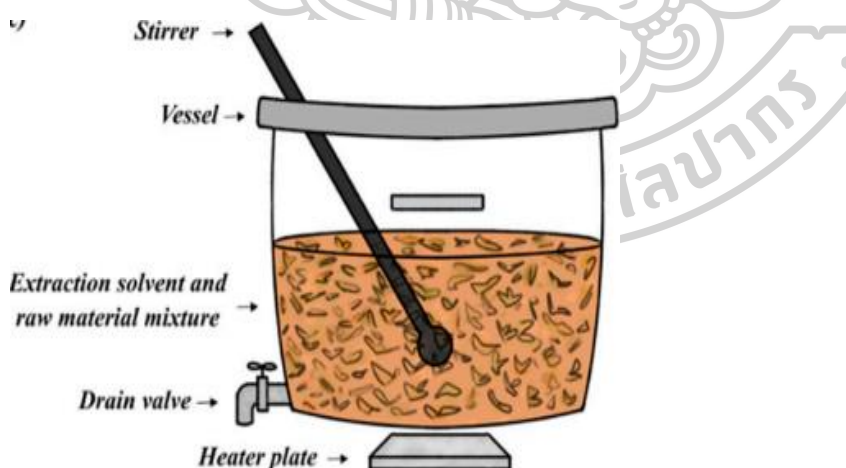
Figure 7. Schematic Representation of the Decoction Extraction Method (79).

Advantages (76)	**Disadvantages** (76)
- Suitable for heat-stable compounds	- Not suitable for the extraction of heat damaged constituents
- Not required more and expensive equipment	
- Easy to perform	
- No need specialized operator	

2.3.2. Non-conventional extractions methods

2.3.2.1. Microwave-assisted extraction (MAE)

MAE technique is based on the principle of dielectric heating with a time-varying electric field. Microwaves start ionic conduction, which is based on the electrophoretic transfer of ions and electrons, producing an electric field. Dielectric heating with a time-varying electric field causes polar molecules to be displaced, resulting in dipole rotation, and forces the molecules to align with the existing electric field. Microwaves generate heat by interacting with ionized compounds in the sample matrix, such as water and some organic components, using the ionic conduction and dipole rotation mechanisms. In MAE, heat and mass transfer observe concurrently, leading to a cumulative effect that enhances the extraction process and increases yield of extract. Moisture evaporation causes high pressure within the plant cell, causing swelling and subsequent leakage. This process aids in the release of the active substances from the leakage cells into the surrounding medium. MAE can also be performed without using solvents. In dry or solvent-free MAE, natural occurring water in the samples serves as the solvent, promoting cell lysis. Solvent-free MAE has applied to extract essential oils and antioxidants from aromatic plants. This technology can be used to attain high-value compounds extracted from natural sources, including phytonutrients, nutraceuticals, and functional food ingredients, and pharmaceutical active compounds from biomass. Many parameters, including the microwave power, time, temperature, dielectric properties of the sample materials, and type of solvent, should be adjusted to obtain desired product attributes (80) (Figure 8). The procedure can be optimized for commercial or economic considerations, resulting in the production of high-quality extracts from a wide range of materials (70, 81).

Ling et al. investigated the optimum processing conditions of MAE for the extraction of anthraquinones (aloe emodin) and flavonoids (kaempferol 3-gentiobioside and kaempferol) from SA. The screening of MAE extraction parameters was determined using a one-factor-at-a-time and two-level factorial design. A central composite design (CCD) was employed to identify the ideal conditions for maximizing the production of the desired compounds. The highest yields of kaempferol 3-gentiobioside (4.27 mg/g dry weight), kaempferol (8.54 mg/g dry weight), and aloe emodin (0.86 mg/g dry weight) were achieved at 90.5% *v/v* ethanol and 18.6 W/mL microwave power (82).
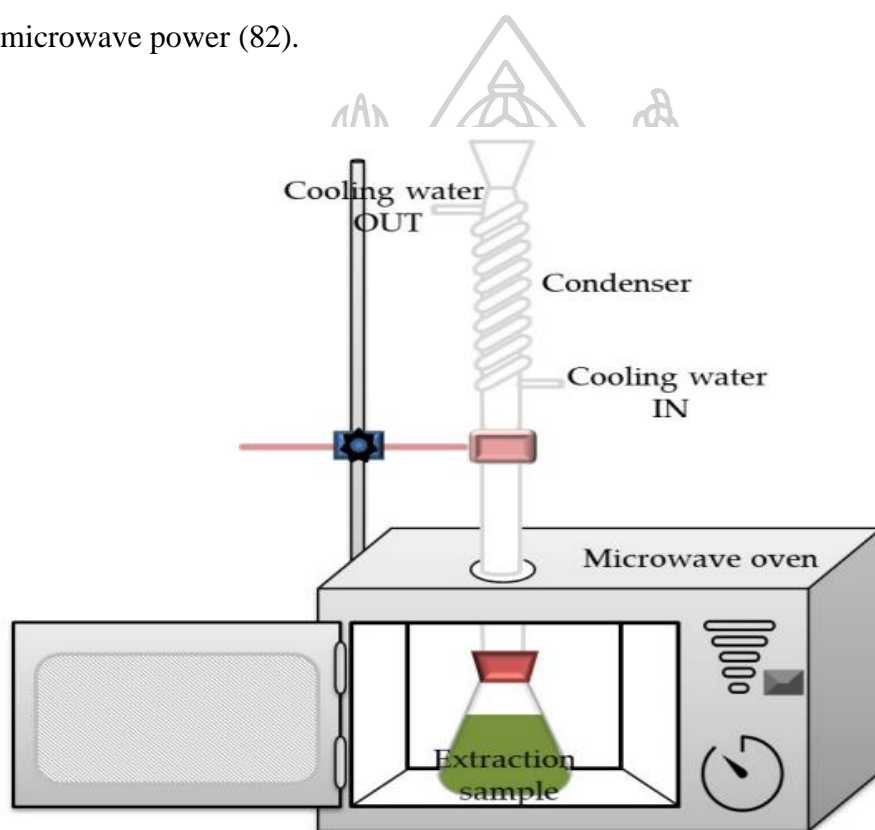
Figure 8. A Diagram Illustrating the Process of Microwave-Assisted Extraction (80).

Advantages (71, 81, 83, 84)	Disadvantages (71, 81, 83, 84)
- Improved extract quality by increasing the purity and stability of marker compounds and allowing for the use of fewer toxic solvents	- Need for special equipment - Low selectivity - High dependency of solvent nature and extraction temperature

- Minimal processing costs; high recovery and purity of marker compounds; rapid extraction rates; reduced energy and solvent consumption	- Unavoidable reaction at high temperatures

2.3.2.2. Supercritical fluid extraction (SFE)

SFE involves a substance that is subjected to temperature and pressure above its critical point. It is called a supercritical fluid and is used as an extraction solvent in SFE. It exhibits solubility characteristics resembling liquids and diffusivity like a gas, enabling it to dissolve a broad spectrum of natural compounds. These solvent properties undergo significant alterations in the vicinity of their critical points, responding sensitively to minor pressure and temperature fluctuations. SFE utilizes gases, typically CO_2, as a solvent, achieved by compressing them into a dense liquid state. This liquid is then transported through a cylinder containing the material to be extracted. The extract containing liquid is further transferred into a separation chamber where the extract is isolated from the gas, and the gas is reclaimed for future use (85) (Figure 9). Because of its appealing properties, such as its low critical temperature (31 °C), selectivity, inertness, low cost, non-toxicity, and ability to extract thermally labile compounds, supercritical CO_2 was widely used in SFE. Supercritical CO_2 is ideal for the extraction of non-polar natural products such as lipids and volatile oils due to its low polarity. The solvent characteristics of CO_2 can be controlled and modified by adjusting the pressure and temperature during the extraction process. This method is particularly well-suited for food components with comparable polarities, like oils and fats. It is an efficient method for selective extraction of specific compounds from the medicinal plants with various compositions (70).

Lo et al. employed SFE and preparative high-performance liquid chromatography to isolate a large scale of chrysophanol swiftly and efficiently, one of the anthraquinones in *Rheum palmatum* Linn. Under the same extraction time, the extraction efficiency of chrysophanol with SFE was found to be 25 times greater than that of boiled water extraction. The hydrophobic selectivity of supercritical CO_2 extraction led to the highest chrysophanol content in crude extracts, achieving 77%,

whereas other extraction methods yielded significantly lower amounts, with 8.4% from solvent extraction and 20% from reflux extraction in the crude extracts. The optimal extraction conditions for SFE were found to be 210 atm of pressure and 85 ºC of temperature for 30 minutes (85).
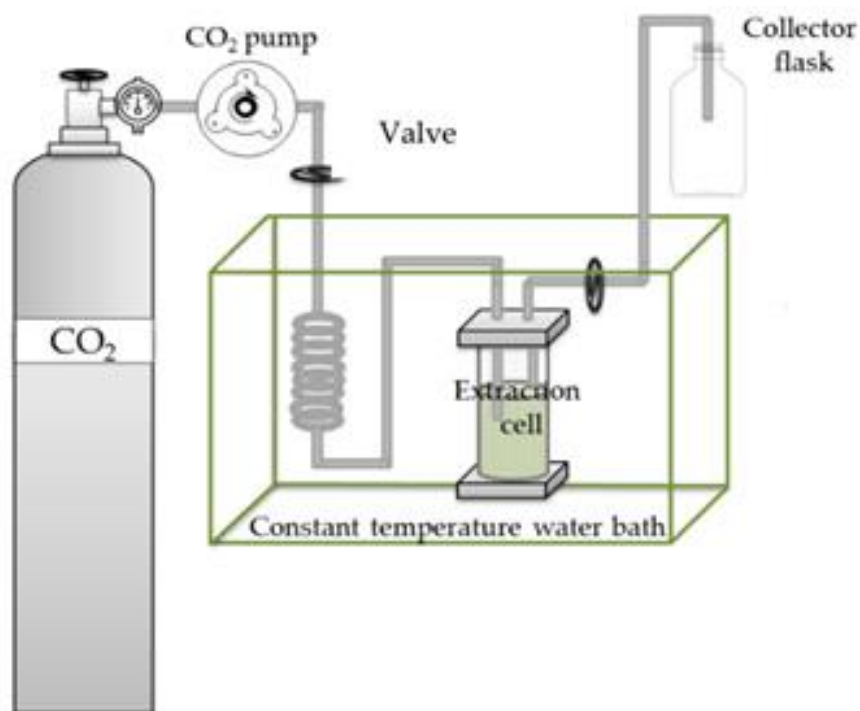
Figure 9. A Diagram Illustrating the Process of Supercritical Fluid Extraction (80).

Advantages (83)	**Disadvantages** (83)
- Faster extraction process	- Costly technology
- Enhanced selectivity of target compounds	- Required elevated pressures
- Reduced solvent usage	- Operates under unconventional conditions
- Automated sample handling	- Involves intricate phase behaviour
- Superior extraction efficiency	
- No solvent residues are left in the extract due to the complete evaporation of CO_2, which is often used as a supercritical fluid.	

2.3.2.3. Ultrasound-assisted extraction (UAE)

The underlying principle of UAE relies on the induction of cavitation effects, which amplify mass transfer, and promote close interaction between the solvent and the plant tissues. The key components of ultrasonic equipment are transducers for the transformation of mechanical or electrical energy into acoustic waveforms. During UAE, when the transducers produce acoustic vibration, the sound waves propagate throughout the vessel, which is filled with the medium, generating cycles of compression and rarefaction, leading to the formation of high- and low-pressure regions. During the rarefaction phase, the acoustic pressure surpasses the attractive forces between the molecules of the liquid medium, resulting in the creation of cavitation bubbles. These bubbles form during the rarefaction phase when the acoustic pressure decreases, and they implode during the compression phase when the acoustic pressure increases. This process generates microturbulence and shock waves, which improve mass transfer and promote the solid-solvent interaction, ultimately improving the extraction efficiency (86) (Figure 10(a)). Stable cavitation occurs when cavitation bubbles oscillate but cannot reach the specific size for implosion. This type of cavitation generates relatively less energy and may have a milder effect on the extraction process. In contrast, transient cavitation occurs when the acoustic pressure is high enough to rapidly grow cavitation bubbles until they reach their critical size, leading to violent collapse or implosion (Figure 10(b)). The implosion of cavitation bubbles near the surfaces of tissue creates microjets, leading to tissue damage and facilitating the deep permeation of solvent into the matrix (87) (Figure 11). Additionally, they release energy in the form of heat, augmenting mass transfer. Throughout the UAE, the combined effects of cavitation, thermal changes, and mechanical forces due to ultrasound lead to cell wall disruption, particle size reduction, plant matrix degradation, and improved mass transfer. These processes increase mass transfer without altering the structure and function of the extracted compounds. With the help of ultrasound, elevated temperatures during the extraction process are not required, protecting heat-sensitive compounds (71).

(a)   (b)
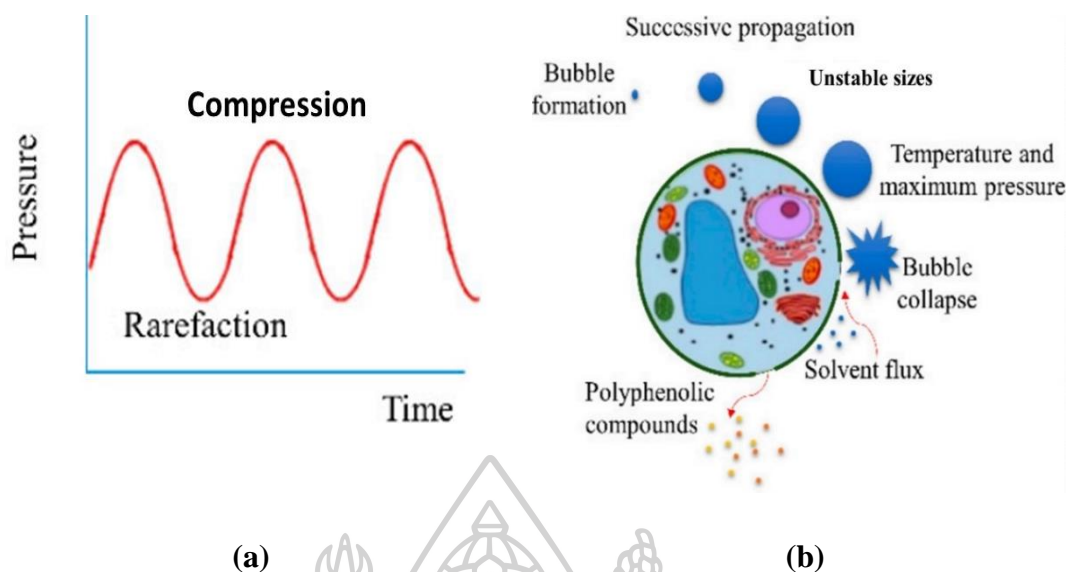
Figure 10. Principle of Acoustic Cavitation **(a)** and Mechanism of UAE **(b)** (86).
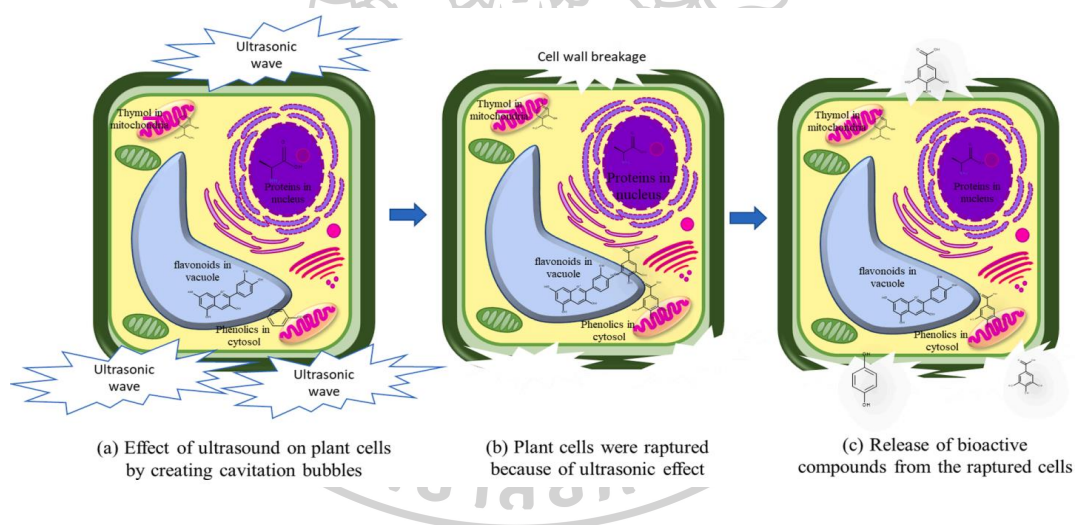
Figure 11. Mechanism of Ultrasound-Assisted Extraction (87).

The ultrasonic devices employed in UAE are briefly classified into 3 categories according to their operational mode, including the ultrasonic bath mode (88) (Figure 12(a)), the sonotrode (ultrasonic probe) mode (Figure 12(b)) and special-design mode basically derived from the first two modes.
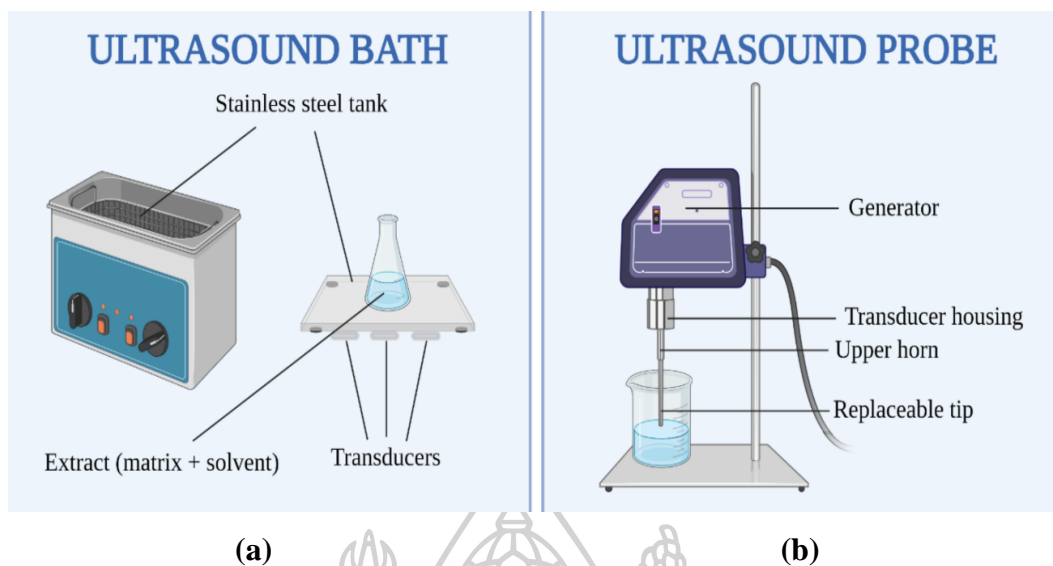
Figure 12. Two Types of Ultrasonic Devices; Ultrasound Bath Mode **(a)**, Ultrasound Probe Mode **(b)** (88).

The most commonly used and easily accessible method is the ultrasonic cleaning bath. Generally, it comprises a transducer, a container, time monitor, and heat controller. The transducers convert electrical current into sound energy, which is then transmitted into the medium within the bath. Typically, in lab-scale extraction, a flask or tube acts as the extraction container, is partially immersed in water, the coupling liquid, and is kept in a specific position to maximize cavitation. For large scale UAE, the ultrasonic bath is applied as an extraction vessel. Throughout this process, the matrix is prevented from floating or sinking and escaping the ultrasonic irradiation by stirring with a mechanical stirrer.

In the probe mode devices, the system typically comprises of an ultrasonic probe, a container fitting with the probe, and sometimes a stirrer and a temperature-control system. For mass production of extract, the special-design mode utilizes a more potent probe equipped with an adequate number of big bores and valves in suitable positions to pass through the matrix and solvent easily (89).

Since each analyte within different sample types binds to the matrix in a unique manner, the optimization of the extraction process should be conducted separately for each compound and matrix. On the other hand, variable recovery rates may be observed

based on the specific analyte. UAE is a cheap, uncomplicated, and effective replacement for traditional extraction methods if it is optimized.

Alam et al. studied the optimization of UAE conditions to increase the contents of sennoside A, sennoside B, aloe-emodin, emodin, and chrysophanol from *Senna alexandrina* (aerial parts). The three independent extraction parameters such as temperature, time, and solvent-to-solid ratio, were optimized using BBD. Phytoconstituent determination was performed using high performance liquid chromatography coupled with ultraviolet detection (HPLC–UV). The optimum extraction conditions were determined to be 64.2 ℃ extraction temperature, 52.1 minutes extraction time, and a solvent-to-solid ratio of 25.2 mL/g. The actual observed values of sennoside A, sennoside B, aloe-emodin, emodin, and chrysophanol (2.237%, 12.792%, 2.457%, 0.261%, and 1.529%, respectively) compared with those predicted by RSM models (2.152%, 12.031%, 2.331%, 0.214%, and 1.411%, respectively). *S. alexandrina* methanol extract exhibited antioxidant properties with a DPPH assay (IC_{50} = 59.7 1.93 µg/mL) and 2,2′-azino-bis-(3-ethylbenzothiazoline-6-sulfonic) acid (ABTS) method (IC_{50} = 47.2 1.40 µg/mL) when compared to standard ascorbic acid (IC_{50} = 6.8 ± 0.9 µg/mL for DPPH and 5.9 ± 1.3 µg/mL for ABTS) (90).

Yingngam et al. investigated the optimal extraction parameters of a high amount of rhein from the fruit pulp of *Cassia fistula* using UAE. A couple of one-variable-at-a-time and CCD were applied to define the most suitable parameters for optimizing the extraction process and to examine the relationship between factors. They reported that the optimum conditions for UAE were found to be 1:40 g/mL solid-to-liquid ratio and 10% v/v aqueous ethanol as a solvent at 75 ℃ for 40 minutes. The average experimental value of rhein content was observed with 14.98 ± 0.93 mg/g (91).

Advantages (71, 81, 88, 89)	**Disadvantages** (71, 81, 88, 89)
- Minimal energy and solvent consumption	- Heat generated during UAE can damage heat-labile compounds
- Enhanced extraction yield	- The various effects of the ultrasound waves depending on the position of the container
- Decreased extraction duration	
- Lower temperatures	

| | containing the solid samples and solvent inside the bath. |
| | - Lack of bath temperature and adequate power control lead to inefficiency in the energy transfer within the container holding the extract. |
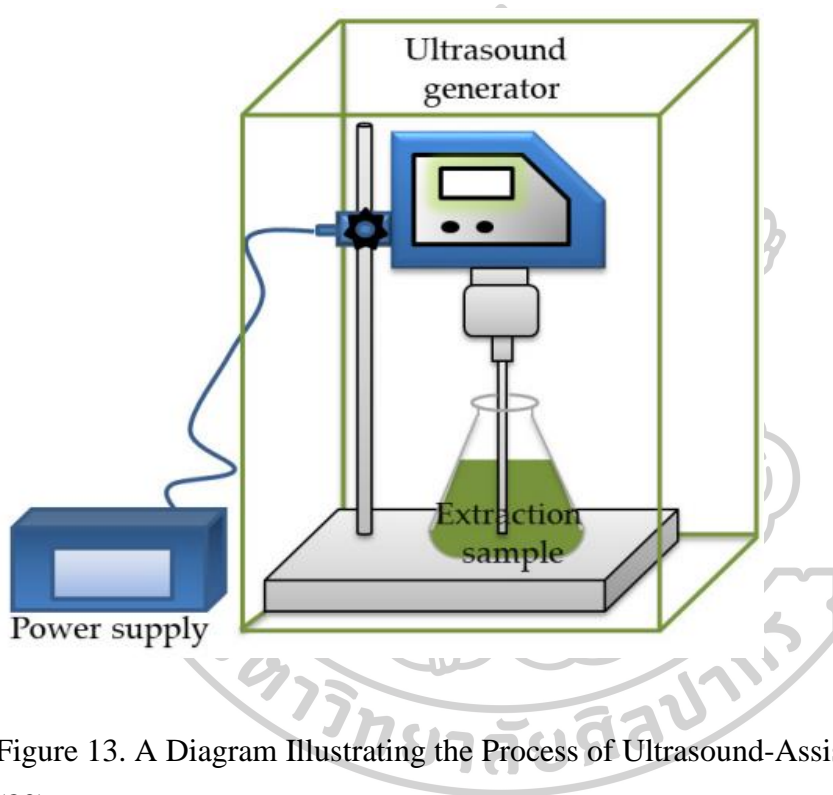
Figure 13. A Diagram Illustrating the Process of Ultrasound-Assisted Extraction (80).

2.4. Optimization of extraction conditions using design of experiments

The extraction of plant materials is a complex process influenced by numerous parameters that play a pivotal role in achieving the efficient quality and quantity of the extract. Selection of appropriate extraction methods is one of the important parameters to obtain the high-quality active components for pharmaceutical products.

Among many extraction methods, UAE is regarded as an environmentally friendly extraction method along with the advantages of inexpensive, simplicity, efficient, high extraction yield, lower operating temperature, minimal energy, and

solvent requirement. There are many parameters affecting UAE methods such as type and concentration of solvent, extraction temperature, extraction time, solvent- to-solid ratio, particle size of the plant materials, ultrasound frequency (80) (Figure 13). Due to numerous factors affecting the UAE, design of experiments (DOE) can be applied to identify the optimum conditions for achieving the high content of desired compound. The optimization process for the extraction conditions is illustrated in Figure 14 (80).
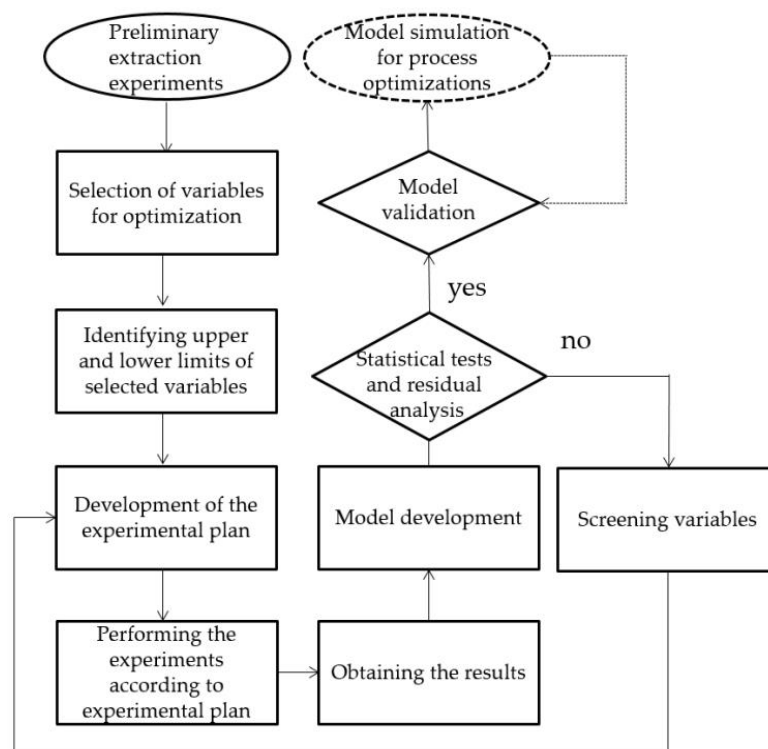
Figure 14. Flow Chart for Optimization Process.

Screening designs, the basic step of the DOE, can be used to define the individual factors affecting response variable and their levels. Some screening designs include one factor at a time (single factor analysis), full factorial design, fractional factorial design, and Plackett-Burman design.

A fundamental strategy that has been extensively applied in scientific and engineering testing is the one factor at a time (single factor analysis). When using a single factor analysis approach, a starting baseline is chosen by changing one factor level at a time while keeping the other factor levels constant. The best level is then chosen, and that level is maintained while the other levels are changed sequentially.

The procedure of conducting single factor analysis experiments involves sequential learning. We can find out more quickly whether a factor has any effects. Contrary to orthogonal fractional factorial designs, data can be monitored more promptly, enabling for the necessary response to be made without having to wait for the entire experiment to be completed (92).

After the independent factors affecting the response and their experimental ranges was identified by screening experiments, RSM is a favourable method for the optimization of extraction conditions. The purposes of the optimization study are to maximize the quantity of desired bioactive compound and to decrease the number of experimental trials and examine the combined effects among multiple factors (93). BBD is one of the experimental designs used for the optimization study. Number of experimental runs was generated by using the equation (1),

$$N = 2k (k-1) + Cp. \quad N = 2k (k-1) + Cp \quad\quad\quad (1)$$

where,

N = number of experiments

k = number of factors

Cp = number of centre points

When compared to CCD with the same number of factors, BBD frequently has fewer design points and can be less expensive to conduct. Axial points outside the "cube" are typical in central composite designs. These locations might not be relevant or might be impractical to conduct as they are above safe operating limitations. Since BBD lacks axial points, all design points are guaranteed to be within the safe operating range.

2.5. Electrospinning

Nanofibers have been created by various techniques, including drawing, template synthesis, phase separation, self-assembly, and electrospinning. Electrospinning is a technique to create continuous nanosized fibers with several uses. The great technological advancement in electrospinning makes it feasible to design and

synthesize novel polymer materials with outstanding properties. Electrospinning is an electrohydrodynamic process that involves electrically charging droplets to create a jet, which is then stretched and dried to produce fibers (94). A typical electrospinning system consists of a high-voltage DC or AC power supply, a syringe pump, and a fiber collector as depicted in Figure 15 (95). In general, the electrospinning process includes four stages: (1) charging the droplet, resulting in the formation of a Taylor cone or conical jet; (2) elongating the jet, composed of droplets with like charges, along a straight path; (3) the jet deviating from a straight path and continuously whipping in all directions; and (4) the solidification of fibers through solvent evaporation, followed by collection on a grounded collector (96). It is a highly cost-efficient technology capable of transitioning laboratory scale into industrial-scale production. In addition, this technology offers the possibility of obtaining specially structured nanofiber arrangements characterized by a significant specific surface area and noteworthy porous structure of inter- and intra-fiber. It also enables the blending two or more substances, potentially regulating the controlled or burst release of a drug, in addition to achieving modified release profiles. The electrospinning technique could spin a broad range of both natural and synthetic polymers with adjustable surface morphology, high interconnected porosity, and the tunable pore size (94, 96).

Significant characteristics of electrospinning are:

- Appropriate solvents must be available for polymer dissolution.

- The solvent should have an appropriate vapor pressure, evaporating at a rate that ensures the fiber maintains its structural integrity upon reaching the collector, yet not so rapidly that it solidifies before reaching the nanometer scale.

- The solvent's viscosity and surface tension must strike a balance, avoiding extremes that might hinder jet formation or disrupt the polymer solution's flow from the nozzle.

- The critical level of voltage should be applied to overcome the polymer solution's viscosity and surface tension, enabling the formation and sustenance of a jet from the syringe tip. The gap between the tip and the grounded surface must be neither too narrow, risking electrode sparks, nor too wide, allowing sufficient time for solvent evaporation and fiber formation (97).

Advantages of Electrospun fibers

Electrospun nanofibers have distinct properties in contrast to other nanostructures:

(a) They possess elevated porosity like the natural extracellular matrix (ECM), which facilitates cell adhesion, proliferation, and migration.

(b) A large, defined contact area offers advantages in managing wound exudate, dispersing drugs, and improving the solubility of poorly water-soluble medications.

(c) Their fiber morphology is particularly well-suited as a versatile material for wound dressing applications.

(d) Drug-encapsulation efficiency can be improved.

(e) Surface morphology of fibers can be adjusted to meet the specific requirements.

(f) Prevent immediate rapid release and create opportunities for effective surface customization through the suitable selection of a drug-polymer-solvent system (94, 98).
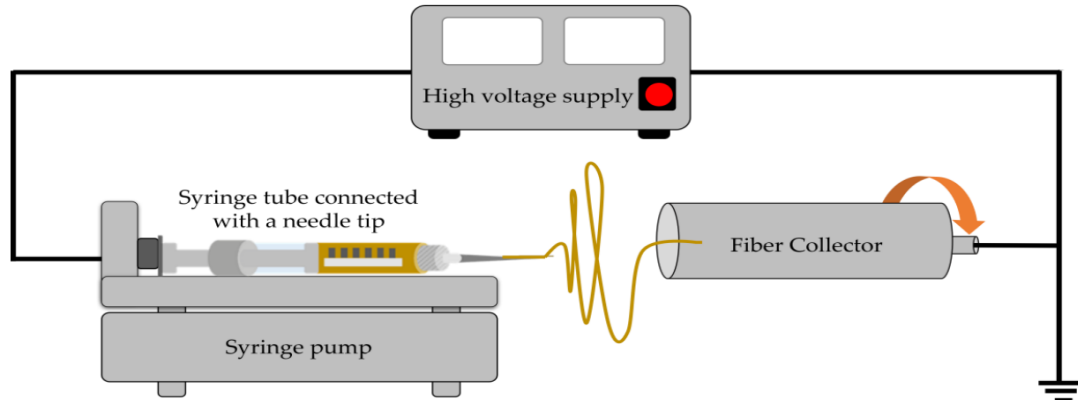
Figure 15. Schematic Representation of Electrospinning Process (95).

2.6. Fabrication of electrospun nanofibers loaded with herbal extracts

Medicated nanofibers are produced from a mixed solution or melt comprising a carrier polymer and the active components, typically processed using single fluid electrospinning (99). These nanoscale fibers, which replicate the native structure of the natural extracellular matrix, can enhance cellular functions like attachment and proliferation. Electrospun fibers possess remarkable attributes, including a substantial specific surface area, high porosity, good biocompatibility, and degradability. As a

consequence, they have found extensive applications in the pharmaceutical field, serving as biosensors, medical implants, drug delivery systems, wound dressings, and scaffolds for tissue engineering (33). Their versatility extends to drug loading, amorphization of crystalline active ingredients, and the extension of physical storage stability (94). Nanofibrous structures possess the distinctive capability of enhancing wound healing more effectively when contrasted with conventional dressings. Nanofibers have the unique capacity to efficiently absorb exudates, creating a conducive moist environment for cellular respiration and proliferation. They mitigate bacterial infections, offer excellent permeability, and safeguard injured tissue from dehydration. Additionally, the electrospinning process enables the incorporation of drugs and various bioactive substances, including growth factors, nanoparticles, antimicrobial agents, and anti-inflammatory agents, within the nanofibers. Biodegradable electrospun wound dressings further foster healing and accelerate cell growth rates, thanks to their exceptional compatibility with blood and tissues (34).

Bioactive properties of natural herbal extracts manifest within a polymeric nanoscale matrix. Numerous crude plant extracts have been effectively incorporated in electrospun fibers.

In a study involving Sprague-Dawley rats, the application of electrospun gelatin membranes with *Centella asiatica* extract as transdermal dressings for wounds demonstrated superior cutaneous wound-healing activity compared to alternative treatments. Notably, rats treated with the electrospun membranes exhibited enhanced wound healing compared to those treated with gauze (used as a control), gelatin membranes lacking *C. asiatica* extract, and a commercial product. The gelatin membranes containing *C. asiatica* extract exhibited antibacterial and anti-inflammatory activities, which contributed to the enhanced wound-healing activity (100).

The wound dressings, consisting of chitosan/polyethylene oxide electrospun nanofibers loaded with green tea (*Camellia sinensis*) extract, exhibited superior healing effects on rat wounds compared to other prepared wound dressings. They demonstrated potent antibacterial activities against *E. coli* and *S. aureus*, along with high swelling properties, indicating their ability to retain moisture on the wound surface. This moisture retention facilitated a moist environment throughout the healing process, thereby contributing to effective wound healing (101).

One of the reports described in detail the assessment of antioxidative, antibacterial, and *in vivo* wound healing properties, as well as *in vitro* release and stability studies, of *Garcinia mangostana*-loaded chitosan-ethylenediaminetetraacetic acid/polyvinyl alcohol (CS-EDTA/PVA) electrospun mats. The fibers demonstrated the capacity to retard the growth of *S. aureus* and *E. coli*, with the effectiveness depending on the concentration of the entrapped extract within the fibers. Notably, fibers loaded with 3% w/w of extracts exhibited full recovery within an 11-day period, marked by skin re-epithelialization and the replacement of granulation tissue with hair follicles. The mats can retain 90% of α-mangostin content for up to 3 months (102).

Chiu et al. have studied the crude extract of *Curcuma comosa* Roxb. incorporated electrospun gelatin fibers to achieve the suitable electrospinning conditions as well as antioxidant, anti-tyrosinase and antibacterial activities and its freeze–thaw stability. The ideal parameters for generating electrospun gelatin fibers were determined to be a gelatin concentration of 30% w/v, employing a co-solvent system of acetic acid/water (9:1 v/v), a feed rate of 3 mL/h, and an applied voltage of 15 kV. Nanofibers with the minimal amount of loading 5% w/v ethanol extract exhibited remarkable activities in terms of DPPH radical scavenging, anti-tyrosinase, and antibacterial properties against *S. aureus* and *S. epidermidis* (103).

In the field of drug delivery and nanotechnology utilizing natural products, several biopolymeric materials are instrumental in advancing the creation of innovative drug delivery systems with improved characteristics. Specifically, the next section extensively explores shellac, a natural polymer, and its significance in this context.

2.7. Shellac

Shellac is one of the natural polymers, obtained from the purified resinous secretion of lac insects, *Laccifer lacca.* It is a complex compound of polyesters and single esters having hydroxyl and carboxyl groups (Figure 16) (104). The main components of shellac are shellolic acid and aleuritic acid. Shellac is a semicrystalline polymer possessing low crystallinity, with a melting temperature between 50 °C and 75 °C (105). Owing to its several properties, such as excellent film formation, water resistance, flexibility, non-toxicity, biodegradability, high gloss, good acid resistance and poor permeability to gases and water vapor, shellac can be used in many areas,

including food technology and pharmaceutical technology (26). Shellac has been widely employed in the food industry for various purposes including as an oil gelling agent and emulsifier, a food foaming agent, and a material for food packaging films, coatings, waxes, and delivery systems. Its applications aim to minimize the loss of water and volatile flavoring substances while also inhibiting microbial growth to extend shelf life. In the pharmaceutical industry, shellac finds utility in tablet coating formulations, microencapsulation processes, matrix formation, enteric coating applications, and as a binder in various pharmaceutical products. Furthermore, shellac serves as a valuable ingredient in cosmetic products, contributing to their formulation and functionality (106). Furthermore, multiscale shellac-based delivery systems have been established from the nanometer to the micrometer scale, such as nanofibers, microparticles, hydrogels, etc (107). However, shellac has some drawbacks; batch-to-batch variation, poor mechanical property, and instability. Shellac undergoes aging due to polymerization occurred by self-esterification. The hydrogen bond between hydroxy group and carboxy group of shellac in acid form become cross linkage to form esters (108) (Figure 17). This esterification reaction may decline the properties of shellac; less soluble, decreased acid value, increased glass transition temperature, loss of gastric resistance, decrease in intestinal fluid solubility leading to major changes in drug dissolution profiles.

Various types of shellac can be obtained through the refinement of sticklac extracted from lac-bearing twigs. The production process of shellac begins with sticklac, derived from the resin secreted by lac insects on branches. To obtain seedlac, sticklac undergoes a series of steps including pulverization, screening, cleaning with water and an alkaline solution, and ultimately air-drying to remove any remaining insects, twigs, and other impurities (109). The purified seedlac is then processed further to yield the valuable substance known as shellac. There are two primary methods for preparing shellac. In the first method, the seedlac is melted, filtered, and shaped into thin sheets. Alternatively, in the second method, the seedlac is dissolved in an organic solvent, filtered to remove sediment, evaporated, and then formed into a thin film (109). Among them, bleached shellac is obtained by dissolving seedlac in aqueous alkali solutions, followed by treatment with sodium hypochlorite and the addition of sulfuric

acid to precipitate. The precipitate is filtrated to remove wax, obtaining bleached, dewaxed shellac.

R=CHO, R' = CH$_2$OH   Jalaric acid
R=CHO, R' = CH$_3$ Laccijalaric acid
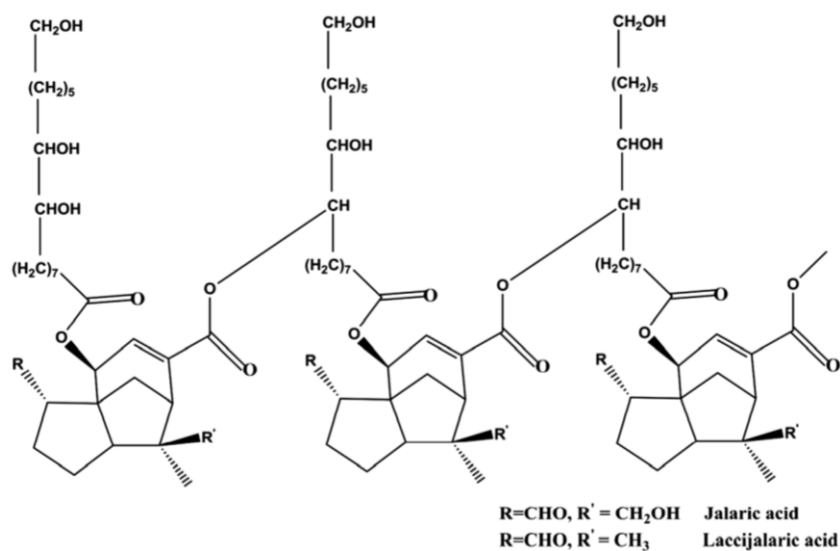
Figure 16. Structure of Shellac (104).
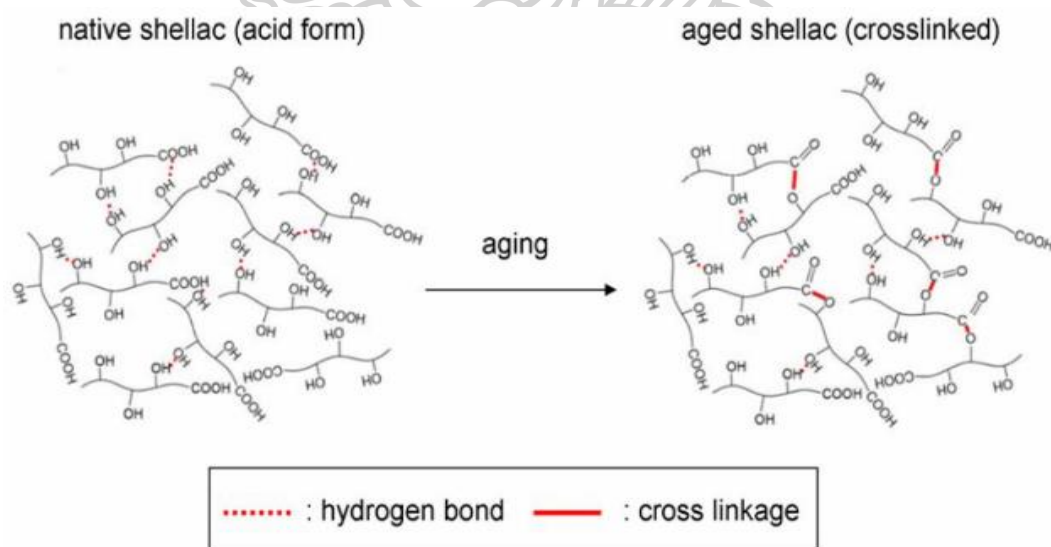
Figure 17. Aging of Shellac (108).

Numerous investigations have been conducted on the utilization of shellac in the electrospinning process to create nanofibers. Wang et al. investigated a study exploring the production of medicated shellac nanofibers designed for colon-specific

sustained release through coaxial electrospinning. The core solution consisted of a blend of 75% w/v shellac and 15% w/v ferulic acid in ethanol, while the shell was comprised of a mixture of ethanol and N, N-dimethylformamide (8/10 v/v). Analytical findings from X-ray diffraction and differential scanning calorimetry confirmed the amorphous dispersion of ferulic acid within the fibers. Furthermore, Infrared (IR) spectra revealed the presence of hydrogen bonding between the shellac and ferulic acid. Given that ferulic acid and shellac both possess -OH and -C=O groups, the distinct peaks associated with ferulic acid's -C=O groups at 1689, 1663, and 1619 cm^{-1} were merged into a singular peak observed at 1698 cm^{-1} in the fiber spectra. Additionally, several peaks in the fingerprint region of the ferulic acid spectrum were no longer discernible in the fiber spectra. These observations confirm that ferulic acid molecules form composites with shellac via hydrogen bonds. *In vitro* dissolution tests revealed that the release of ferulic acid was minimized at pH 2.0 and sustained in a neutral dissolution medium (110).

Chinatangkul et al. studied the variables affecting the creation and characteristics of shellac nanofibers infused with the antimicrobial compound monolaurin, using a full factorial design, characterization study of fibers, and antimicrobial activities with a time kill kinetics study. The impact of formulation and process parameters including shellac content (35 - 40% w/w), monolaurin content (1 - 3% w/w), applied voltage (9-27 kV), and flow rate (0.4-1.2 mL/h) on the properties of nanofiber were studied. According to the results, the shellac concentration exhibited the key parameter influencing the diameter of fiber and had a negative relation with bead formation. Small (488 nm) and beadless (0.48) fibers with the weight ratio of shellac and monolaurin (37.5 : 1.1) were obtained using the optimum area at an applied voltage of 18 kV and a flow rate of 0.8 mL/h. Time kill-kinetic studies revealed that shellac nanofibers loaded with monolaurin had excellent antibacterial activity against *S. aureus* (111).

The features of electrospun nanofibers plays a pivotal role in defining their ultimate physical and chemical characteristics, predominantly dictated by the electrospinning process. Influential factors that impact fiber morphology within the electrospinning process fall into three primary categories: process parameters, solution parameters, and environmental conditions. By manipulating these parameters, the

morphology and structure of nanofibers can be managed. Consequently, it becomes essential to meticulously examine the optimal electrospinning conditions to achieve the targeted range of beadless and ultrafine nanofibers.

2.8. Optimization of electrospinning parameters

The electrospinning parameters need to be optimized in order to achieve nanofibers with a desired morphology, structure, and properties. Attaining the desired properties of electrospun fibers relies on various parameters like applied voltage, flow rate, a concentration and viscosity of the spinning solution, solution conductivity, distance between the collector and needle tip, solvent used to dissolve the drugs or the extracts, etc. Parameters influencing electrospinning process and effects are described in Table 2 (94, 97, 112, 113). Utilizing the DOE approach can be advantageous for optimization of parameters influencing the desired morphology and properties of electrospun fibers.

Table 2. Parameters Effecting the Electrospun Nanofibers.

Parameters	Effects on the diameter, morphology, and structure of nanofibers
Flow rate	When the flow rate is low, the polymer solution would have adequate time for polarization. If it is exceedingly high, both the rapid drying time and the minimal stretching resulted in the formation of bead fibers with thick diameters (113).
Applied voltage	Increasing the voltage generally enhances the production of finer fibers, although it may also lead to the ejection of more fluid, resulting in thicker fiber diameters. Once the voltage surpasses a critical threshold, the diameter initially decreases, followed by an increase beyond a certain point. The initial reduction in diameter is attributed to increased repulsion forces (94).
Distance	The instability stage at which the deposition of jet on the collector is determined by the working distance from tip of the spinneret to collector. A sufficiently long distance is necessary to ensure complete extension and solidification of the jet, resulting in the fibers formation.

Parameters	Effects on the diameter, morphology, and structure of nanofibers
	In fact, long distance can form thinner fibers. When the space between the tip of the spinneret and the collector reaches a specified limit, the fiber could not be thinner as the distance increases due to jet solidification. There is insufficient time for solvent evaporation at a short distance resulting the creation of flattened structures with beaded fibers (97).
Relative molecular mass	The molecular weight of a polymer significantly influences the rheological characteristics and electrical properties of the solution. Generally, lower molecular weights tend to result in the formation of beads instead of fibers due to limited chain entanglement (112).
Viscosity of polymer solution	Reduced viscosity facilitated the creation of finer fibers. However, lowering the solution viscosity could result in the formation of beaded nanofibers, as a higher concentration of solvent molecules reduced chain entanglements and decreased the density of surface charges. Conversely, if the viscosity became excessively high, it would become challenging to extrude the solution from the spinneret (97).
Surface tension	Lower surface tension leads to proper jet initiation facilitating the thinner fibers production and allowed the beads to disappear gradually (94).
Relative volatility of polymer solution	Excessive volatility is detrimental to the fiber-spinning process, as the jet may solidify almost instantly upon exiting the spinneret. Conversely, when volatility is too low, the fibers will remain wet when deposited on the collector. A porous microstructure may develop due to higher volatility levels (112).
Conductivity of the solution	Solutions with elevated conductivity exhibit a greater capacity to carry charge, leading to the application of higher voltages. Consequently, higher voltages contribute to a reduction in fiber diameter and an increased distribution of fiber diameters (94).
Solubility of solvent	The solubility parameter of the solvent is critical for the formation of a homogeneous polymer solution, but a solvent characterized by a

Parameters	Effects on the diameter, morphology, and structure of nanofibers
	high solubility parameter is not necessary to create a suitable solution for electrospinning. The critical factor determining suitability is the solvent's volatility or vapor pressure, as it dictates the rate of evaporation and, consequently, the solidification rate of the jet (112).
Temperature	Elevated temperatures lead to a reduction in both the surface tension and viscosity of the polymer solution, enabling the creation of finer fibers. Nonetheless, higher temperatures also accelerate solvent evaporation, restricting the extension of the jet. As such, temperature exerts two opposing effects on fiber diameter, necessitating careful optimization (112).
Relative humidity	Relative humidity plays a critical role in influencing the solvent's evaporation rate and, consequently, the solidification rate of the jet. Reduced relative humidity favours the creation of finer fibers with a drier surface. However, if the relative humidity drops too low, rapid solvent evaporation constrains the jet's extension. When the relative humidity reaches a certain threshold, water vapor in the air can penetrate the jet, resulting in morphological alterations in the nanofibers (112).

2.9. Design of experiments (DOE)

Experimental design, commonly known as DOE, is a structured methodology geared towards uncovering the key factors that impact response variables, such as product performance, process efficiency, or physical characteristics. This approach aims to systematically identify independent variables and assess their significance or insignificance in influencing the desired outcomes. By analysing the interactions between various process and product variables, DOE helps optimize system performance while enhancing desirable attributes. Employing statistical techniques, DOE allows for the thorough examination of data and the estimation of product properties under diverse experimental conditions within the constraints of the design. This approach ensures the generation of essential information with minimal experimentation. Employing DOE offers the advantage of producing, analysing, and

evaluating systematic data to make at effective and objective conclusions. An experimental design involve four phases including the planning, designing, conducting and analysis of experiments as shown in Figure 18 (114). Three types of experimental designs; mixture designs, factorial designs, and response surface designs are commonly used in various fields of science and engineering.
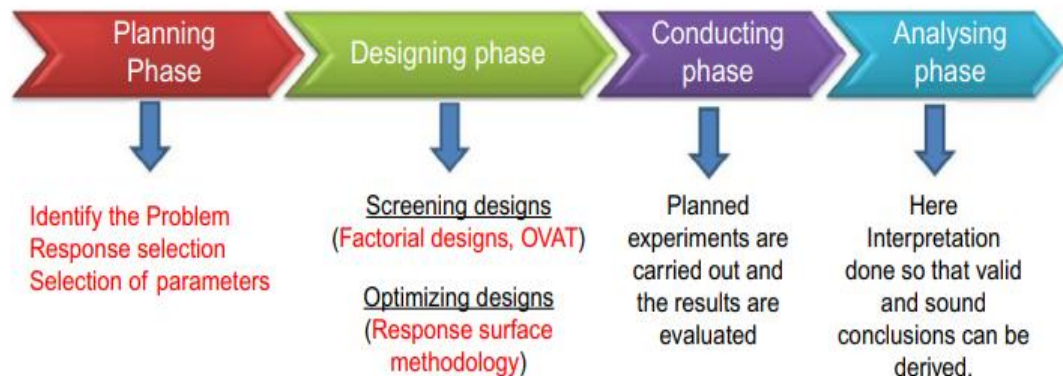
Figure 18. Different Phases Involved in Design of Experiments (114).

2.9.1. Mixture designs

Mixture designs are specifically tailored for optimizing formulations in which the independent variables represent different components or ingredients within a mixture or recipe. The objective of formulation optimization is to determine the ideal proportions of these components by assessing the performance of various properties (dependent variables or responses) across a range of compositions. Mixture experiments can be considered as a specialized subset of response surface experiments, as they focus on modelling and improving the relationship between ingredient proportions and desired outcomes (115).

2.9.2. Factorial designs

Factorial designs are employed to systematically examine multiple independent variables to identify the significant factors and interactions that influence the performance of various response variables under investigation. The initial step in conducting a factorial design is to establish the experimental range for each independent variable, setting the boundaries within which the variables will be tested. Factorial designs are typically two-level designs with a low and high level for each factor.

A full factorial design involves generating experimental data points by systematically testing all possible combinations of factor levels in each complete trial or replication of the experiment. In this approach, the number of experiments required is determined by 2^k, where 'k' represents the number of independent variables. For instance, in a scenario with five independent variables, a full factorial design necessitates conducting 25 or 32 experiments. This means that the high and low values for each independent factor are explored in conjunction with the high and low values of all other independent variables in a comprehensive manner. The resulting response model encompasses not only the main effects of the individual factors but also all possible interactions among them, allowing for a thorough examination of their combined influence on the outcomes of the study.

A fractional factorial design is one of the most significant statistical developments to explore the influences of numerous controllable factors on an interest response. It is not only well-known design features to carefully reduce the size of an experiment, but it can also limit the loss of important data that would result from omitting to thoroughly investigate all the combinations of the levels of the factors of interest (116). Fractional factorial designs are employed to determine the main effects and the effect of some possible interactions. This design reduces the number of experiments but does not account for all possible interactions among independent factors in the space of experiments. A two-level fractional factorial design is typically described as 2^{k-p}, where p represents the fraction of the full 2^k factorial (i.e., $1/2^p$). A 1/2 factorial with five independent variables generates 16 experiments, while a 1/4 factorial needs eight experiments. Fractional factorials are typically one of the initial phases in an evaluation approach. It is possible to recognize the crucial factors and then perform a more thorough evaluation. Following the completion of screening experiments, notable factors are chosen to proceed with a response surface DOE, aimed at pinpointing the ideal processing conditions. Alternatively, a factorial design incorporating a central point and repeated experiments may be employed to further explore significant variables.

A three-level factorial design requires three experiments for each input variable because it includes a center point, high level, and low level for each independent variable. The number of experiments significantly increased by the third level. While

three-level factorial designs result in a vast array of experimental configurations or trial combinations, alternative response surface designs have been devised to minimize the number of tests needed to achieve comparable insights.

2.9.3. Response surface designs

Response surface designs are often preferred over three-level factorial designs. This is because three-level factorial designs involve testing low, high, and centre values for each independent variable, and they tend to require a greater number of experiments to gather equivalent information. In contrast, response surface designs offer a more efficient and effective approach for achieving the same level of insight with fewer experimental trials.

Response Surface Methodology (RSM) represents a fusion of statistical design and numerical optimization approaches used to construct empirical models. It serves for both optimizing processes and designing products, providing a framework for constructing and leveraging models to enhance efficiency and design across various applications. Once essential factors are identified, response surface designs are employed to refine processes, offering a detailed analysis of their interconnections and curvature within the experimental space. This approach enables the prediction of second-order effects of factors that two-level factorial designs cannot evaluate. Unlike factorial designs, response surface experiments reveal curvature, presenting a graphical demonstration in two or three dimensions when plotting a response variable against independent factors. Compared to two-level factorial or fractional factorial designs, response surface designs offer richer information about output or response variables. By fitting responses to quadratic or cubic equations using multilevel experimental points, a better model of the response variable in the experimental space can be established. Central Composite Design (CCD) and Box-Behnken Design (BBD) prove more useful than three-level factorial designs in this context (117-119).

2.9.3.1. Central Composite Design (CCD)

A Box-Wilson central composite design, often referred to as Central Composite Design (CCD), is a common approach used in RSM to create a second-order polynomial model for response variables. It accomplishes this without the need for a

full factorial design of experiments. The CCD is essentially an extension of a two-level factorial design, with the inclusion of 2^k (where k is the number of independent variables) points positioned between the axes, in addition to replicates at the centroid as presented in Figure 19 (114). In experimental design, it's essential to have a minimum of three levels for each variable to determine the coefficients of a polynomial with quadratic terms accurately. The CCD incorporates three distinct types of points: factorial points, central points, and axial points.
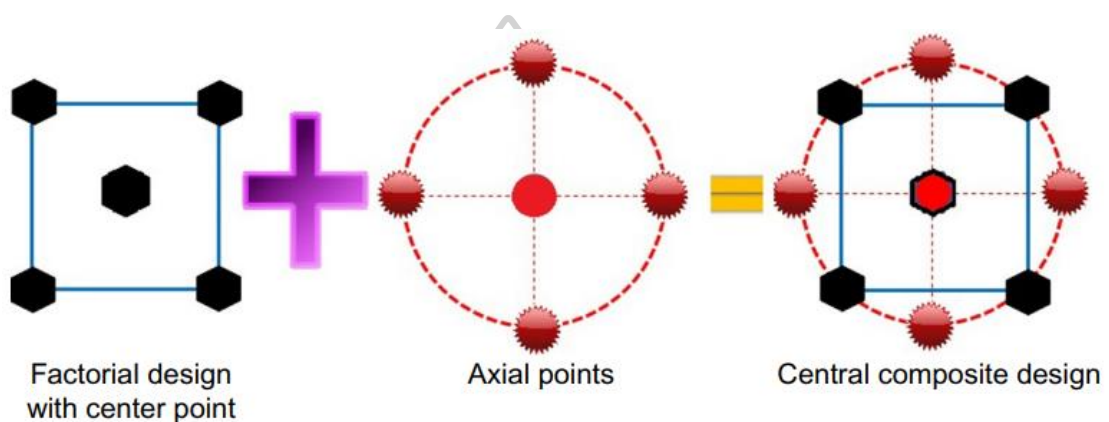
Figure 19. A Graphical Representation of Central Composite Design (114)**.**

1. **Factorial Points:** These points are located at the edges of an n-dimensional cube, typically originating from full or fractional factorial designs. In these designs, factor levels are typically coded as -1 and +1.
2. **Central Points:** The central point is positioned at the centre of the experimental design space. It's used as a reference point to help assess the behaviour of the system around its centre.
3. **Axial Points:** Axial points are strategically placed along the axes of the coordinate system. They are symmetrically located concerning the central point and are usually situated at a distance denoted as α from the design centre. These points are used to explore the behaviour of the system at a distance from its central point and are particularly useful for estimating quadratic effects.

These points, along with the factor level settings, allow for a systematic exploration of the response surface and the determination of the coefficients in a

polynomial equation, making it possible to model and optimize complex processes or experiments (119).
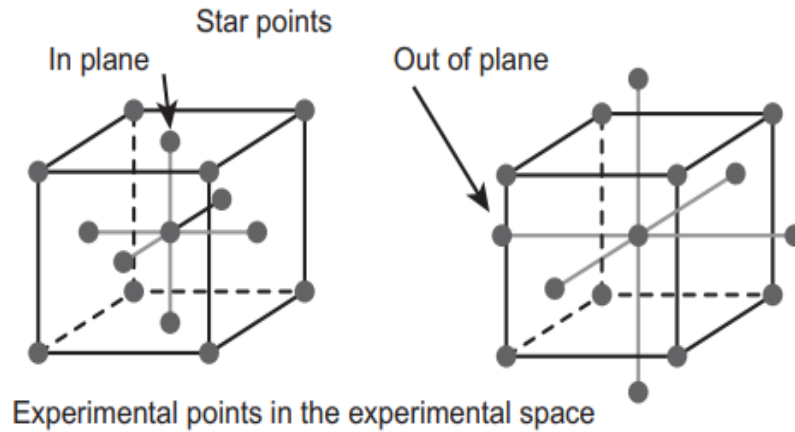
Figure 20. Central Composite Design with Star Points (117).

The experimental space for a three-factor CCD is depicted in Figure 20 (117). The star points or central points within each surface may extend beyond the surface, depending on the specific design. However, it's essential to recognize that placing star points outside the designated plane might not be feasible under practical processing conditions. Therefore, they must be situated within the plane alongside the other coordinate points. In any given design, it's critical that all experimental points are physically viable and attainable for processing. Since the star points are observed to be outside the hypercube, adjustments must be made for each factor, typically requiring five levels instead of three. However, achieving these adjusted values for factors can sometimes pose challenges (120).

2.9.3.2. Box-Behnken Design (BBD)

The Box-Behnken design (BBD) is a statistical experimental design utilized in the field of DOE. It falls under the umbrella of RSM and aids in optimizing processes or products by investigating the relationship between multiple independent variables and their effect on the measured outcome (output). The primary objective of a BBD is to construct a predictive model of the response variable while efficiently conducting experiments with a relatively small number of runs. Unlike other designs, the BBD is

an isolated quadratic design without incorporating factorial or fractional factorial designs into its structure. It is rotatable and necessitates three levels for each factor. Besides the lower and upper bounds, a central point is included for each factor within the BBD. This central point facilitates the estimation of quadratic effects and assists in evaluating curvature in the response surface. Treatment combinations in this design are positioned at the midpoints of limits of the process range and in the center, as illustrated in Figure 21 (114).
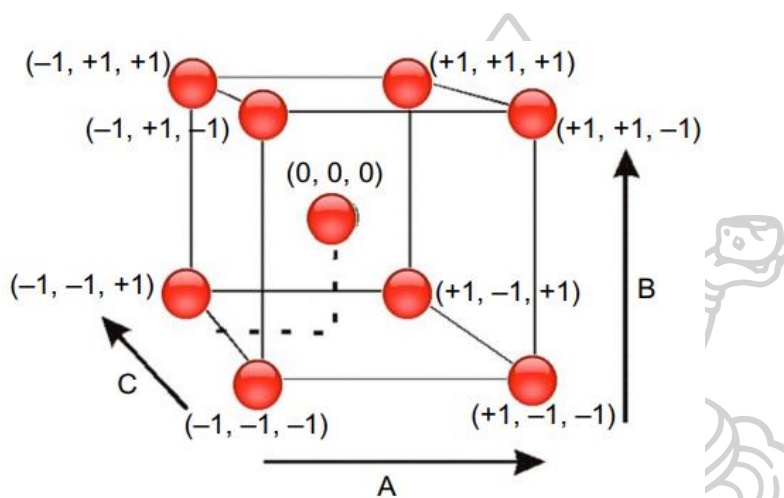
Figure 21. A Visual Representation of Box-Behnken Design (117)**.**

BBD is particularly suitable for experiments involving more than two factors and when the optimum is anticipated to lie within the middle of the factor ranges. It proves valuable for determining optimal conditions without necessitating an excessive number of experiments. Once the response surface model is set up, optimization methods can be employed to identify the best conditions, whether they aim to maximize or minimize the response variable. This approach finds frequent application in product formulation, process optimization, and quality improvement endeavors.

Chapter 3
Methodology

3.1. Materials and instrumentation

3.1.1. Materials

1) Acetonitrile HPLC grade (99.93 % v/v) (Fisher Scientific Korea Ltd., Seoul, Korea)

2) Bleached shellac (Excelacs Co., Ltd., Bangkok, Thailand)

3) Diclofenac sodium (Bureau of Drug and Narcotic, Department of Medical Sciences, Ministry of Public Health, Nonthaburi, Thailand)

4) Dimethyl sulfoxide (DMSO) (Fisher Scientific, Loughborough, Leicestershire, UK)

5) Distilled water

6) *Escherichia coli* DMST 4212

7) Ethanol (99.8 % v/v) (VWR International, Fontenay-sous-Bois, France)

8) Fresh chicken egg

9) Isopropyl alcohol (QRëC, Auckland, New Zeland)

10) Native shellac (Mahachai Shellac Company Limited, Samut Sakhon, Thailand)

11) Neomycin sulfate (Greater Pharma Manufacturing Co., Ltd., Nakhon Pathom, Thailand)

12) Orthophosphoric acid (85% w/w) (Ajax Finechem Pty Ltd., Auckland, New Zealand)

13) Potassium phosphate monobasic (KH_2PO_4) (QRëC, Auckland, New Zeland)

14) *Pseudomonas aeruginosa* ATCC 9027

15) *Senna alata* leaves (Charoensuk Osot, an herbal shop in Nakhon Pathom, Thailand)

16) Sodium chloride (NaCl) (Ajax Finechem Pty Ltd., Auckland, New Zealand)

17) Sodium hydroxide (QRëC, Auckland, New Zeland)

18) Sodium phosphate dibasic (Na_2HPO_4) (Ajax Finechem Pty Ltd., Auckland, New Zealand)

19) Standard rhein (95 % w/w) (MilliporeSigma Supelco, Darmstadt, Germany)

20) *Staphylococcus aureus* ATCC 6538P

21) Tryptic Soy Agar (HiMedia Laboratories Private Limited, Mumbai, India)

22) Tryptic Soy Broth (Becton, Dickinson and company, Sparks, MD, USA)

23) Tween 80

24) Ultrapure water (UltraPure Water Machine, TKA Wasseraufbereitungssysteme GmbH, Niederelbert, Germany)

3.1.2. Instruments

25) 0.45 µm nylon syringe filter (TTK Science Co., Ltd., Bangkok, Thailand)

26) Agar plate

27) Agilent 1100 HPLC-DAD (Agilent Technologies, CA, USA)

28) Analytical balance (Satorius, Göttingen, Germany)

29) Bacterial incubator (Contherm Biosyn 6000CP; Contherm Scientific Ltd., Wellington, New Zealand)

30) Biosafety cabinet (Model S2010, Holten, Denmark)

31) Differential scanning calorimeter (DSC 8000, Perkin Elmer, Rodgau, Germany)

32) Drop shape analyzer (First Ten Angstroms, Portsmouth, Virginia, U.S)

33) Duran bottle 1000 mL, 500 mL, 250 mL, 100 mL (Schott Duran, Germany)

34) Electrical conductivity meter (Model EC400, Extech instruments corporation, Pittsburgh, PA, USA)

35) Electrospun machine (kd Scientific, Holliston, USA)

36) Fourier transform infrared (FTIR) spectrometer (Nicolet Avatar 360, Ramsey, MN, USA)

37) Freeze dryer (Model 6112974, Labconco Corporation, Kansas City, MO, USA)

38) Freezer (Model- DF 9007, ilShinBioBase Co., Ltd., Dongducheon-si, Gyeonggi-do, Korea)

39) Incubator shaker (ES-20 Incubator, Gibthai Co., Ltd, Bangkok, Thailand)

40) Luna Omega Polar C18 column (5 μm, 100 Å, 4.6 mm x 250 mm) (Phenomenex Inc., Torrance, CA, USA)

41) Magnetic stirrer (ST10, Finepcr, Seoul, Korea)

42) Needle 16 - gauge (G), 18 - gauge (G), 20 - gauge (G) (Nipro (Thailand) corporation Limited, Phra Nakhon Si Ayutthaya 13110, Thailand)

43) pH meter (Mettler Toledo, Schwerzenbach, Switzerland)

44) Powder X-ray diffractometer (PXRD) (MiniFlex II, Rigaku Corporation, Tokyo, Japan)

45) Rotary evaporator (R-100, Buchi, Japan)

46) Scanning Electron Microscope (SEM) (MIRA 3, Tescan, Brno, Czech Republic)

47) Syringe 10 cc, 1 cc (Nipro (Thailand) Corporation Limited, Phra Nakhon Si Ayutthaya 13110, Thailand)

48) Ultrasonicator (Model 230D, Crest Ultrasonics Corp., Ewing Township, NJ, USA)

49) UV-vis spectrophotometer (Cary 60, Agilent Technologies, Santa Clara, CA, USA)

50) Viscometer (RM 100 CP 2000 Plus, LAMY Rheology, Champagne au Mont d'Or, France)

51) Whatman filter paper No. 1 (GE Healthcare UK Limited, Amersham Place Little Chalfont, Buckinghamshire, UK)

3.2. Optimization of extraction conditions and evaluation of rhein-rich (optimized) extract

3.2.1. Preparation of extracts

SA leaves were extracted using UAE method under various conditions as per experimental plan. An exact amount (2.5 g) of dried SA leaves powder (particle size 323.83 ± 2.42 μm) was thoroughly mixed with a specified volume of solvents within a Duran bottle. Subsequently, the bottle was submerged in an ultrasonic water bath operating at a frequency range of 42 - 45 kHz (set at level 9) and the extraction process was carried out under controlled parameters, including extraction time and temperature. After the marc and menstruum were separated by filtration through Whatman filter paper No. 1, each extracted solution was concentrated using a rotary evaporator setting at a pressure of 35 mbar and a temperature of 40 °C. In the next step, the concentrated extract solution was kept in deep freezer overnight, after which it undergoes complete drying using a freeze dryer. Before conducting additional analysis, all dried extracts were kept at ‑20 °C and protected from light exposure.

3.2.2. HPLC method validation

The analytical technique used to measure rhein in SA leaf extracts was subjected to validation to ensure compliance with the International Conference on Harmonization (ICH) Q2 (R1) guideline. This validation encompasses assessing specificity, linearity and range, accuracy, precision, as well as determining the limit of detection (LOD) and the limit of quantitation (LOQ) (121).

The method's specificity was validated through three replicates, including the extract solution, a standard solution of rhein, and a blank solution with mobile phase. To evaluate linearity, a calibration curve was constructed, encompassing concentrations ranging from 10 µg/mL to 30 µg/mL, with each concentration level analyzed in triplicate. The determination of Limit of Quantification (LOQ) and Limit of Detection (LOD) employed a statistical approach based on the linearity data, utilizing the line slope and regression coefficient deviation as key parameters.

According to the ICH guidelines, method validation should encompass a concentration range falling within 80% to 120% of the test concentration. Repeatability was evaluated by injecting 9 samples at rhein concentrations of 15 µg/mL, 20 µg/mL, and 25 µg/mL. These analyses were conducted by the same analyst, utilizing the same instrument, on the same day. On the other hand, intermediate precision was assessed through three repetitions of analyses using three concentrations within the working range from the rhein reference solution, performed on three different days. Precision assessment involved calculating the relative standard deviation (RSD) and Horwitz ratio (HorRat value), following the methodology outlined in a prior research report (122).

To ascertain accuracy, an analysis was conducted on a sample solution treated at three different concentration levels using a standard rhein solution: 75%, 100%, and 125%. Accuracy assessment involved preparing samples in triplicate for each of these recovery levels, with injections also carried out in triplicate. The percentage of recovery was calculated using equation (2).

Recovery (%) = (Recovered concentration/Injected concentration) $\times$ 100   (2)

where recovered concentration is the concentration of the spiked sample minus the concentration of the non-spiked sample and injected concentration represents the concentration of the standard rhein that was added to the sample.

The study assessed robustness by examining variations in the oven temperature of the column, which fluctuated by ± 2 ºC, and changes in the mobile phase flow rate, which varied by ± 0.1 mL. As part of this analysis, the method's robustness for quantifying rhein in samples was evaluated, utilizing standard rhein as a reference to gauge method reliability under various conditions.

In order to examine the chemical stability of the rhein standard solution and the extract sample solution during storage, both solutions were subjected to testing at room temperature for two time points: 0 h and 36 h. This evaluation included the verification of rhein's chromatographic profile and an analysis of peak areas to ensure the integrity and stability of the chemical components.

3.2.3. Quantitative determination of rhein content

The standard stock solution of rhein (0.1 mg/mL) was dissolved in ethanol. Working standard solutions ranging from 2 μg/mL to 30 μg/mL were prepared for the calibration curve using a serial dilution technique. Individually, the resulting extracts (0.02g) were dissolved in the extraction solvents and then adjusted to 10.00 mL with the same solvent. Prior to analysis, all solutions were filtered using a 0.45 µm nylon syringe filter. Quantitative analysis is performed using the Agilent 1100 HPLC-DAD. The separation was carried out at 30 °C using a Luna Omega Polar C18 column (5 μm, 100 Å, 4.6 mm x 250 mm). The mobile phase was composed of acetonitrile and 0.1 % v/v orthophosphoric acid in aqueous solution (65:35, v/v) with a flow rate of 1.00 mL/min via the isocratic elution system. The injection volume, total run time, and detection wavelength were set to 10 µL, 20 min, and 254 nm, respectively. All experiments were repeated three times.

3.2.4. Design of Experiments

3.2.4.1. Single factor analysis

Rare information is available regarding the experimental parameters and UAE conditions for SA plants. Therefore, single factor analysis was used in this work to

identify the experimental level and key variables influencing the UAE conditions. It was employed to investigate the individual factors of extraction conditions affecting rhein content in SA leaf extracts. The specific parameters and their corresponding experimental ranges are described in Table 3.

Table 3. Parameters and Experimental Ranges of Single Factor Analysis.

Parameters	Extraction Conditions				
Solvent Type	50% Ethanol		95% Ethanol		Distilled water
Ethanol concentration (%)	60	70	80	90	95
Extraction temperature (°C)	30	40	50	60	70
Extraction time (min)	5	10	15	20	25
Solvent- to -solid ratio (mL/g)	10:1	20:1	30:1	40:1	50:1

3.2.4.2. Box-Behnken Design (BBD)

To obtain the largest composition of rhein in SA leaf extracts, the extraction procedure was optimized. BBD was selected to provide information to identify the optimal level of each factor and interactions between factors. The significant effects of BBD can be evaluated by analysis of variance test (ANOVA) and the optimal responses can be investigated by regression model.

The independent variables and levels of experiments were illustrated in Table 4. Design-Expert 8.0.6 software (Stat-Ease, Inc., Minneapolis, USA) was utilized along with a BBD including 17 experiments for optimization study. The extract obtained from optimized conditions was evaluated by investigating its biological properties.

Table 4. Parameters and Experimental Ranges in BBD.

Independent variables	Symbol	Levels		
		-1	0	1
Temperature (°C)	X_1	40	50	60
Time (min)	X_2	10	15	20
Solvent-to-solid ratio (mL/g)	X_3	20	30	40

3.2.5. Antibacterial capacity assay

For assessing the antibacterial efficacy of the optimized extract against *S. aureus* ATCC 6538P, *E. coli* DMST 4212, and *P. aeruginosa* ATCC 9027, a broth dilution method recommended by the Clinical Laboratory Standards Institute (CLSI) was employed.

A loopful of microbial culture was introduced into Tryptic Soy Broth (TSB), and its turbidity was measured at a wavelength of 600 nm using a UV-Vis spectrophotometer. The absorbance from 0.08 to 0.1, indicating a microbial load of approximately 0.5 McFarland standard, equivalent to 10^7 to 10^8 CFU/mL.

The extract solution (10 mg/mL) was serially diluted with TSB to obtain concentrations ranging from 0.3125 mg/mL to 5 mg/mL. Bacterial culture was added to each concentration, and after 24-hour incubation at 37°C, the MIC, representing the lowest concentration inhibiting bacterial growth, was determined. Growth control (inoculated TSB), control (uninoculated TSB), and negative control (mixture of uninoculated TSB and extract) were also evaluated. Neomycin sulfate (in a range between 0.0078 mg/mL and 0.50 mg/mL) served as the positive control for assessing antibacterial activity using the same procedure.

Test solutions showing no growth were spread on sterile Tryptic Soy Agar (TSA) plates. After incubation at 37°C for 24 hours, the concentration at which no visible growth occurred was recorded as the MBC. Each experiment was performed in triplicate, with neomycin sulfate used as a positive control.

3.2.6. Anti-inflammatory activity

The evaluation of anti-inflammatory properties was conducted using an adapted version of the protein anti-denaturation assay outlined by Rick-Leonid et al (123). The heat-induced egg albumin denaturation bioassay is a well-established, validated, sensitive, rapid, and reliable *in vitro* method for assessing anti-inflammatory potential of natural substances. When albumin solution is subjected to heat, it transforms from a clear solution to turbid one indicating the denaturation of albumin. Compounds possessing anti-inflammatory properties have the capability to inhibit this turbidity in white albumin. They effectively prevent heat-treated albumin from denaturation. This

ability of the extract to inhibit denaturation in heat-treated egg albumin serves as the basis for this assay.

3.2.6.1. Preparation of phosphate-buffered saline (PBS pH 6.4)

To prepare one liter of solution, 1.79 g of sodium phosphate dibasic (Na_2HPO_4), 1.36 g of potassium phosphate monobasic (KH_2PO_4) and 7.2 g of sodium chloride were gradually added to a clean container containing distilled water. The solution was continuously stirred until these components were completely dissolved. Next, the pH of the solution was adjusted using hydrochloric acid (HCl) or sodium hydroxide (NaOH) as needed, while monitoring the pH with a pH meter to achieve a pH level of 6.4. Finally, the solution was made up to a total volume of one liter.

3.2.6.2. Preparation of test solutions

In a 10-mL volumetric flask, 0.1 g of the optimized extract was weighed and completely dissolved in DMSO. The stock solution was diluted to prepare different concentrations in a range of 0.5-4 mg/mL. As a positive control, diclofenac sodium solutions were also prepared at concentrations of 0.25-2.5 µg/mL using the same procedure.

3.2.6.3. Preparation of egg albumin solution

Albumin (2 mL) was extracted from a fresh egg through a filtration process, and it was subsequently combined with 28 mL of PBS with a pH of 6.4 until a thoroughly uniform mixture was achieved.

3.2.6.4. Protein anti-denaturation assay

For each concentration of the test solution (1.5 mL), it was combined with 2 mL of albumin solution. A comparable volume of PBS served as the negative control. These reaction mixtures were then incubated for 15 minutes at 37 °C. Following incubation, the mixtures were heated for 5 minutes at 70 °C and subsequently allowed to cool to room temperature. The absorbance of each solution was measured using a UV-vis spectrophotometer at 660 nm. The percentage of inhibition was computed using equation (3). A dose-response curve was utilized to determine the concentrations of the

sample solution required to achieve 50% inhibition, commonly known as the IC_{50} (half-maximal inhibitory concentration). Each sample underwent testing in triplicate.

$$\% \text{ Inhibition} = \frac{\text{Abs of control} - \text{Abs of sample}}{\text{Abs of control}} \times 100 \tag{3}$$

3.3. Fabrication and optimization of SA leaf extract loaded shellac electrospun nanofibers

3.3.1. Preliminary study for the selection of shellac type and solvent type

3.3.1.1. Preparation of shellac solutions

Different contents (32.5% w/w, 35% w/w, 37.5% w/w, 40% w/w, 42.5% w/w) of the bleached shellac and native shellac were prepared by dissolving in 95% v/v ethanol. Solutions were allowed to stir in room condition for overnight. After stirring, each shellac solution was diluted to achieve the desirable concentrations. For the selection of solvents, ethanol and isopropanol were used.

3.3.1.2. Assessment of solutions properties

Solution properties were evaluated by measurement of viscosity, surface tension and electrical conductivity.

- Viscosity

The viscosity of shellac solutions was examined using a viscometer. The measurement was conducted at 25 °C in triplicate with shear rate ranging from 600 to 1500 s^{-1}.

- Surface tension

The surface tension of shellac solutions was measured by image analysis of drop shape analyzer. Each shellac solution was first loaded in a syringe and then pumped out. The surface tension values were calculated by FTA32 software in triplicate.

- Conductivity

The conductivity was performed by immersing the probe into shellac solutions in room condition using electrical conductivity meter.

3.3.1.3. Fabrication of shellac electrospun fibers

The shellac solution was transferred into a 10 mL syringe fitted with a needle (18-G), inner diameter of 0.84 mm, at the nozzle and connected to a high-voltage power supply. The electrospinning process was conducted with a feed rate of 0.8 mL/h and an applied voltage of 18 kV. The distance between the tip and collector was maintained at 20 cm. The acquired fibers were deposited on the aluminum foil fitted with the rotating drum. Each run was performed under the control of temperature 23-25 °C and 40-60 % RH.

3.3.2. Design of Experiments

3.3.2.1. Fractional Factorial Design (FFD)

Based on the results of preliminary study, a FFD was used to examine the main effects and interaction of factors influencing the response factors of SA leaf extract loaded shellac fibers. Nineteen experiments including three center points were carried out in accordance with a design matrix. Parameters and the experimental range were presented in Table 5. Fiber diameter and bead-to-fiber ratio were used as dependent variables. Design expert software 8.0.6 version (Stat-Ease Inc., Minneapolis, MN, USA) was applied to generate the design matrix and conduct the data analysis.

Table 5. Parameters and Experimental Ranges in FFD.

Independent variables	Symbol	Level		
		Low (-1)	Center (0)	High (+1)
Shellac content (% w/w)	X_1	35	40	45
SA leaf extract content (% w/w)	X_2	1	2.5	4
Applied voltage (kV)	X_3	9	18	27
Feed rate (mL/h)	X_4	0.4	0.8	1.2
Needle tip diameter (mm)	X_5	0.61	0.84	1.06

3.3.2.2. Box-Behnken Design (BBD)

BBD was employed to examine the optimal electrospinning conditions after the critical parameters have been defined and their levels established. In this design, fiber diameter, bead-to-fiber ratio and entrapment efficiency were used as multiple response variables. The level and range of each parameter was illustrated in Table 6. Twenty-nine runs of experiments including five center points were performed.

Table 6. Parameters and Experimental Ranges in BBD.

Independent variables	Symbol	Level		
		Low (-1)	Center (0)	High (+1)
Shellac content (% w/w)	X_1	35	40	45
SA leaf extract content (% w/w)	X_2	1	2.5	4
Applied voltage (kV)	X_3	9	16.5	24
Feed rate (mL/h)	X_4	0.4	0.8	1.2

3.3.3. Preparation and assessment of shellac-SA leaf extract solutions

An accurate weight of optimized SA leaf extract was dissolved in 95% v/v ethanol using a sonicator to ensure full solubility of the components. Subsequently, various weights of bleached shellac were added to each solution and left to stir at room condition overnight using a magnetic stirrer. After stirring, each solution was adjusted with 95% v/v ethanol to achieve the desired concentrations. The properties of shellac-extract solution, such as viscosity, conductivity, and surface tension, were evaluated as described in section 3.3.1.2.

3.3.4. Fabrication of shellac electrospun fibers loaded with SA leaf extract

In the electrospinning process, individual solutions were transferred into a 10-mL syringe containing a needle at the nozzle, which was then connected to a high-voltage power supply. The resulting fibers were deposited onto aluminum foil mounted on a rotating drum. The distance between the needle tip and the collector remained constant at 20 cm for all samples. Each operation was performed under the control of temperature 23-25 °C and 40-60 % RH.

3.3.5. Entrapment efficiency of shellac electrospun fibers loaded with SA leaf extract

The quantity of extract encapsulated in nanofibers was examined through quantitative analysis of rhein content, serving as a specific marker for the electrospun fibers. The entrapment efficiency of SA leaf extract was calculated based on the calibration curve of standard rhein. Standard rhein solution was serially diluted in a range of 2 μg/mL to 30 μg/mL to construct the calibration curve. Each fiber sample (0.2 g) was immersed in 10 mL of 95% v/v ethanol until all materials were completely dissolved. The test solutions were filtered using 0.45 µm syringe filter. The rhein content was then analyzed using the developed method of HPLC-DAD. The separation was carried out with an isocratic elution system at column temperature 40 °C. The mobile phase consisted of acetonitrile and 0.1 % v/v aqueous orthophosphoric acid (55:45, v/v) with a flow rate of 0.6 mL/min. The injection volume, total run time, and detection wavelength were set to 10 μL, 40 min, and 254 nm, respectively. The entrapment efficiency (%) of the extract was calculated using the equation (4) (124).

$$\text{Entrapment efficiency (\%)} = \left(\frac{\text{Amount of rhein in the extract entrapped in the fibrous matrix}}{\text{Amount of rhein in the extract added to the polymer solution}} \right) \times 100 \qquad (4)$$

3.4. Characterization and evaluation of optimized nanofibers
3.4.1. Scanning Electron Microscope (SEM)

The analysis of fiber morphology, including fiber diameter and bead-to-fiber ratio was performed using a Scanning Electron Microscope (SEM). JMicro-Vision 1.2.7 software, Geneva, Switzerland, was used to analyze fiber diameters and bead-to-fiber ratio based on SEM pictures.

3.4.2. Fourier Transform Infrared (FTIR) spectroscopy

The chemical components and functional properties of SA leaf extract, bleached shellac, their physical mixtures, and fibers were studied using FTIR spectrometer. The pellets were prepared by mixing samples with KBr powder (1:3 ratio of sample and KBr), compacted into a pellet under hydraulic pressure, and then put in the sample

holder. The spectrum was recorded in wavenumbers ranging from 4000 to 400 cm^{-1} with a resolution of 4 cm^{-1}.

3.4.3. Powder X-ray Diffraction (PXRD)

The crystallinity of bleached shellac, SA leaf extract, their physical mixtures, and fibers was investigated by using a powder X-ray diffractometer. The analysis was performed with Cu Kα radiation (λ = 1.5406 Å) at 40 mV and 30 mA. The samples were scanned in the 2θ range of 5 ° to 40 ° at 4 °/min to monitor the crystalline or amorphous nature of all samples.

3.4.4. Differential Scanning Calorimetry (DSC)

A differential scanning calorimeter was applied to evaluate the thermal properties of bleached shellac, SA leaf extract, their physical mixtures, and fibers. Each sample was weighed between 2-5 mg in an aluminum pan. Subsequently, the aluminum pan was sealed with a cover under pressure. All samples were then heated at a rate of 10 °C/min in the range of 25 °C to 210 °C. An analysis was performed under nitrogen gas flow with a flow rate of 20 mL/min.

3.4.5. *In vitro* release study

In vitro release behaviors of extract from the fiber were examined using direct immersion method. The releasing medium with PBS pH 7.4 and pH 6.8 were used to study the release behaviors under different pH conditions. Surfactants are often added to dissolution mediums to enhance the solubility of drugs that do not dissolve well in water. They achieve this by reducing the medium's surface tension. When the concentration of surfactants surpasses a certain threshold, known as the critical micelle concentration (CMC), they can form micelles. These micelles can encapsulate poorly water-soluble drugs within their hydrophobic centres, aiding in their solubilization (125). In this research, tween 80 (1.5% w/v) was added to each medium in order to improve the solubility of fibers containing shellac and rhein-rich extract, which were known for their limited aqueous solubility. Rhein served as a marker compound employed for the release study of extract from the fibers. As a result, the determination of the released rhein content from the samples was carried out using HPLC-DAD.

For the purpose of comparing the release properties of the extract, six fiber samples were selected: Run 3 (446.89 nm) and Run 18 (426.59 nm) which had larger diameters, Run 19 (277.07 nm) and Run 25 (226.21 nm) which featured smaller diameters, along with two additional samples that represented the optimized fiber and extract. The test sample was kept in an incubator maintained at a constant temperature of 37 °C and agitated at 100 rpm while submerged in 10 mL of medium for dissolution up to 24 h. Samples were collected at various intervals: 10 min, 20 min, 30 min, 40 min, 50 min, 1 hour, 2 hours, 4 hours, 6 hours, 8 hours, 10 hours, 12 hours, and 24 hours. At each time point, 1 mL of the sample solution was withdrawn and immediately replenished with an equal volume of new medium to keep the volume constant. The determination of rhein release from all samples was accomplished by utilizing the reference curve of rhein for calibration.

3.4.6. Release kinetics

The examination of the release mechanism involved analysing the dissolution patterns of all samples by applying them to different kinetic models, such as zero order, first order, Higuchi, and Korsmeyer-Peppas, utilizing the DD Solver version 1 add-on for Excel. The optimal model was chosen according to several factors: the minimal Akaike Information Criterion (AIC), the maximal model selection criterion (MSC), and the greatest adjusted R-squared (Adj R^2) values.

3.4.7. Antimicrobial activity of optimized nanofibers

The time-kill kinetics assay is a microbiological method utilized to assess the effectiveness of a substance against microbial growth within a designated timeframe. In line with prior research, the antimicrobial effectiveness of optimized fibers against *S. aureus*, *E. coli*, and *P. aeruginosa* was evaluated over a period of time (126).

Bacterial culture was prepared by subculturing the target microbes from a well-isolated colony on a suitable agar plate into a new tube containing sterile growth medium, specifically TSB. The culture was incubated in the bacterial incubator at 37 °C until 18-24 h. After incubation, a UV-vis spectrophotometer at 600 nm was applied to assess the microbial culture to obtain an absorbance falling within the range of 0.08 to 0.1 which was correlated with a bacterial concentration of approximately 0.5

McFarland standard, correspondent to 10^7-10^8 CFU/mL. The MIC values obtained from the prior broth dilution assay outlined in section 3.2.5.2 were employed for each microbe. The bacterial suspension was mixed with TSB to obtain the concentration of 10^6 CFU/mL. Prior to the test, test samples underwent UV sterilization for 30 min, and subsequently, they were combined with bacterial medium to achieve the desired concentrations: 3.15 mg/mL for *S. aureus* and 6.25 mg/mL for *E. coli* and *P. aeruginosa*, representing 5 times the MIC of the extract. Reference and negative control samples consisted of extract and corresponding microbial culture, respectively. All samples were incubated in bacterial incubator at the temperature 37 ℃. At each predetermined time point, 100 µL of each sample was withdrawn and reduce the concentration to 10^5 CFU/mL. Subsequently, the diluted samples were spread onto a sterile agar plate. All agar plates were then kept in an incubator at 37 ℃ until 18-24 h to allow colony growth. Following that, the colonies present on agar plate were enumerated, and the results were documented. Survival rate of bacterial cells over time was calculated using equation (5). The percentage of living microbial count over time was plotted to create a time-kill curve.

$$\text{The percentage of viable bacterial cells} = (C_t \times 100)/C_0 \qquad (5)$$

C_0 denotes the microbial load in CFU/mL at the starting point, while C_t represents the microbial load in CFU/mL at each specified point.

3.4.8. Stability study

Accelerated stability tests were conducted according to the guidelines established by the ICH (127). This accelerated stability test was designed to evaluate the capacity of the fibers to retain rhein content under extreme conditions over a specified period.

A sufficient number of replicates of the optimized nanofibers were kept both in room temperature at 25 ℃ and in a humidity chamber controlled at 40 ℃ ± 2 ℃ and 75% ± 5% RH. At designated intervals, specifically at 0, 30, 60, and 90 days, representative samples were withdrawn from the chamber. The samples were subjected to an assessment for the quantitative determination of rhein content using HPLC-DAD.

The percentage of retained rhein in the optimized fibers and extract was determined using equation (6).

Retaining rhein content (%) = $(R/R_i) \times 100$ (6)

where, R represents the quantity of rhein content retaining in the sample at each sampling time point, and R_i denotes the initial rhein content at the starting time point of sampling.

Chapter 4

Results and Discussion

4.1. Optimization of extraction conditions and evaluation of rhein-rich extract

4.1.1. Introduction

Optimal extraction conditions play a pivotal role in achieving high productivity and superior extract quality of plant, encompassing essential natural plant compound and desired bioactive properties. A key focus in enhancing the efficacy of SA leaf extracts lies in maximizing the concentration of rhein, a crucial active component. Traditional extraction methods face limitations in terms of time, energy, and solvent utilization. In contrast, UAE serves as an alternative technique, efficiently production of numerous active compounds within a minimal duration, while reducing energy and solvent. Non-heat-based extraction processes like UAE are particularly advantageous in preserving the effectiveness of bioactive compounds. Numerous factors related to UAE, such as frequency, ultrasound power, temperature, duration, type of solvent, concentration of solvent, and the ratio of solvent to solid, can be adjusted to enhance optimization results (128-130).

Historically, methanol has been a commonly employed extraction solvent in preparing SA leaf extracts (43, 131, 132). However, the well-acknowledged toxicity of methanol raises concerns. Non-toxic solvents such as ethanol, water, or their combinations are gaining prominence as safer alternatives. These solvents are recognized for their safety in human consumption and are believed to be effective in extracting bioactive compounds from herbs (133-135).

HPLC is a powerful analytical technique widely used for analysing diverse compounds, including various phytochemical classes present in plant extracts. In comparison to other analytical methods for determining phytochemicals, HPLC is the preferred choice due to its versatility, compatibility with a range of compounds, and its ability to offer both quantitative and qualitative insights (136). HPLC offers exceptional sensitivity, enabling the accurate detection and quantification of active components in plant extracts, even at low concentrations. Additionally, its selectivity helps in distinguishing and separating closely related compounds, providing accurate results. Its ability to provide accurate concentration data is essential for assessing the potency of

herbal remedies or plant-based pharmaceuticals (137). Validating an HPLC method is crucial for establishing its reliability, accuracy, and robustness in analytical procedures, providing confidence in the results obtained during routine sample analysis. Method validation ensures the dependability and capability of the HPLC method to consistently deliver accurate and valid results.

In a previous study, the determination of rhein concentrations in *Cassia fistula* fruit pulp extracts utilized HPLC–UV/Vis detection. The analysis involved a reverse phase (RP) -C18 column, employing a mobile phase of methanol with 0.5% v/v aqueous acetic acid in a ratio of 60:40, and detection at 435 nm (138). Conversely, when assessing rhein in SA leaf extracts through HPLC–DAD, an RP-C18 column was employed along with a mobile phase comprising methanol with 2% v/v aqueous acetic acid in a ratio of 70:30, with detection at 254 nm (139). Notably, the use of DAD in this context proves advantageous over UV/Vis detection. DAD's capability to analyse peak purity enhances its superiority, particularly in the identification of co-eluting contaminants on HPLC chromatograms. This feature is crucial for ensuring analytical accuracy, mitigating the risk of misleading data, and serves as a valuable addition to standard quality control practices, especially in pharmaceutical and food analyses (140).

Employing a DOE to assess and optimize extraction processes offers the advantage of gathering highly valuable information with a reduced number of experiments, leading to cost efficiency, and enhanced desired outcomes. RSM emerges as a powerful statistical technique for constructing an empirical model that considers the most influential variables and effects (90, 141). Specifically, BBD, an RSM technique, has demonstrated efficacy in optimizing herbal extraction processes (142). Notably, BBD necessitates merely three levels per factor and a small quantity of experimental trials facilitating the determination of optimal conditions. This approach enhances the overall efficiency and practicality of the optimization process.

The primary objective of this part was to generate a SA leaf extract enriched with rhein, showcasing notable biological activities. Additionally, the study aimed to establish an HPLC–DAD method for the accurate determination of rhein quantity The research encompassed three key steps: (1) optimizing the conditions for extracting rhein from SA leaves employing the UAE technique; (2) development and validation of the

HPLC–DAD analytical technique for quantifying rhein in the extracts; and (3) evaluating the rhein content and assessing the bioactivities including microbial effectiveness and anti-inflammatory activity of the optimized extract. This comprehensive approach was not only to optimize the extraction process but also to establish a dependable method for quantifying the target compound. Simultaneously, the study aimed to explore the potential bioactive properties inherent in the resulting extract.

4.1.2. HPLC method development and validation

4.1.2.1. Screening of optimized HPLC conditions

The HPLC parameters, including mobile phase composition, column temperature, and flow rate, were systematically optimized, as detailed in Table 7 (143). Efficient separation of rhein, a bioactive marker, was successfully achieved through isocratic elution within a reasonable timeframe. The selection of a 254 nm wavelength was based on the absorption of UV light by the aromatic chromophore present in rhein (refer to Figure 1). Table 7 provides an overview of the exploration of various binary eluents for the mobile phase, encompassing different composition of organic solvents and weak acid solutions.

Table 7. Different Conditions of the HPLC System for Determination of Rhein.

Parameters	Chromatographic Conditions		
	I	II	III
Column	Luna Omega Polar C18 column (5 µm, 100 Å, 4.6 mm × 250 mm) (Phenomenex Inc., Torrance, CA, USA)		
Column temperature	25 °C	30 °C	30 °C
Flow rate	1 mL/min	0.8 mL/min	1 mL/min
Injection volume	10 µL	10 µL	10 µL
Detection wavelength	254 nm	254 nm	254 nm
Mobile phase	Methanol: 2% v/v aqueous acetic acid (70:30)	Acetonitrile: 0.5% v/v aqueous acetic acid (60:40)	Acetonitrile: 0.1% v/v aqueous phosphoric acid (65:35)
Run time	20 min	15 min	15 min
Resolution	10.79	0.88	6.80
Symmetry factor	0.85	1.20	0.85
Theoretical plate	17,520	3315	8968
Retention time (min)	16.403	9.482	6.315
Purity factor	238.174	893.232	996.654

The HPLC chromatograms of SA leaf extract operating different analytical settings are presented in Figures 22(a–c). After conducting several tests, it was found that, as shown in Table 7, an ideal ratio of 65:35 (acetonitrile: 0.1% v/v orthophosphoric acid) (condition III) produced enhanced peak separation and higher purity level. The optimization of the mobile phase not only addressed issues of peak broadening but also prevented tailing problems during the analysis.
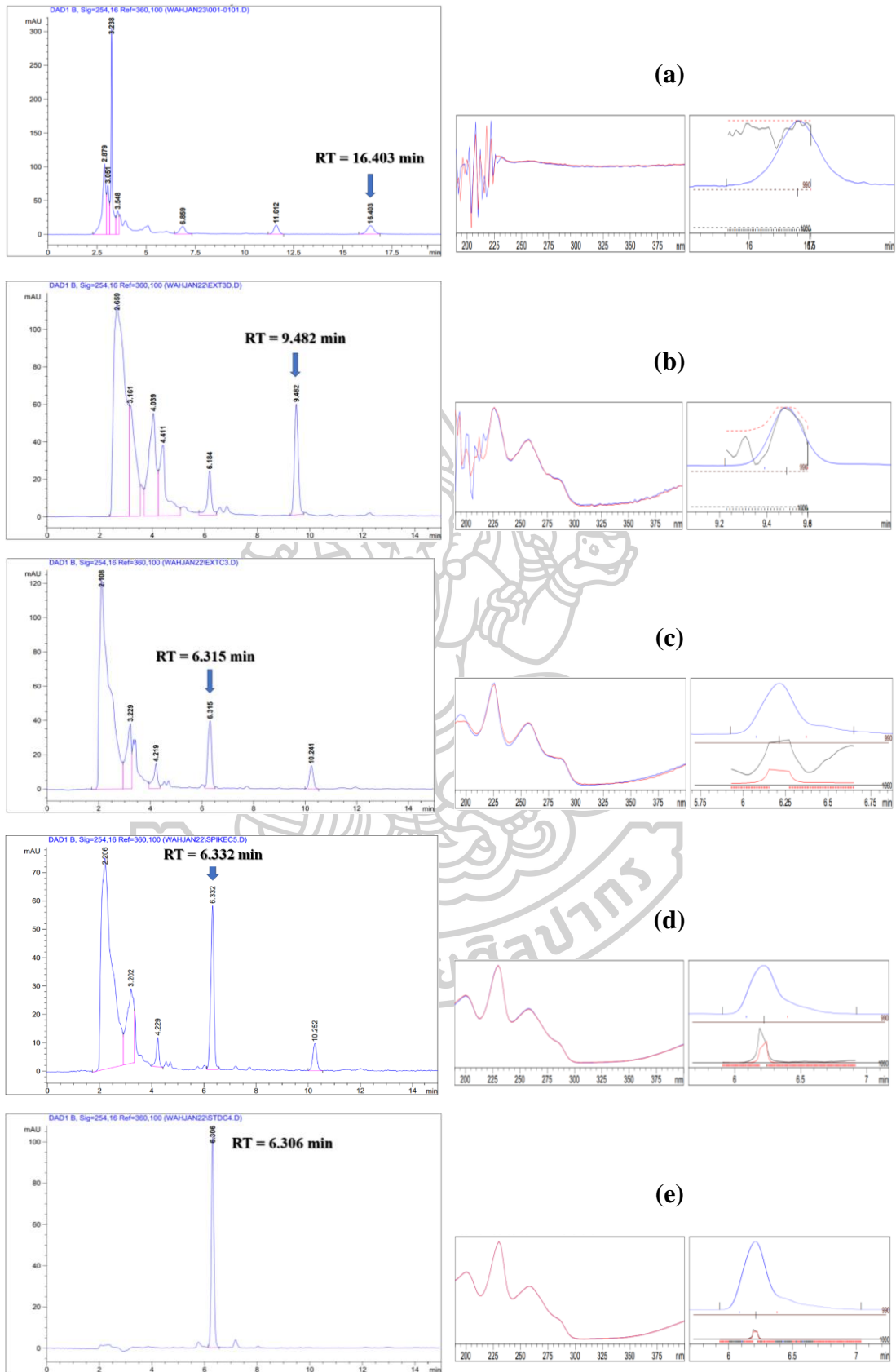
Figure 22. HPLC Chromatograms of SA Leaf Extract Analyzed using Condition I **(a)**, Condition II **(b)**, Condition III **(c)** Chromatograms of the Extract Spiked with Rhein Analyzed using Condition III **(d)** and Standard Rhein Analyzed using Condition III **(e)**

Subsequently, a reverse-phase Luna Omega Polar C18 column was validated using a mobile phase of 65:35 acetonitrile to 0.1% v/v aqueous orthophosphoric acid (condition III) with 1mL/min flow rate at the detection wavelength 254 nm. As shown in Figure 22(c), the rhein peak showed a retention time of 6.3 min under these optimized conditions. Chromatograms of SA leaf extract spiked with rhein (Figure 22(d)) and standard rhein (Figure 22(e)) were examined under condition C. When comparing these findings to previously reported rhein determination methods (129, 130), HPLC conditions in this study required less solvent and had a shorter run time. Notably, condition C, as shown in Table 7, had the greatest purity factor, with a value of 996.654.

4.1.2.2. Method validation
- System suitability

The chromatograms acquired under optimal conditions underwent a suitability assessment to gauge the peak area response's RSD, theoretical plates, and symmetry factor. The system suitability testing findings demonstrated a symmetry factor of 0.85, theoretical plates ranging from 22,453 to 22,787, and an RSD of the peak area response at 0.20% (143). These values align well with the specifications outlined in the USP 43-NF 38 regulations, which require symmetry factors within the range of 0.8 to 1.5, theoretical plates exceeding 2000, and a peak area response RSD of no more than 2% (144).

- Specificity

The system's capacity to identify rhein from other constituents of extract while maintaining the same retention time effectively confirmed its specificity (Figure 22(c, d)). To evaluate the purity of the rhein peak, the chromatographic profiles of the original extract and the extract fortified with standard rhein were consulted. In this assessment, the overlapping UV spectra observed at the onset of the peak, middle, and finish were compared. Table 8 shows that both the purity factor and the resolution met the

acceptable parameters, with the purity factor falling between 996 and 999 and the resolution between 7.34 and 7.87. These findings highlight the specificity of the approach by confirming the lack of disturbance affecting the peak corresponding to rhein.

- Linearity

In accordance with the guidelines provided by the Association of Official Agricultural Chemists (AOAC) (145), the method developed exhibited linear behaviour within a concentration range spanning from 10 µg/mL to 30 µg/mL. The coefficient of determination (R^2) for the standard rhein was determined to be 0.9990, as indicated in Table 8 (143), and this consistently high value was observed across all replicates (n = 3). The method's linearity was confirmed using the regression equation y = 22.4138x + 13.2070.

Table 8. Validation Summary of Analytical Method (143).

Validation Parameters	Acceptance Criteria *	Results
Specificity	Resolution ≥ 2	Resolution = 7.34–7.87
	Purity factor ≥ 950	Purity factor = 996–999
Linearity and range	$R^2 \geq 0.99$	$R^2 = 0.9990$
Accuracy	Recovery = 80–110%	Recovery = 91.69–105.89%
Repeatability	RSD ≤ 7.3%	RSD = 5.0–6.3%
(Intra-day precision)	HorRat value = 0.5–2.0	HorRat value = 0.8–0.9
Intermediate precision	RSD ≤ 7.3%	RSD = 6.0–7.2%
(Inter-day precision)	HorRat value = 0.5–2.0	HorRat value = 0.6–0.7
Robustness	Robust	Robust
Limit of detection	-	2.44 µg/mL
Limit of quantitation	-	7.39 µg/mL

*AOAC, 2016 (145)

- Accuracy

A pre-analysed sample solution with a defined concentration was mixed with standard rhein solutions at pre-determined concentrations (15, 20, and 25 µg/mL) to evaluate accuracy. As presented in Table 8, the developed method demonstrated accuracy, as evidenced by the high recovery values ranging from 91.69% to 105.89%. Notably, all recovery values were well within the acceptance criterion of 80% to 110%, affirming the accuracy of the method (145).

- Precision

The RSD values for repeatability (intra-day) and intermediate precision (inter-day) were determined to be within the range of 5.0% to 6.3% and 6.0% to 7.2%, respectively, as indicated in Table 8. The HorRat values were observed to be 0.8 to 0.9 for repeatability and 0.6 to 0.7 for intermediate precision. According to the acceptance criteria outlined in (145), the % RSD values and HorRat values should be ≤7.3% and 0.5–2.0, respectively. The obtained results, falling within these specified limits, confirm that the method is reasonably accurate in terms of repeatability and intermediate precision.

- LOD and LOQ

To estimate LOD and LOQ, signal-to-noise ratios were employed, calculated as 3.3 σ/S and 10 σ/S, respectively. Here, σ represents the standard deviation of the response, and S is the slope derived from the calibration curve. As per the results presented in Table 8, the LOD was determined to be 2.44 µg/mL, while the LOQ was found to be 7.39 µg/mL.

- Robustness

Certain factors were examined in the context of the robustness study, including the column temperature and the flow rate of the eluent. Each condition was tested with sample preparation in triplicate, with analyses conducted in duplicate. Examining the variations in column temperature (±2ºC) revealed no notable influence on the analysis of rhein. This indicates that temperature fluctuations within the specified range had negligible impact on the analytical outcomes. Similarly, the evaluation of mobile phase

flow rate variations (± 0.1 mL) demonstrated no significant impact on the analytical results. The durability of column oven temperature and flow rate was demonstrated by RSD values for rhein concentrations that were below 1.5% and 2.0%, respectively. A p-value larger than 0.05 from an ANOVA with 95% confidence intervals indicates that there are no significant differences in the dataset. This validates the robustness of the method in the analyzed conditions. Furthermore, values within the acceptability requirements were shown in the robustness assessment in relation to the rhein peak. In particular, the theoretical plates ranged from 8965 to 9062, the symmetry factor from 0.84 to 0.91, and the resolution values from 6.70 to 7.00. These results highlight the method's robustness without compromising the effectiveness of separating rhein from other peaks.

- Chemical stability

RSD values of 2.3 and 2.4 for the concentration of rhein were found in the SA leaf extract samples examined at 0 and 36 h, respectively. According to stability data, samples remained stable for up to 36 h at room temperature, with acceptable deviations.

4.1.3. Quantitative determination of rhein

The rhein content within all extracts was assessed utilizing the validated HPLC-DAD method. Utilizing the linear equation derived from the rhein standard curve, the quantity of rhein was determined. According to USP 43-NF 38 (144) and AOAC guidelines (145), the method validation results demonstrated the efficacy of the developed procedure for analyzing rhein in SA leaf extract. Additionally, compared to the earlier research (139), the developed and verified method showed a number of advantages, such as a shorter analysis time and less volume of organic solvent consumed. These improvements contribute to the method's practicality and efficiency in rhein analysis, making it a valuable tool in pharmaceutical and analytical applications.

4.1.4. Design of Experiments

4.1.4.1. Single factor analysis

Following a comprehensive analysis of prior research and other relevant studies on anthraquinone extraction, the selection of input variables and the scope of experimental conditions for this study was determined.

In an earlier study, it was observed that a 95% v/v ethanol extract yielded higher amounts of rhein in comparison to a 50% v/v ethanol extract and an aqueous extract (133). Consequently, ethanol was chosen as the solvent, with concentrations ranging from 60% v/v to 95% v/v.

According to prior research (146), the optimal anthraquinones yield was attained at 67 °C for a duration of 33 min. Beyond this temperature, extraction yields gradually decreased. Interestingly, extraction durations exceeding 33 min did not have a noticeable effect on the extraction yield. The authors discussed that prolonging the extraction time could enhance the degradation of anthraquinones, leading to a decreased result. However, this study revealed a contrasting trend, as the amount of rhein declined following a duration of 25 min. As a result, an experimental temperature and time were chosen within a temperature span from 30 °C to 70 °C and a time frame ranging from 5 min to 25 min, respectively.

Wu et al. (147) investigated that the anthraquinones yields exhibited a notable increase with an increase in the solid-liquid ratio ranged between 20:1 mL/g to 26:1 mL/g, while the extraction temperature varied from 70°C to 80°C. This increase was particularly prominent at elevated temperatures and a moderate solvent-to-solid ratio. Consequently, the experimental range for this factor in our study was set from 10:1 mL/g to 50:1 mL/g.

(a)

(b)

(c)

(d)

(e)
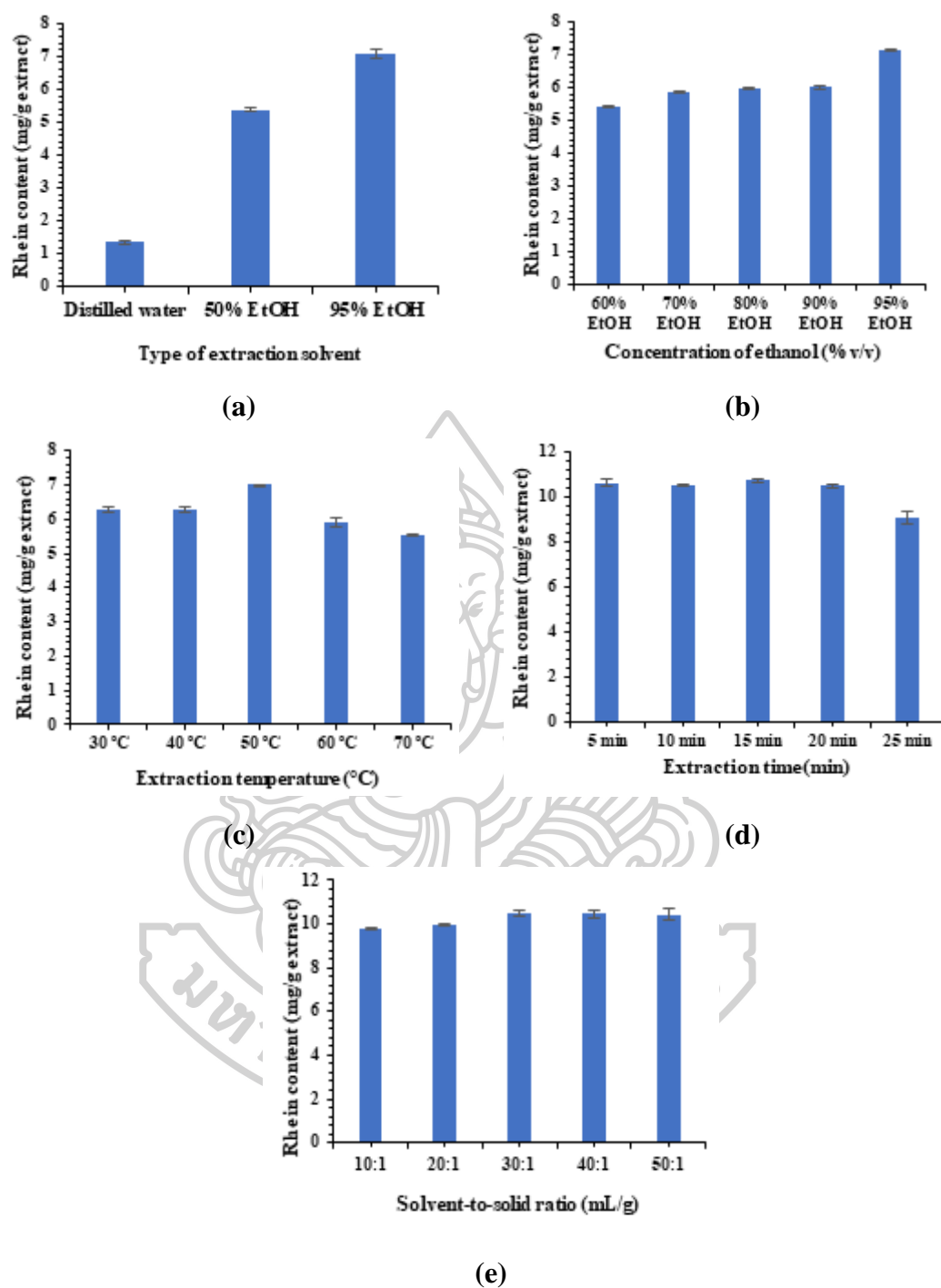
Figure 23. Factors Affecting on the Rhein Content in the Extracts, Solvent type **(a)**, Solvent concentration **(b)**, Extraction Temperature **(c)**, Extraction Time **(d),** and Solvent-to-Solid Ratio **(e)** (143).

Figure 23 (143) demonstrated the effect of individual factor affecting rhein content. The impact of various extraction solvents (distilled water, 50% v/v ethanol, and 95% v/v ethanol) on the rhein content in the extracts is depicted in Figure 23(a), indicating that 95% v/v ethanol emerged as the most efficient solvent.

Figure 23(b) illustrates a rise in rhein content corresponding to higher ethanol concentrations, suggesting that rhein exhibits increased solubility in 95% v/v ethanol. These results are consistent with prior studies indicating rhein's semi-lipophilic nature, with enhanced solubility in organic solvents (19). Moreover, it is recognized as safe for human consumption. Hence, 95% v/v ethanol was chosen as the solvent for extraction.

Figure 23(c) depicts the impact of temperature on rhein content, with an initial increase from 30 °C to 50 °C followed by a gradual decrease. Elevated temperature could facilitate rhein extraction from SA leaf powders by reducing solvent viscosity, enhancing the diffusion coefficient, and improving the dissolvability of the active ingredient (148). Consequently, the temperature applied for extraction was defined at 50 °C.

Figure 23(d) demonstrates the impact of extraction time on the rhein content of extracts. It was noted that the rhein content exhibited a gradual increase as the extraction time extended from 5 min to 15 min, beyond which it began to decrease gradually. Thus, the duration of extraction was determined to be optimal at 15 min.

As the solvent-to-solid ratio rises, Figure 23(e) shows that the rhein concentration progressively rises and stabilizes at ratios more than 30:1 mL/g. As a result, 30:1 mL/g was determined to be the ideal solvent-to-solid ratio for further optimization.

4.1.4.2. Box-Behnken Design (BBD)

- Optimization of the extraction conditions

The outcomes of a single-factor experiment were used as the basic steps for investigation of ideal extraction conditions through the BBD, focusing on the independent factors; extraction temperature (X_1), extraction time (X_2), and solvent-to-solid ratio (X_3). The matrix of design and output variable are presented in Table 9 (143). Through multivariable regression analysis, Equation (7) was developed to express the correlation of the rhein content and the input factors.

Rhein content = 9.64 + 0. 31 (X_1) + 0.38 (X_2) − 0.69 (X_3) + 0.72 (X_1X_2)

$\qquad$ + 0.46 (X_1X_3) − 0.35 (X_2X_3) − 0.55 $(X_2{}^2)$ − 0.94 $(X_3{}^2)$ $\qquad$ (7)

Table 9. Matrix Design and Experimental Results of BBD (143).

Run	Independent Variables			Response (n=3)
	X_1 Temperature (°C)	X_2 Extraction time (min)	X_3 Solvent-to-solid ratio (mL/g)	R Rhein content (mg/g extract) (Mean ± SD)
1	0 (50.00)	0 (15.00)	0 (30:1)	9.49 ± 0.05
2	0 (50.00)	-1 (10.00)	-1 (20:1)	8.12 ± 0.02
3	+1 (60.00)	-1 (10.00)	0 (30:1)	8.36 ± 0.12
4	0 (50.00)	0 (15.00)	0 (30:1)	9.45 ± 0.06
5	+1 (60.00)	+1 (20.00)	0 (30:1)	10.42 ± 0.10
6	-1 (40.00)	+1 (20.00)	0 (30:1)	8.50 ± 0.10
7	-1 (40.00)	-1 (10.00)	0 (30:1)	9.31 ± 0.11
8	-1 (40.00)	0 (15.00)	+1 (40:1)	7.35 ± 0.05
9	+1 (60.00)	0 (15.00)	+1 (40:1)	9.02 ± 0.14
10	0 (50.00)	+1 (20.00)	+1 (40:1)	7.39 ± 0.03
11	0 (50.00)	-1 (10.00)	+1 (40:1)	7.19 ± 0.07
12	+1 (60.00)	0 (15.00)	-1 (20:1)	9.24 ± 0.07
13	0 (50.00)	0 (15.00)	0 (30:1)	10.15 ± 0.19
14	-1 (40.00)	0 (15.00)	-1 (20:1)	9.39 ± 0.06
15	0 (50.00)	0 (15.00)	0 (30:1)	9.35 ± 0.04
16	0 (50.00)	+1 (20.00)	-1 (20:1)	9.71 ± 0.10
17	0 (50.00)	0 (15.00)	0 (30:1)	9.58 ± 0.05
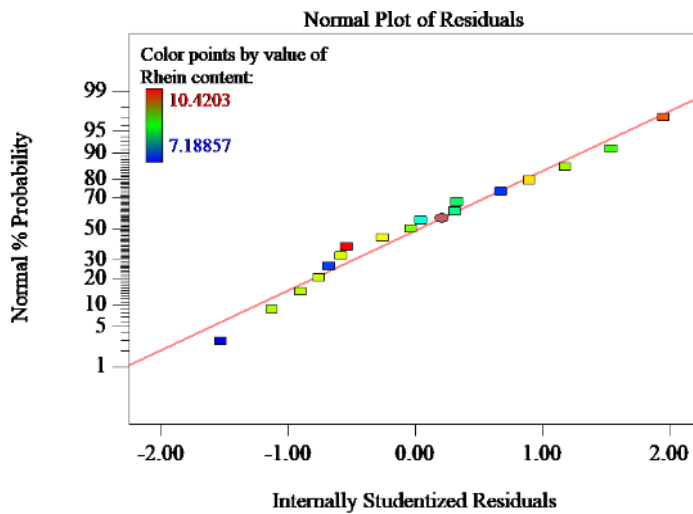
Figure 24. Plot Illustrating the Normal Probability of Internally Studentized Residuals for Rhein Content.

The examination of the residuals plot for normality is crucial in assessing the appropriateness of the selected model for the experimental dataset. In this regard, the plot illustrates that the data points adhere to a normal distribution, as indicated by the linear pattern observed (Figure 24). This observation implies that the residuals, signifying the variances between the observed and predicted values derived from the model, are distributed in a manner consistent with a normal distribution. This consistency confirms the reliability and validity of applying the model to the experimental data.

Table 10 (143) presents the analysis of variance (ANOVA) for the quadratic response surface model. The results revealed that the mathematical model was highly significant, as indicated by a p-value less than 0.01. The model's coefficient of determination (R^2) was 0.9575, suggesting a strong fit to the data. Furthermore, the lack of fit was not statistically significant, with a p-value greater than 0.05, affirming that the quadratic regression model adequately predicts the data trends.

Table 10. ANOVA for Response Surface Reduced Quadratic Model (143).

Source	Sum of Squares	df	Mean square	F value	P value Prob>F
Model	14.39	8	1.80	22.51	0.0001*
X_1—Extraction temperature	0.77	1	0.77	9.68	0.0144**
X_2—Extraction time	1.16	1	1.16	14.50	0.0052*
X_3—Solvent-to-solid ratio	3.78	1	3.78	47.36	0.0001*
X_1X_2	2.06	1	2.06	25.83	0.0010*
X_1X_3	0.83	1	0.83	10.39	0.0122**
X_2X_3	0.49	1	0.49	6.08	0.0389**
X_2^2	1.27	1	1.27	15.84	0.0041*
X_3^2	3.77	1	3.77	47.16	0.0001*
Residual	0.64	8	0.080		
Lack of fit	0.24	4	0.060	0.60	0.6854***
Pure Error	0.40	4	0.10		
Cor Total	15.03	16			
$R^2 = 0.9575$		Adj $R^2 = 0.9149$		Pred $R^2 = 0.8078$	

Significant * $p < 0.01$; ** $0.01 < p < 0.05$; not significant ***.

The "Pred R-Squared (Pred R^2)" value of 0.8078 and the Adj R^2 value of 0.9149 were closely related, indicating the model's reliability for prediction purposes. Additionally, the individual effects of temperature, duration, and solvent-to-solid ratio were found to be statistically significant at a p-value more than 0.05. The model analysis reveals that there are significant interconnections among all factors, indicating the combined effects of extraction temperature, time, and solvent-to-solid ratio on the rhein content. Additionally, the quadratic factors of extraction time and solvent-to-solid ratio were found to be statistically significant. This implies that the relationship between each of these variables and the rhein content is not purely linear, and the quadratic terms play a meaningful role in influencing the overall outcome. These findings highlight the importance of considering both interactions and quadratic effects when understanding and optimizing the extraction conditions for rhein content.
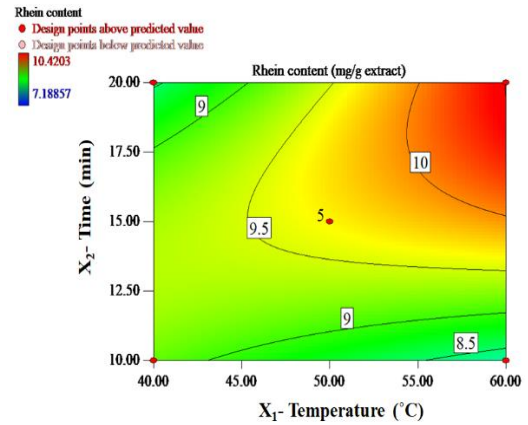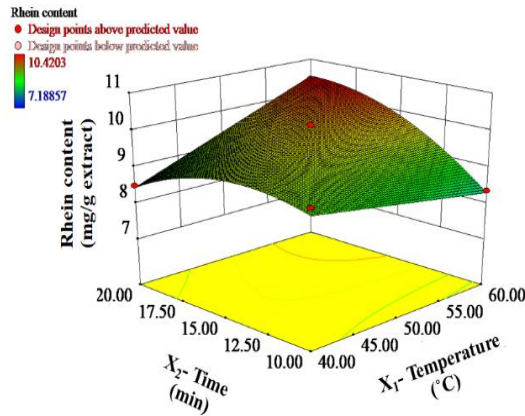
Actual factor - X₃ – Solvent-to-solid ratio = 30:1 mL/g

(a)   **(b)**

Actual factor - X₂ – Extraction time = 15 min

(c)   **(d)**

Actual factor - X₁ – Extraction temperature = 50 ˚C

(e)   **(f)**

Figure 25. Combination of Factors Affecting Rhein Content Illustrated by 3D surface Plots and Contour plots: Temperatures and Times **(a, b),** Temperatures and Solvent-to-Solid Ratios **(c, d)**, and Extraction Times and Solvent-to-Solid Ratios **(e, f)** (143).

The quadratic polynomial equation, designed to express the relationships between input factors and their impact on rhein amount, was utilized to generate 3D response surface plots and contour plots (Figure 25) (143). The colour gradient, transitioning from blue to red in various shades, signifies increasing rhein content.

Figures 25(a) and 25(b) depict the impacts of extraction temperature and duration on rhein content, while maintaining a constant solvent-to-solid ratio. The rhein content exhibited an increase with higher values for both factors, while short period of extraction and reduced temperatures leading to a minimal amount. The connection between extraction temperature and time had a pivotal impact in influencing extraction of rhein from SA leaves. This observation aligns with prior studies focusing on rhein optimization using UAE from *Cassia fistula* pod pulp (91).

As shown in Figure 25(c) and 25(d), the maximum rhein content was achieved with a moderate solvent-to-solid ratio, elevated temperature, and a constant extraction time. This outcome could be attributed to the higher solubility of rhein at high temperatures. Conversely, a lower temperature combined with increased solvent-to-solid ratio resulted in a reduced rhein content. Notably, the solvent-to-solid ratio positively influenced the extraction process, as indicated by the higher phytochemical yield with increased ratios. This aligns with the principle of mass transfer, where the difference in concentration between the solid and the liquid's overall volume, serves as the driving force. An increased solvent-to-solid ratio enhances this concentration gradient, facilitating the extraction of more phytochemicals (149). In contrast to the findings discussed earlier, prior research investigated that elevating the temperature and reducing the solvent-to-solid ratio led to higher concentrations of phytochemicals. This observation aligns with the common understanding that when less solvent is employed, the phytochemicals become more concentrated (150).

Figures 25(e) and 25(f) depict the impact of the interconnection between extraction time and solvent-to-solid ratio on rhein content. The maximum rhein content was observed with an extended extraction time and a mild to medium levels of solvent-

to-solid ratio. Higher solvent-to-solid ratios were expected to facilitate swift exchange of mass between the solvent and plant materials. However, in this study, an elevated solvent-to-solid ratio led to a decrease in the amount of rhein, aligning with findings from prior research (147, 151). It's worth noting that variations in experimental conditions, methodologies, and the nature of the specific plant materials can lead to different outcomes in extraction studies.

- Verification of optimized conditions

As indicated in Table 11 (143), the optimum extraction conditions were identified as 59.52 °C, 18.4 min, and a solvent-to-solid ratio of 25.48:1 (mL/g). The software anticipates a predicted value of 10.44 mg/g extract using these specified conditions. Three additional experiments were conducted using the optimal conditions to verify the model, resulting in a mean value of 10.36 ± 0.27 mg/g extract. Notably, the actual value fell within the 95% confidence interval of the predicted value. This alignment between the predicted and observed values suggests that the model generated by the software for the optimal conditions is reliable and can be determined to possess a high level of precision.

Table 11. Predicted and Observed Values for Confirmation of Optimized Conditions (143).

	Temperature (ºC)	Time (min)	Solvent-to-solid ratio (mL/g)	Rhein content (mg/g extract)
Optimal conditions	59.52	18.4	25.48	10.44 (Predicted value)
Experimental conditions	60	18	25	10.36 ± 0.27 (Actual value)

4.1.5. Antimicrobial activity of rhein-rich (optimized) extract

The antimicrobial efficacy of the optimized extract was assessed using strains of *E. coli*, *S. aureus*, and *P. aeruginosa*. Persistent wounds, especially in individuals with diabetes mellitus who have unmanaged blood sugar levels, often harbour bacteria that can cause infections. The occurrence of bacteria such as *S. aureus* or anaerobic organisms in these wounds poses a significant challenge to treatment (152). To ensure the accuracy and reliability of the experimental results, neomycin sulfate served as a positive control. The rhein-rich extract exhibited antibacterial properties against all three strains, as detailed in Table 12 (143).

As per the investigation conducted by Doughari and Okafor (153), the methanolic extract of SA roots and leaves demonstrated MICs of 12 mg/mL, 15 mg/mL, and 20 mg/mL against *S. aureus*, *E. coli*, and *P. aeruginosa*, respectively. Additionally, Ehiowemwenguan et al. (154) reported that the methanolic extract from the leaves of SA exhibited MICs of 6 mg/mL, 8 mg/mL, and 10 mg/mL against *S. aureus*, *E. coli*, and *P. aeruginosa*, respectively. Pham and colleagues showed that using bioassay-guided fractionation techniques, they were able to pinpoint antimicrobial substances within the SA leaf extract. Remarkably, they discovered a significant presence of the antimicrobial agent rhein in the SA leaf extracts, which were soluble in methanol and ethyl acetate (132). The current research demonstrated that the optimized extract displayed antimicrobial activity against microorganisms of both Gram-positive (*S. aureus*) and Gram-negative (*E. coli and P. aeruginosa*) categories. Consistent with prior study (155), the optimized SA leaf extract shows promise as a possible candidate for antibacterial agents in the management of wounds.

The analysis of SA leaf extracts' antibacterial activity observed that the rhein-rich extract displayed exceptional effectiveness against *S. aureus*. The antimicrobial effectiveness, as measured by the MIC of SA leaf extracts, exhibited a positive correlation with the quantity of rhein (143). This suggests that rhein plays a crucial role as an antimicrobial component in SA leaf extract, particularly in inhibiting the growth of *S. aureus*. Consistent with earlier research (23), the hydroxyanthraquinone nucleus of rhein, an anthraquinone derivative, has been proposed to be responsible for its antibacterial activity. This core structure features two ketone functionalities located at the C9 and C10 positions, alongside two hydroxyl groups at the C1 and C8 positions.

Moreover, a polar carboxylic group substituent at the C3 position (Figure 1) in rhein may increase its antibacterial effectiveness. This study underscores the beneficial impact of rhein content in SA leaf extracts on antibacterial activity against *S. aureus*.

Table 12. MIC and MBC Values of Rhein-Rich (Optimized) Extract (143).

| Tested microorganisms | Rhein-rich Extract | | Neomycin Sulfate | |
	MIC (mg/mL)	MBC (mg/mL)	MIC (mg/mL)	MBC (mg/mL)
S. aureus ATCC 6538P	0.63	5.00	0.063	0.125
E. coli DMST 4212	1.25	2.50	0.016	0.031
P. aeruginosa ATCC 9027	1.25	5.00	0.031	0.250

4.1.6. Anti-inflammatory activity of rhein-rich (optimized) extract

In vitro assessment was conducted to evaluate the anti-inflammatory impact of the optimized extract against egg protein denaturation. Various concentrations of the extract were incubated with albumin solution under controlled experimental conditions, and absorbance levels were measured. Figure 26 illustrates that the optimized extract exhibited concentration-dependent suppression of protein denaturation. The reference drug, diclofenac sodium, demonstrated a comparable concentration-dependent inhibition, surpassing the efficacy observed in the test extract.

In comparison with other SA leaf extracts, including de-chlorophyll extracts treated with different decolorizing agents, the optimized extract revealed the highest concentrations of rhein and superior effects on albumin denaturation (143). Consequently, the anti-inflammatory effects observed in the optimized extract are likely attributed to the presence of rhein. These results are consistent with earlier investigations (156, 157) that have demonstrated the anti-inflammatory properties of rhein.

In response to harmful stimuli like pathogens and irritants, inflammation serves as the body's protective response. This complex process involves increased vascular permeability, membrane modifications, and heightened protein denaturation (158). Assessing the impact of an optimized extract on protein denaturation, as part of the inflammatory process, could provide insights into its potential as an anti-inflammatory

agent. These findings could be valuable for studies related to anti-inflammatory agents or substances.
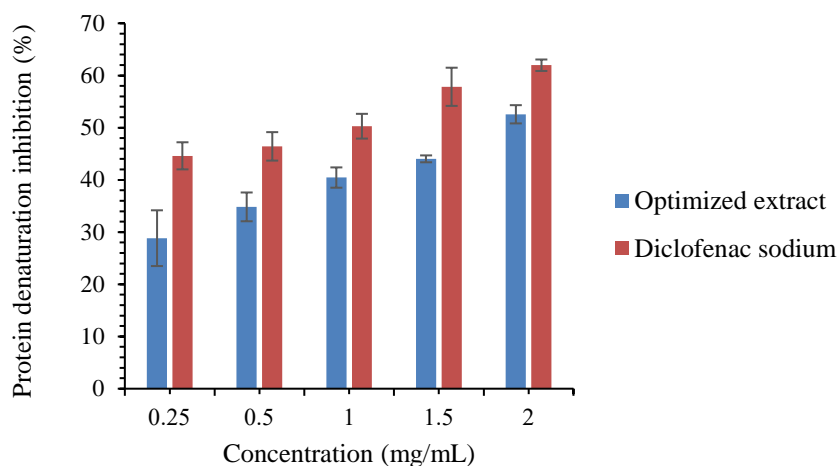
Figure 26. *In Vitro* Anti-inflammatory Activity (Protein Denaturation Method) of the Rhein-Rich (Optimized) Extract and Diclofenac Sodium (n=3).

4.1.7. Conclusion

The effectiveness of extracting bioactive compounds from natural sources relies heavily on the chosen extraction methods and parameters. To obtain a bioactive high rhein content from SA leaves, the efficiency of UAE was enhanced by investigating key parameters: solvent concentration and type, temperature, duration, and solvent-to-solid ratio. HPLC-DAD method was developed for determination of rhein content and also successfully validated. RSM was applied for optimizing the process parameters using BBD. The optimal conditions included using 95% v/v ethanol as the extraction solvent at 59.52 °C for 18.4 min, with a solvent-to-solid ratio of 25.48:1 (mL/g), resulting in a predicted value of rhein content 10.44 mg/g extract. The actual rhein content (10.36 ± 0.27 mg/g extract) closely correlated with the predicted value within an acceptable range. The biological activities of optimized rhein-rich extract, including anti-inflammatory and antimicrobial properties, were evaluated through protein denaturation assay and broth dilution method. The extract demonstrated anti-inflammatory effects as indicated by the percent inhibition of albumin denaturation. Additionally, the optimized extract exhibited antimicrobial effectiveness against *S. aureus*, *P. aeruginosa*, and *E. coli*.

4.2. Fabrication and optimization of SA leaf extract loaded shellac electrospun nanofibers

4.2.1. Introduction

S. alata (family – Fabaceae) and is indigenous to the Amazon Rainforest. While it is prominently found in Asia and Africa, it holds particular significance in the Philippines, Thailand, and Indonesia, where it is cultivated for medicinal purposes. Notably, the leaves are favoured in traditional medicine due to their higher concentration of active constituents compared to other parts (1). The therapeutic importance of this plant is underscored by its widespread use in folk medicine to address ailments such as constipation, stomach pain, ringworm, and various skin disorders (41).

SA leaf extract is abundant in various bioactive compounds (15). A study by Ahmed, and Shohael highlighted the presence of antifungal anthraquinones in SA leaves, specifically aloe-emodin, chrysophanol, emodin, and rhein (159). Rhein was identified as a key component accountable for the reported antimicrobial properties of SA leaves, as noted by Khare in Indian Medicinal Plants (42). The significant presence of rhein in SA leaf extract has been linked to its antioxidant, anti-inflammatory, and antibacterial attributes (143). These studies suggest that the extract possesses significant biological potential, positioning it as a favourable candidate for the formulation of pharmaceutical products. The presence of diverse bioactive compounds showcases the medicinal value of SA leaf extract and supports its traditional use in addressing various health concerns.

Shellac, a naturally occurring polymer derived from the resinous secretions of insects (*Laccifer lacca*), is distinguished by its makeup of polyesters and individual esters derived from aleuritic acid and terpenic acids. These terpenic acids may include jalaric acid or laccijalaric acid (104). This semi-crystalline polymer demonstrates limited crystalline structure and typically melts at temperatures ranging from 50°C to 75°C (105). With its versatile qualities, shellac can be used in various fields, notably in food and pharmaceutical technologies. Additionally, researchers have developed shellac-based delivery systems with sizes ranging from nanometers to micrometers, such as nanofibers, microparticles, hydrogels, and more (107). This versatility in form allows for diverse applications and innovations in drug delivery and other related fields.

Commercial shellac is categorized into three types based on the production methods employed: hand-made, machine-made, and bleached. The process of obtaining bleached shellac involves specific steps aimed at enhancing its properties. To create bleached shellac, seedlac undergoes dissolution in an alkaline water-based solution before being subjected to treatment with sodium hypochlorite. The bleached shellac is subsequently precipitated by adding sulfuric acid. After precipitation, the resulting mixture is filtered to remove wax, resulting in dewaxed or bleached shellac (160).

While numerous studies have explored the applications of bleached shellac in various fields such as drug enteric coating (30), as an edible surface coating for fruits and vegetables (31), formation of microparticle in antibacterial oils (161), and formation of gel for treating periodontitis (162), there is a lack of scientific investigation into the potential applications and properties of electrospun nanofibers derived from bleached shellac. Such investigations could contribute to expanding the range of applications involving bleached shellac in nanotechnology and related fields.

Nanotechnology-based drug delivery systems use nanosized substances to precisely target and controlled release of drug, offering advantages in the treatment of chronic disorders by enabling localized and precision-targeted drug delivery. The clinical applications of discovering nanomaterials and utilizing them to enhance natural products are complicated and challenging to comprehend (163).

Regarding drug delivery and nanotechnology based on natural products, several biopolymeric materials play a crucial role, including shellac (111), chitosan (164), xanthan gum (164), and cellulose (165). These biopolymers contribute to the development of innovative drug delivery systems with enhanced properties. The aim is to identify and harness their pharmacological potential, with the goal of developing active ingredients that exhibit fewer side effects and greater safety compared to existing synthetic compounds (166).

Nanofibers, characterized by less than 1000 nm diameter, find extensive applications in delivery of drug, cosmeceuticals, and wound dressing due to their several advantages. These benefits encompass good stability, precise delivery of drug to the target site, low toxicity, superior ability of drug encapsulation, remarkable mechanical characteristics, and appropriateness for temperature-sensitive compounds (167). The production of nanofibers involves techniques such as electrospinning, which

includes variations like multi-jet electrospinning, coaxial electrospinning, and emulsion electrospinning, as well as interfacial polymerization, phase separation, and self-assembly (168). Among these methods, electrospinning stands out as the most prevalent and effective process for nanofiber production. In the electrospinning process, whether single-fluid or multi-fluid, mixed with active substances fed through an electrospun instrument subjected to high voltage (10-50 kV), resulting in the creation of fine fibers (99).

Several factors, including polymer type, polymer concentration, and applied voltage, play a pivotal role in determining the characteristics of fibers (126). The electrospinning technique employs electrostatic forces to elongate the electrospinning solution into nano-sized fibers, closely resembling the native structure of the extracellular matrix in tissues. Consequently, these nanofibers can actively support normal cellular functions, including cell attachment and proliferation. Nanofibers produced through electrospinning demonstrate exceptional characteristics, including a substantial specific surface area, heightened porosity, favourable biocompatibility, and biodegradability. These unique characteristics make electrospun nanofibers highly versatile, leading to their widespread applications in the pharmaceutical industry (33).

The characteristics and attributes of electrospun nanofibers are significantly influenced by their morphology, primarily controlled by the electrospinning process. There are three key categories of factors that play a crucial role in shaping the morphology of nanofibers during electrospinning: operational factors, solution characteristics, and ambient settings (169). Adjusting these factors allows for the manipulation of the form and arrangement of the nanofibers. Achieving the desired range of beadless nanofibers with fine diameters requires a careful examination and optimization of electrospinning conditions. This process is essential to ensure the production of nanofibers that meet specific requirements for various applications.

A fractional factorial design stands as a notable statistical method employed for evaluating the influence of several manageable variables on a particular outcome of concern. Thoughtfully minimizing the scope of an experiment is a recognized design strategy that not only conserves resources but also safeguards against the omission of crucial data by not assessing every conceivable combination of factor levels (116). This design serves as an initial step in the evaluation process, identifying critical factors

before proceeding to a more comprehensive assessment. While the fractional factorial design allows for a reduction in the test run, it is noteworthy that it does not account for all possible interactions among independent factors within the experimental space. As such, it provides a practical and efficient means of screening and identifying key factors but may necessitate further investigation to fully understand complex interactions and relationships between factors in subsequent stages of experimentation.

After screening experiments, key factors are selected for further investigation using either a response surface design or a full factorial design, which incorporates a center point and recurring trials. Response surface designs, compared to three-level factorial designs, offer a more efficient approach, providing valuable insights with fewer trials. Response surface designs analyze curvature and interactions within the experimental domain to create a more refined model of the output factor (117-119). Therefore, to achieve the best possible outcome, it is necessary to consider implementing a different optimization design. The Box-Behnken design (BBD) is aimed at optimization by studying the relationship between multiple parameters and their influence on an outcome. BBD is rotatable, necessitates three levels for each parameter, and includes a centre value for the estimation of quadratic effects. It is suitable for experiments with more than two factors, offering an efficient means of finding optimal conditions without excessive trials (114). This systematic approach enhances the efficiency of experimentation and aids in achieving optimal process conditions.

Electrospun nanofiber dressings offer enhanced wound healing capabilities compared to traditional dressings. They excel in exudate absorption, fostering a moistened area conducive to cellular metabolism and growth while reducing bacterial infection and inflammation. These nanofibers ensure optimal permeability and safeguard damaged tissues against dehydration (34). The electrospinning process enables the incorporation of various substances into matrix of fibers, including drugs, growth factors, bioactive nanoparticles, and plant extracts. Biopolymer dressings produced through electrospinning, particularly those containing herbal extracts or natural compounds, exhibit biodegradable nature, excellent compatibility with human body as well as anti-infective and anti-inflammatory activities. This combination of

features makes them particularly effective in promoting wound healing and cell growth (170-172).

While previous studies (35-39) have identified significant antimicrobial potential in SA leaf extract, there is a remarkable gap in research regarding the incorporation into electrospun nanofibers. The distinct properties of shellac fibers, coupled with the proven antimicrobial abilities of SA leaf extract, offer a potential avenue for creating electrospun shellac fibers infused with this extract. This approach has the potential to enhance wound healing by using the synergistic effects of the electrospun fibers and the antimicrobial properties of SA leaf extract.

In this research, electrospinning was used to create shellac fibers containing SA leaf extract. A screening process was adopted to pinpoint the most efficient electrospinning conditions for achieving the desired nanofiber structure, employing a fractional factorial experimental approach. Subsequently, the Box-Behnken Design (BBD) was employed to identify the best values for each dependent parameter. The study also examined the entrapment efficiency and release kinetics of rhein from shellac electrospun fibers laden with SA leaf extract. Furthermore, an evaluation of the antibacterial characteristics of fibers was conducted, specifically emphasizing the inhibition of microbial growth with the aim of potentially expediting the wound healing process. This comprehensive approach aimed to explore the potential of shellac electrospun fibers incorporating SA leaf extract for advanced wound care applications.

4.2.2. Preliminary study for the selection of shellac type and solvent type

4.2.2.1. Type of shellac

Two types of shellac, namely native shellac, and bleached shellac, were employed for a comparative analysis of morphological features, including fiber diameter and bead-to-fiber ratio, in the electrospun fibers. The SEM images were analysed by the utilization of JMicro-Vision 1.2.7 software to quantify the number of individual beads and nanofibers. Following the enumeration of beads and fibers, the bead-to-fiber ratio was calculated using the equation (8).

$$\text{Bead-to-Fiber Ratio} = (\text{Number of Beads}) / (\text{Number of Fibers}) \qquad (8)$$

Figure 27 illustrates SEM images of various shellac electrospun fibers under identical spinning conditions. When maintaining a shellac content of 42.5% w/w, the fiber diameters of native shellac were notably larger compared to those of bleached shellac, as depicted in Figures 27(a, b). Figures 27(c, d) display distinct outcomes in the bead-to-fiber ratio between the two shellac types at a concentration of 35% w/w. These findings indicated that native shellac exhibited higher values for both fiber diameter and bead-to-fiber ratio in comparison to bleached shellac. Following that, bleached shellac was chosen for further examination.

Diameter = 881.21 nm

(a)

Diameter = 407.42 nm

(b)

Bead to fiber ratio = 2.35

(c)

Bead to fiber ratio = 1.24

(d)
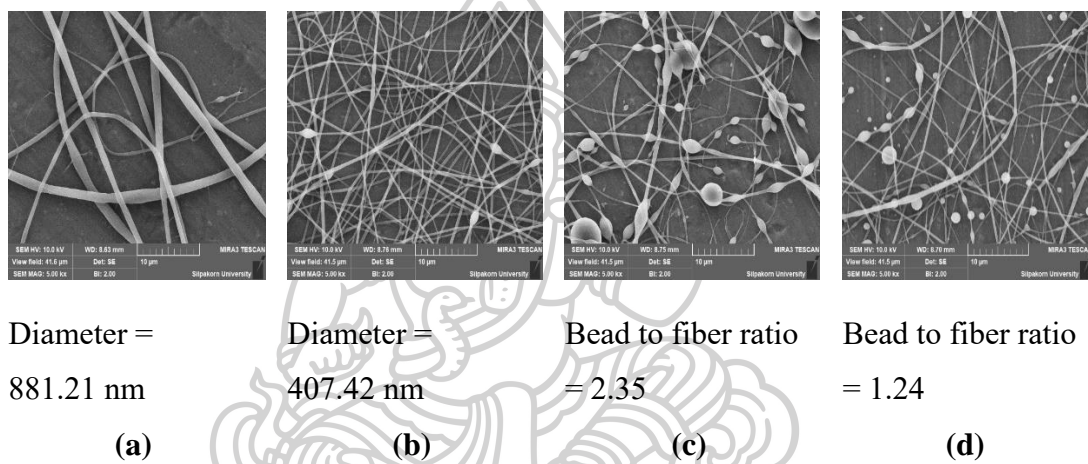
Figure 27. Comparison of Fiber Diameter, Native Shellac **(a)**, Bleached Shellac **(b)** and Bead-to-Fiber Ratio, Native Shellac **(c),** Bleached Shellac **(d)**.

4.2.2.2. Type of solvent

The choice of solvent in the electrospinning fluid is a crucial factor affecting the spinnability of the process. In this study, ethanol and isopropanol were employed as solvents, and the outcomes were illustrated in Figure 28(a-d).

Diameter =	Diameter =	Bead-to-fiber ratio	Bead-to-fiber ratio
2118.08 nm	400.67 nm	= 0.12	= 1.24
(a)	**(b)**	**(c)**	**(d)**

Figure 28. Comparison of Fiber Diameter with 42.5% w/w Shellac Content, Isopropanol **(a),** Ethanol **(b)**, and Bead-to-Fiber Ratio with 35% w/w Shellac Content, Isopropanol **(c),** Ethanol **(d)**.

The fiber diameter derived from the electrospinning fluid utilizing isopropanol was approximately five times greater than that of solutions using ethanol. There was a notable difference in the bead-to-fiber ratio between the two solvents as well. As a result, ethanol was used as the suitable solvent for the electrospinning fluid in subsequent investigations.

4.2.3. Design of Experiments

4.2.3.1. Fractional Factorial Design (FFD)

Nineteen experimental runs, including three centre points, were carried out based on the experimental plan created by Design-Expert software. Detailed plan and outcomes are outlined in Table 13.

Table 13. Matrix Design and Experimental Results of FFD (173).

	Independent Variables					**Responses (n=3)**	
Run	X_1 **Shellac Content (% w/w)**	X_2 **Extract Content (% w/w)**	X_3 **Applied Voltage (kV)**	X_4 **Feed Rate (mL/h)**	X_5 **Needle Tip Diameter (mm)**	R_1 **Fiber Diameter (nm) (Mean ± SD)**	R_2 **Bead-To-Fiber Ratio (Mean ± SD)**
1	−1 (35.00)	−1 (1.00)	1 (27.00)	1 (1.20)	1 (1.06)	401.02 ± 22.79	4.45 ± 1.30
2	−1 (35.00)	−1 (1.00)	−1 (9.00)	1 (1.20)	−1 (0.61)	398.99 ± 3.71	5.27 ± 1.07
3	0 (40.00)	0 (2.50)	0 (18.00)	0 (0.80)	0 (0.84)	360.93 ± 13.26	0.32 ± 0.11
4	1 (45.00)	−1 (1.00)	1 (27.00)	1 (1.20)	−1 (0.61)	773.52 ± 25.61	0.17 ± 0.02
5	1 (45.00)	1 (4.00)	1 (27.00)	1 (1.20)	1 (1.06)	749.96 ± 15.79	0.16 ± 0.12
6	−1 (35.00)	1 (4.00)	1 (27.00)	−1 (0.40)	1 (1.06)	396.22 ± 10.62	0.56 ± 0.29

7	−1 (35.00)	−1 (1.00)	1 (27.00)	−1 (0.40)	−1 (0.61)	368.51 ± 8.74	1.39 ± 0.61
8	−1 (35.00)	1 (4.00)	−1 (9.00)	−1 (0.40)	−1 (0.61)	374.57 ± 9.27	1.43 ± 0.81
9	1 (45.00)	1 (4.00)	−1 (9.00)	1 (1.20)	−1 (0.61)	394.49 ± 9.52	0.02 ± 0.01
10	1 (45.00)	−1 (1.00)	1 (27.00)	−1 (0.40)	1 (1.06)	727.32 ± 4.43	0.17 ± 0.07
11	−1 (35.00)	1 (4.00)	1 (27.00)	1 (1.20)	−1 (0.61)	330.31 ± 10.38	4.12 ± 0.68
12	1 (45.00)	1 (4.00)	1 (27.00)	−1 (0.40)	−1 (0.61)	680.65 ± 8.98	0.28 ± 0.12
13	−1 (35.00)	1 (4.00)	−1 (9.00)	1 (1.20)	1 (1.06)	343.44 ± 6.93	4.45 ± 1.47
14	1 (45.00)	1 (4.00)	−1 (9.00)	−1 (0.40)	1 (1.06)	419.49 ± 3.24	0.02 ± 0.01
15	1 (45.00)	−1 (1.00)	−1 (9.00)	−1 (0.40)	−1 (0.61)	425.40 ± 11.30	0.02 ± 0.01
16	0 (40.00)	0 (2.50)	0 (18.00)	0 (0.80)	0 (0.84)	323.91 ± 7.84	0.34 ± 0.08
17	−1 (35.00)	−1 (1.00)	−1 (9.00)	−1 (0.40)	1 (1.06)	387.38 ± 2.71	1.03 ± 0.26
18	1 (45.00)	−1 (1.00)	−1 (9.00)	1 (1.20)	1 (1.06)	435.88 ± 5.41	0.02 ± 0.01
19	0 (40.00)	0 (2.50)	0 (18.00)	0 (0.80)	0 (0.84)	349.50 ± 3.19	0.57 ± 0.14

Pareto charts (Figure 29) (173) are employed to analyse the individual impacts and interconnections among input factors. From left to right, these variables are arranged in decreasing sequence of frequency, from most often to least frequent. The independent variables are represented by orange bars on the Pareto chart, which indicate positive impacts, and blue bars, which indicate negative impacts.
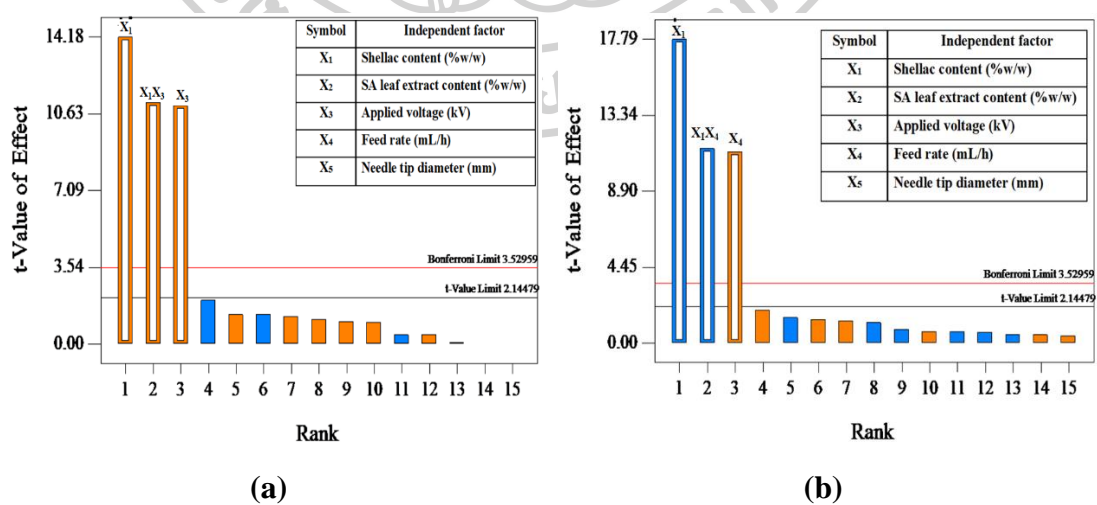
Figure 29. Pareto Chart Illustrating the Impact of Factors on Fiber Diameter (**a**) and Bead-to-Fiber Ratio (**b**) The orange-colored bars and blue-colored bars indicate positive effects, and negative effects, respectively (173).

Figure 29(a) depicts that the t-values for the applied voltage and content of shellac exceeded the standard t-limit, suggesting substantial favourable effects on fiber width. The favourable interaction between these two factors further corroborated the positive influence on diameter of fiber. Figure 29(b) shows that the bead-to-fiber ratio correlated positively with feed rate of the solution and negatively with shellac concentration. The connection between these factors revealed a detrimental association with formation of bead. Significantly, shellac content appeared as the most influential factor affecting both the fiber diameter and bead-to-fiber ratio.

To assess the relationships of input factors for each response, three-dimensional (3D) surface, and two-dimensional (2D) contour graph (Figure 30) (173) are provided. As shown in Figure 30(a) and 30(b), the simultaneous increase in electrical voltage and a significant concentration of shellac could lead to the generation of large diameter fibers. The interplay between feed rate and shellac proportion on the bead-to-fiber ratio is demonstrated in Figure 30(c) and 30(d). The combination of a rapid solution input rate and a low amount of shellac resulted in bead formation.
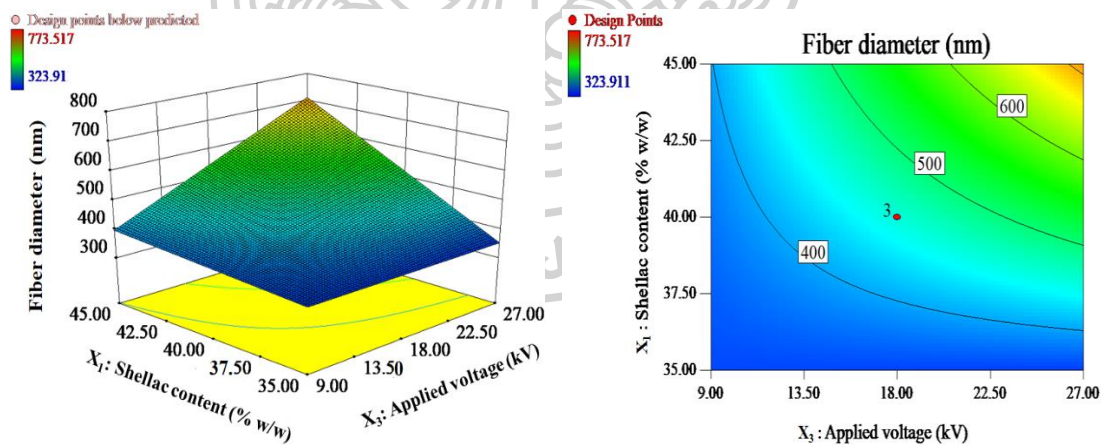
Actual Factors

X$_2$: SA leaf extract content = 2.5 % w/w   X$_4$: Feed rate = 0.80 mL/h

X$_5$: Needle tip diameter = 0.84 mm

(a)   **(b)**
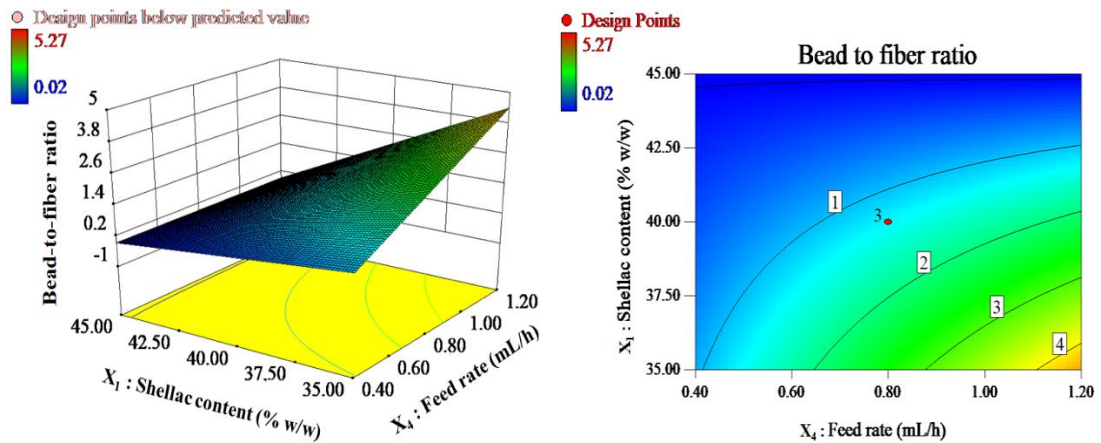
Actual Factors

X₂: SA leaf extract content = 2.5 % w/w   X₃: Applied voltage = 18 kV

X₅: Needle tip diameter = 0.84 mm

(c)   **(d)**

Figure 30. Contour Plots Illustrating the Relationship of Factors on Fiber Diameter (**a,b**), and Bead-to-Fiber Ratio (**c,d**) (173).
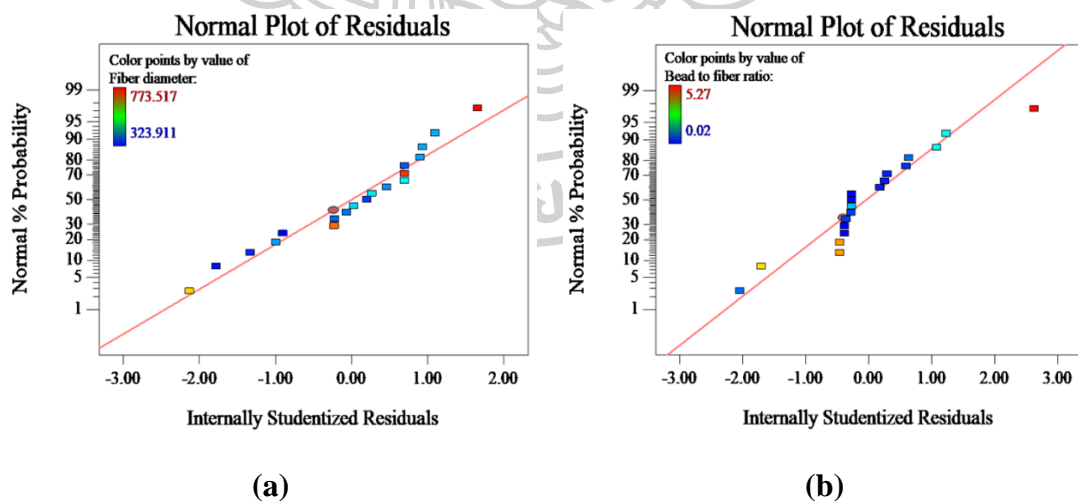
(a)   **(b)**

Figure 31. Plot Illustrating the Normal Probability of Internally Studentized Residuals for Fiber Diameter (**a**), and Bead-to-Fiber Ratio (**b**) (173).

To make sure that the selected model for the experiment efficiently captures the data, a normal plot of residuals is employed. Figure 31 (173) demonstrates that the data values observed along the straight line exhibited a normal distribution. The analysis of variance (ANOVA) presented in Table 14 indicates that the statistical significance of the mathematical models for all response factors, demonstrating p-values below 0.05. The high R^2 values indicate the accuracy and suitability of the resultant models for all dependent factors. The Pred R^2 values of both responses were found to be closely align with their Adj R^2 values. These findings validate the suitability of the models for making predictions. Moreover, the insignificant lack-of-fit values demonstrated that the model fits well.

Through the application of multiple regression analysis, equations were formulated for each response factor as follows:

$$\text{Fiber diameter} = 454.82 + 100.39\,(X_1) + 77.99\,(X_3) + 79.03\,(X_1X_3) \qquad (9)$$

$$\text{Bead-to-fiber ratio} = 1.30 - 1.36\,(X_1) + 0.86\,(X_4) - 0.88\,(X_1X_4) \qquad (10)$$

Table 14. ANOVA for the Selected Factorial Model (173).

Source	Sum of Squares	df	Mean Square	F Value	p-Value Prob > F
R_1—Fiber diameter					
Model	3.59×10^5	3	1.20×10^5	32.97	<0.0001 *
X_1—Shellac content	1.61×10^5	1	1.61×10^5	44.49	<0.0001 *
X_3—Applied voltage	97320.85	1	97320.85	26.85	0.0001 *
X_1X_3	99939.92	1	99939.92	27.58	<0.0001 *
Residual	54362.18	15	3624.15		
Lack of Fit	53643.40	13	4126.42	11.48	0.0829 **
Pure Error	718.78	2	359.39		
Cor Total	4.13×10^5	18			
$R^2 = 0.8683$ Adj $R^2 = 0.8420$ Pred $R^2 = 0.8274$					
R_2—Bead-to-fiber ratio					
Model	53.90	3	17.97	64.62	<0.0001 *
X_1—Shellac content	29.81	1	29.81	107.22	<0.0001 *

Source	Sum of Squares	df	Mean Square	F Value	*p*-Value Prob > F
X₄—Feed rate	11.83	1	11.83	42.56	<0.0001 *
X₁X₄	12.25	1	12.25	44.06	<0.0001 *
Residual	4.17	15	0.28		
Lack of Fit	4.13	13	0.32	16.47	0.0587 **
Pure Error	0.04	2	0.02		
Cor Total	58.07	18			
$R^2 = 0.9282$	Adj $R^2 = 0.9138$		Pred $R^2 = 0.9016$		

Significant * $p < 0.01$; not significant *

4.2.3.2. Box–Behnken Design (BBD)

The initial identification of factors influencing diameter of fibers and formation of beads was carried out using a FFD. Following this prior investigation, the experimental levels of impact factors were selected for optimization using a BBD. The matrix of design and output of each response are presented in Table 15 (173).

Table 15. Matrix Design and Experimental Results of BBD (173).

Run	Independent Variables				Responses (n=3)		
	X_1 Shellac Content (% w/w)	X_2 Extract Content (% w/w)	X_3 Applied Voltage (kV)	X_4 Feed Rate (mL/h)	R_1 Fiber Diameter (nm) (Mean ± SD)	R_2 Bead-to-Fiber Ratio (Mean ± SD)	R_3 Entrapment Efficiency (%) (Mean ± SD)
1	0 (40.00)	0 (2.50)	0 (16.50)	0 (0.80)	343.99 ± 13.90	0.33 ± 0.02	82.33 ± 4.89
2	0 (40.00)	0 (2.50)	1 (24.00)	−1 (0.40)	335.26 ± 3.92	0.43 ± 0.05	96.04 ± 0.49
3	1 (45.00)	0 (2.50)	1 (24.00)	0 (0.80)	446.89 ± 13.01	0.09 ± 0.08	77.44 ± 3.14
4	−1(35.00)	−1 (1.00)	0 (16.50)	0 (0.80)	310.52 ± 29.01	2.37 ± 0.49	96.81 ± 5.18
5	0 (40.00)	0 (2.50)	0 (16.50)	0 (0.80)	359.51 ± 5.93	0.46 ± 0.12	82.94 ± 2.86
6	1 (45.00)	−1 (1.00)	0 (16.50)	0 (0.80)	355.37 ± 10.94	0.05 ± 0.04	70.53 ± 5.22
7	0 (40.00)	0 (2.50)	1 (24.00)	1 (1.20)	336.23 ± 20.90	0.16 ± 0.03	90.05 ± 6.91
8	−1(35.00)	0 (2.50)	−1 (9.00)	0 (0.80)	325.04 ± 26.16	4.05 ± 0.23	102.99 ± 1.36

9	0 (40.00)	1 (4.00)	1 (24.00)	0 (0.80)	351.06 ± 20.18	0.09 ± 0.01	95.52 ± 1.04
10	1 (45.00)	0 (2.50)	0 (16.50)	1 (1.20)	414.27 ± 19.82	0.02 ± 0.01	68.97 ± 1.47
11	−1(35.00)	0 (2.50)	1 (24.00)	0 (0.80)	312.57 ± 8.51	1.47 ± 0.20	105.42 ± 3.05
12	−1(35.00)	1 (4.00)	0 (16.50)	0 (0.80)	280.29 ± 21.53	1.99 ± 0.65	77.55 ± 1.24
13	1 (45.00)	1 (4.00)	0 (16.50)	0 (0.80)	422.24 ± 22.60	0.02 ± 0.01	66.39 ± 0.71
14	0 (40.00)	0 (2.50)	0 (16.50)	0 (0.80)	319.79 ± 17.05	0.57 ± 0.11	83.54 ± 2.76
15	0 (40.00)	1 (4.00)	0 (16.50)	−1 (0.40)	276.04 ± 10.89	0.09 ± 0.04	76.70 ± 1.79
16	1 (45.00)	0 (2.50)	0 (16.50)	−1 (0.40)	390.48 ± 15.29	0.03 ± 0.01	58.88 ± 4.60
17	−1(35.00)	0 (2.50)	0 (16.50)	−1 (0.40)	259.94 ± 23.12	2.13 ± 0.13	99.81 ± 3.95
18	0 (40.00)	0 (2.50)	−1 (9.00)	1 (1.20)	426.59 ± 11.20	1.65 ± 0.44	80.84 ± 2.10
19	0 (40.00)	1 (4.00)	0 (16.50)	1 (1.20)	277.07 ± 10.24	0.07 ± 0.02	87.74 ± 0.95
20	0 (40.00)	−1 (1.00)	0 (16.50)	1 (1.20)	291.10 ± 7.12	0.34 ± 0.06	93.81 ± 0.78
21	0 (40.00)	0 (2.50)	0 (16.50)	0 (0.80)	310.52 ± 2.16	0.39 ± 0.07	90.24 ± 2.43
22	0 (40.00)	−1 (1.00)	1 (24.00)	0 (0.80)	356.75 ± 23.34	0.22 ± 0.03	99.44 ± 3.71
23	0 (40.00)	1 (4.00)	−1 (9.00)	0 (0.80)	480.01 ± 8.57	1.16 ± 0.40	77.87 ± 2.18
24	1 (45.00)	0 (2.50)	−1 (9.00)	0 (0.80)	523.86 ± 6.69	0.25 ± 0.06	59.84 ± 0.78
25	−1(35.00)	0 (2.50)	0 (16.50)	1 (1.20)	226.20 ± 5.42	2.62 ± 0.97	88.39 ± 3.69
26	0 (40.00)	0 (2.50)	0 (16.50)	0 (0.80)	318.21 ± 2.27	0.38 ± 0.10	82.19 ± 0.84
27	0 (40.00)	0 (2.50)	−1 (9.00)	−1 (0.40)	462.28 ± 7.76	1.31 ± 0.47	74.99 ± 4.13
28	0 (40.00)	−1 (1.00)	0 (16.50)	−1 (0.40)	332.74 ± 10.42	0.37 ± 0.12	85.82 ± 4.46
29	0 (40.00)	−1 (1.00)	−1 (9.00)	0 (0.80)	410.33 ± 6.35	1.48 ± 0.69	95.13 ± 5.67

The outcomes of ANOVA displayed in Table 16 (173) clearly indicate that all response factors are statistically significant. A p-value less than 0.05 signifies the effectiveness of the mathematical models employed for these variables. The regression coefficients, coupled with R^2 values of 0.8406, 0.9780, and 0.8259, signify the appropriateness and predictability of the resultant models for all output factors.

The Pred R^2 values, closely aligned with their Adj R^2 values in each response further support the reliability of these models for prediction. It is also supported by the unsignificant lack-of-fit indicating the models exhibited a good fit.

The following equations were created using multiple regression analysis to describe each output factor:

$$\text{Fiber diameter} = 322.84 + 69.88X_1 - 40.78\ X_3 + 74.40X_3^2 \qquad (11)$$

$$\text{Bead-to-fiber ratio} = 0.36 - 1.18X_1 - 0.12X_2 - 0.62X_3 + 0.60X_1X_3$$
$$+ 0.76X_1^2 + 0.41X_3^2 \qquad (12)$$

$$\text{Entrapment efficiency} = 84.25 - 14.08\ X_1 - 4.98\ X_2 + 6.02\ X_3$$
$$- 4.96\ X_1^2 + 5.36\ X_3^2 \qquad (13)$$

Table 16. ANOVA for Response Surface Reduced Quadratic Model (173).

Source	Sum of Squares	df	Mean Square	F Value	p-Value Prob > F
R$_1$—Fiber diameter					
Model	1.18×10^5	3	39,162.78	43.96	<0.0001 *
X$_1$—Shellac content	58,597.40	1	58,597.40	65.77	<0.0001 *
X$_3$—Voltage	19,954.60	1	19,954.60	22.40	<0.0001 *
X$_3^2$	38,936.35	1	38,936.35	43.70	<0.0001 *
Residual	22,273.41	25	890.94		
Lack of Fit	20,585.04	21	980.24	2.32	0.2151 ***
Pure Error	1688.37	4	422.09		
Cor Total	1.398×10^5	28			
$R^2 = 0.8406$	Adj $R^2 = 0.8215$		Pred $R^2 = 0.7835$		
R$_2$—Bead-to-fiber ratio					
Model	27.59	6	4.60	162.82	<0.0001 *
X$_1$—Shellac content	16.73	1	16.73	592.40	<0.0001 *
X$_2$—Extract content	0.17	1	0.17	5.87	0.0241 **
X$_3$—Voltage	4.61	1	4.61	163.31	<0.0001 *
X$_1$X$_3$	1.46	1	1.46	51.84	<0.0001 *
X$_1^2$	3.94	1	3.94	139.49	<0.0001 *
X$_3^2$	1.18	1	1.18	41.94	<0.0001 *
Residual	0.62	22	0.03		
Lack of Fit	0.59	18	0.03	3.78	0.1032 ***
Pure Error	0.03	4	8.63×10^{-3}		
Cor Total	28.21	28			

Source	Sum of Squares	df	Mean Square	F Value	p-Value Prob > F
$R^2 = 0.9780$	Adj $R^2 = 0.9720$		Pred $R^2 = 0.9546$		

R_3—Entrapment efficiency

Source	Sum of Squares	df	Mean Square	F Value	p-Value Prob > F
Model	3537.04	5	707.41	21.82	<0.0001 *
X_1—Shellac content	2377.95	1	2377.95	73.34	<0.0001 *
X_2—Extract content	297.57	1	297.57	9.18	0.0060 *
X_3—Voltage	434.97	1	434.97	13.42	0.0013 *
X_1^2	169.60	1	169.60	5.23	0.0317 **
X_3^2	198.54	1	198.54	6.12	0.0211 **
Residual	745.75	23	32.42		
Lack of Fit	699.71	19	36.83	3.20	0.1340 ***
Pure Error	46.04	4	11.51		
Cor Total	4282.80	28			
$R^2 = 0.8259$	Adj $R^2 = 0.7880$		Pred $R^2 = 0.7052$		

Significant * $p < 0.01$; ** $0.01 < p < 0.05$; not significant ***.

(a)   (b)

(c)
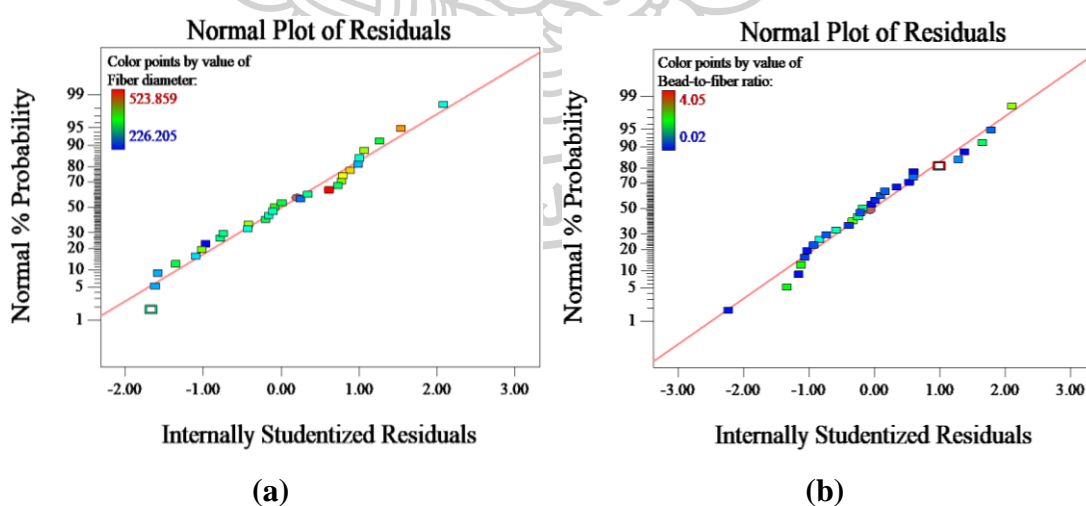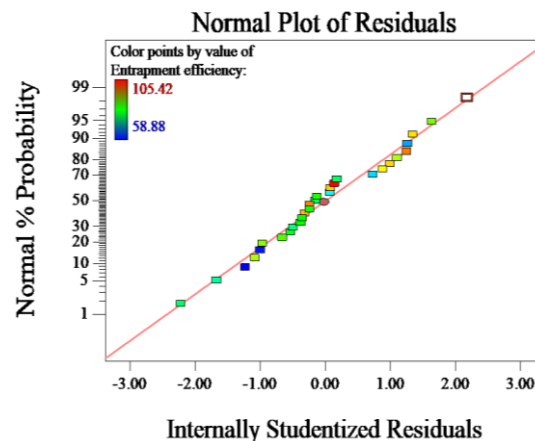
Figure 32. Plot Illustrating the Normal Probability of Internally Studentized Residuals for Fiber Diameter (**a**), Bead-to-Fiber Ratio (**b**), and Entrapment Efficiency (**c**) (173).

The normality of residuals plot serves the purpose of evaluating the appropriateness of the selected model for the experimental data. This is evident in Figure 32 (173), where the data points display a straight-line pattern, indicating a normal distribution. The apparent conformity to a standard normal frequency distribution further supports the credibility and adequacy of the selected model in accurately representing the empirical data.

4.2.4. Factors affecting fiber diameters

The graphical representations in Figure 33 depict the influence of distinct factors affecting each outcome (173). Notably, shellac content and applied voltage emerge as significant factors affecting fiber diameter. Figure 33(a) demonstrates a connection between elevated shellac proportion and the generation of increased fiber widths. Meanwhile, Figure 33(b) illustrates the evident impact of fluctuating voltage intensities affecting fiber thickness. Initially, low voltage induces fiber expansion, followed by a reduction in size at medium voltage levels. Elevated voltage, however, leads to a resurgence of increased diameter of fiber. Low and high levels of voltage, combined with increased shellac content, result in a discernible enlargement of fiber size. These findings showcase the responsiveness of fiber diameter to fluctuations in

shellac amount and electrical voltage, offering valuable insights about the complicated interconnecion between these aspects and subsequent fiber features.

The ability of a polymer solution to be electrospun, as well as the resulting structure and morphology of the nanofibers, is generally influenced by a blend of polymer-specific solution characteristics, processing parameters, and environmental conditions. Key factors impacting the electro spinnability of a polymer solution include its concentration and electrical conductivity. A significant relationship was found between elevated shellac concentration and the production of larger fiber diameters. This association was attributed to the heightened viscosity and intermolecular entanglement within the solution, stemming from the increased concentration of shellac.

The elevated shellac content impedes the resistance to elongate during the electrically induced fiber formation, ultimately resulting in the production of fibers with increased diameters. This understanding of the interaction of shellac ratio and fiber diameter contributes to optimizing the electrospinning process for desired nanofiber characteristics (97).

The adjustment of voltage levels had a notable effect on the diameters of the fibers in the process of electrospinning. Initially, a low voltage led to an expansion of fiber diameter due to diminished electrostatic forces, resulting in reduced stretching of the polymer flow and the production of larger-diameter fibers. Subsequently, a reduced diameter of fibers was observed at a moderate voltage setting, likely due to equilibrium of the electrostatic forces, which allowed the optimal stretching of polymer jet, producing smaller-diameter fibers. Conversely, increasing the voltage resulted in a large-diameter fiber. This implies that an abundance of electrostatic forces may lead to overstretching of the polymer flow, producing fibers with larger diameters (97, 112).

Some studies have suggested that fiber diameter is not affected by the electrical voltage applied during the procedure of electrospinning (174), However, this finding has shown that increasing the voltage can lead to the production of additional charges, thereby increasing the stretching capacity of the polymer solution. This, in turn, leads to the fabrication of finer nanofibers with reduced diameters (175). These findings align with prior research (28, 111, 176) that have reported similar responses, highlighting

the importance of voltage adjustment in controlling fiber diameter during electrospinning.

4.2.5. Factors affecting bead-to-fiber ratio

The specific impacts of each factor on the bead formation are meticulously presented in Figure 33(c–e). A noteworthy relation is evident as higher ratio of shellac and extract content, and increased voltage coincide with a reduction in the bead-to-fiber ratio. Conversely, lower voltage and reduced shellac and extract concentration were identified as factors contributing to bead formation.

Elevated shellac content, extract content, and applied voltage were linked to a reduction in the bead formation, suggesting a preference for generation of more uniform fiber under these circumstances. The addition of shellac increased the solution's viscosity and entanglement, resulting a decreased occurrence of beads and facilitating the creation of fine nanofibers. Increasing the shellac concentration can modify the equilibrium between viscosity and surface tension, leading to a more efficient technique for electrospinning.

On the other hand, diminished proportion of shellac and extract content, along with lower voltage, were related with an increased occurrence of bead formation. Lowering the concentration of shellac decreases the viscosity, enhancing the influence of surface tension across the electrospinning jets. This stronger influence of surface tension, combined with a decrease in molecular entanglements, facilitates the creation of beads on the fiber strands (97). The findings of this study illustrate that the physical characteristics of fibers are significantly influenced by the combination of shellac concentration, extract levels, and the application of electrical voltage.

A higher concentration of extract has the potential to improve the solution conductivity, consequently facilitating the extended polymer flow and minimizing beads. Following the introduction of the extract to the shellac solution, a significant rise in electrical conductivity was found. The noteworthy aspect in this observation is the presence of carboxylic acid in the extract, notably rhein, which can undergo ionization, generating ionized particles that contribute to the increased solution conductivity (177).

Moreover, the incorporation of significant amounts of the extract led to a more viscous solution. This occurrence could potentially account for the observed reduction

in bead generation. Conversely, lower levels of shellac and extract, coupled with reduced voltage, may result in a decrease in both viscosity and conductivity of the solution. This could lead to insufficient stretching of the polymer jet and facilitate in the formation bead. Additionally, increasing the applied voltage has the potential to enhance the electrostatic forces influencing the polymer flow, leading to the development of a more consistent and extended fiber structure and a decrease in the incidence of beads (178). These results highlight the critical effects of processing parameters and extract concentration on the electrospinning process, providing important information for tailoring conditions to achieve targeted fiber morphologies. Improved outcomes in electrospinning for potential materials science applications can be achieved by effectively controlling these variables.

To anticipate the connection of input and output factors, 3D and 2D contour plots were created. The relationship between the shellac and the applied voltage had a noteworthy influence on the beads-to-fibers ratio. As illustrated in Figure 33(i) and 33(j), the results indicate that bead formation was encouraged by combination of reduced voltage and a minimal amount of shellac. On the other hand, when utilizing middle to high levels of voltage along with increased shellac amount, the bead-to-fiber ratio was reduced. These results highlight the complex relationships among the independent factors and their impact on the desired outcome.

4.2.6. Factors affecting entrapment efficiency

In Figure 33(f–h), notable levels of encapsulation efficiency were noted when certain conditions were met, notably with higher electrical voltages and minimal amounts of shellac and extract. Lower contents of both shellac and extract may enhance solubility and decrease the viscosity of the solution, which in turn aids in the effective integration of the extract into the polymer. On the other hand, increasing the content of shellac and extract result in a marked decrease in entrapment capacity.. This decline could be due to the immobilized substances of solution or the limited solubility of constituents (179).

Using higher voltage appears to be a effective approach to improve the ability of entrapment in the electrospinning method. This behaviour can be explained by the increased the electrostatic interactions and the stretching of the polymer jet that occur

throughout the electrospinning process. It is anticipated that the enhanced elongation capacity will lead to better trapping and the efficient integration of the target materials into the matrix. Furthermore, increased applied voltage can create the smoother, more uniform fibers, which enhances entrapment efficiency. The substantial quantity of polymers surface area produced at increased voltage enables the material easier to passively load, which create the high entrapment level (180, 181). These results provide useful information about the networking of solution composition, process parameters, and entrapment efficiency and can be used to optimize electrospinning conditions for successful component incorporation into fibers. This information has practical implications for various applications in materials science.

(a)

(b)

(c)

(d)

(e)

(f)

(g)

(h)
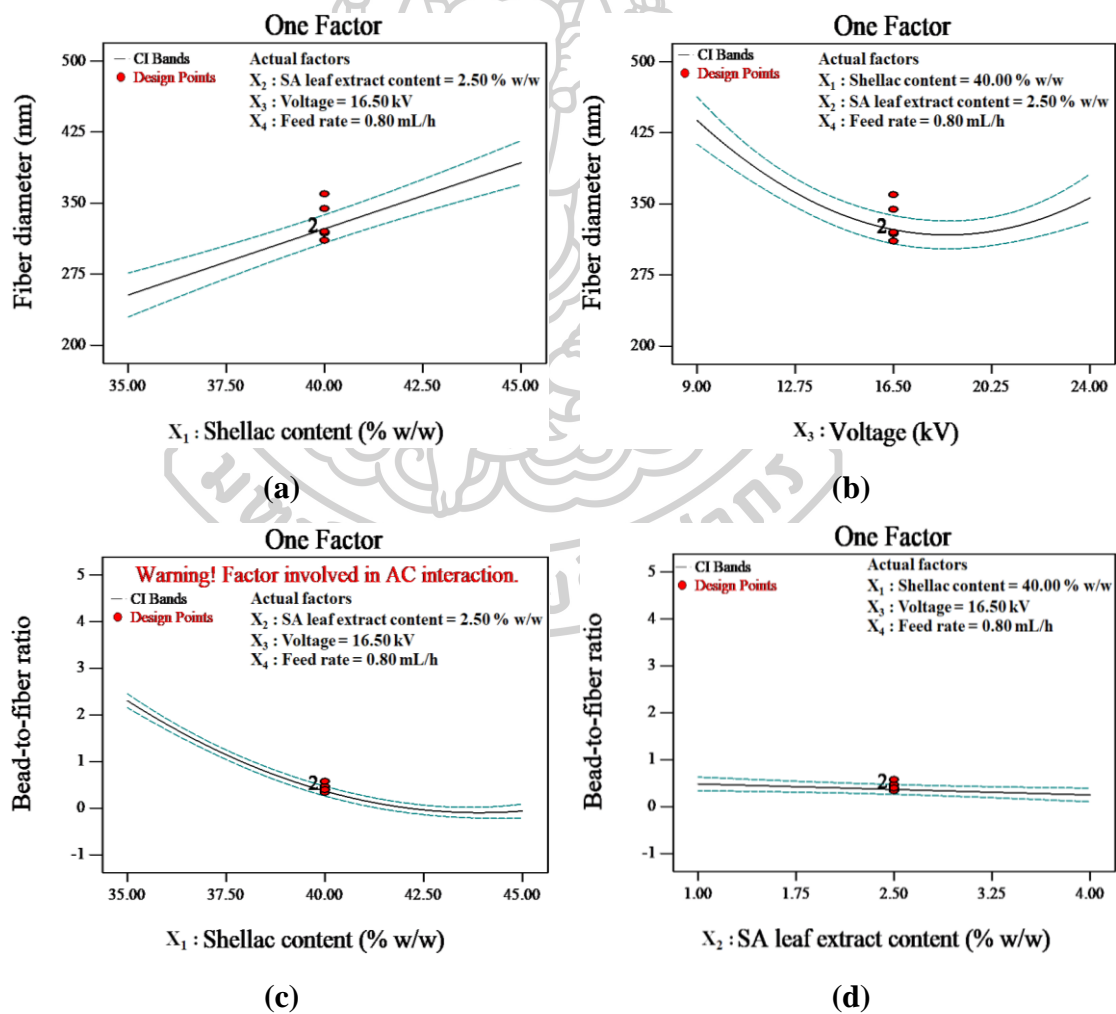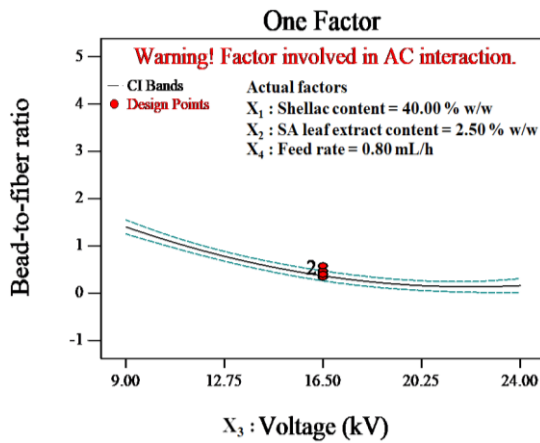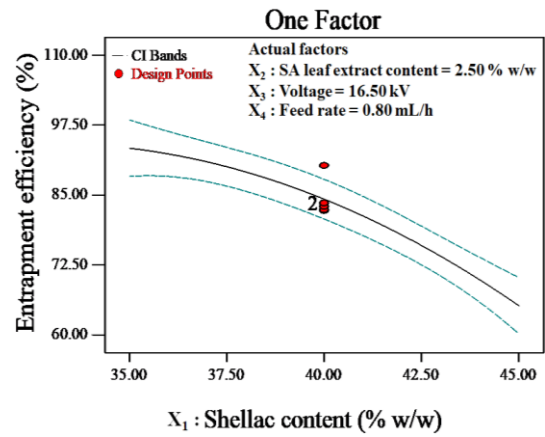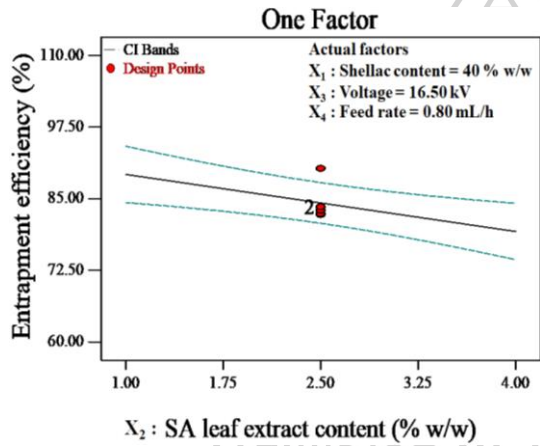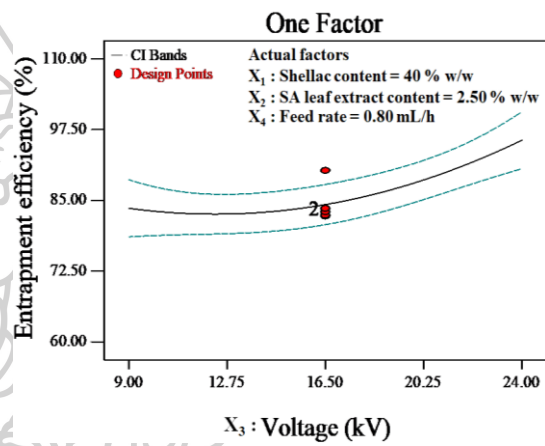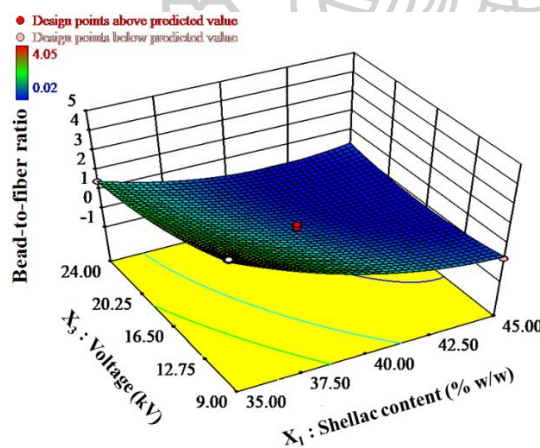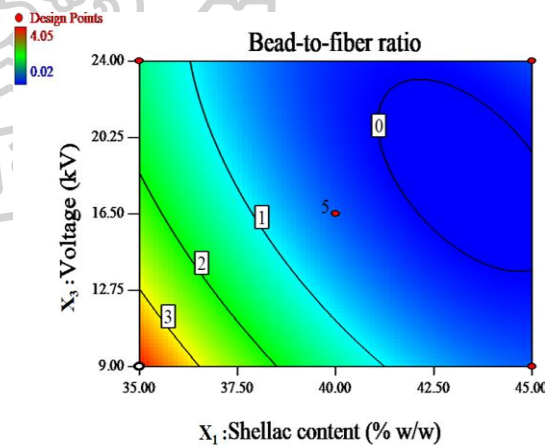
Actual Factors

X₂: SA leaf extract content = 2.5% w/w

X₄: Feed rate = 0.8 mL/h

(i)

(j)

Figure 33. Linear Effect on Fiber Diameter: Shellac Content (**a**) and Applied Voltage (**b**); Linear Effect on Bead-to-Fiber Ratio: Shellac Content (**c**), Extract Content (**d**), and Applied Voltage (**e**); Linear Effect on Entrapment Efficiency: Shellac Content (**f**), Extract Content (**g**), and Applied Voltage (**h**); and 3D- and 2D Surface Plot Showing the Interaction of Shellac Content and Applied Voltage on Bead-to-Fiber Ratio (**i, j**) (173).

4.2.7. Optimization of electrospinning conditions

Table 17 provides a summary of the prameters for optimized electrospinning settings, with a focus on acceptable limits for all response variables to validate the optimized conditions. Since none of the responses showed statistical significance, the feed rate kept constant at 0.8 mL/h (173). Using an overlaid contour graph (Figure 34), the region where the anticipated limits of all dependent factors were maintained within allowable ranges was generated. The yellow-colored region on the contour plot denotes the design space, which represents a set of ideal circumstances that fulfill the requirements of all responses (173). Table 18 displays the ideal conditions for controlling the desired ranges of all responses. Three independent trials were carried out to confirm the validity of these conditions (173). Table 19 presents the verification results thoroughly, providing further confirmation that the actual values were within acceptable limits. This improves the reliability of the optimized electrospinning settings (173).

The resulting fibers, with 306 nm in diameter and reduced bead-to-fiber ratio of 0.29, exhibited a nanoscale morphology devoid of beads under optimal electrospinning conditions. In previous research, larger fibers measuring 488 nm in diameter and with a bead-to-fiber ratio of 0.48 were generated using shellac and monolaurin under optimal electrospinning conditions (111). Furthermore, a separate study utilizing shellac loaded with *Kaempferia parviflora* extract observed larger fiber diameters and increased formation of bead (126). When compared to these prior findings, the ultrafine fibers in this study presented a distinct profile characterized by beadless and smaller diameters.

The morphological difference could be ascribed to the utilization of bleached shellac in this investigation, which is recognized for its exceptional purity achieved through a bleached method. The use of bleached shellac resulted in a naturally low

viscous fluid for electrospinning, which led to the creation of fibers with a propensity to form beads and a lower diameter. Nonetheless, it's crucial to highlight that the addition of extract played a crucial role in adjusting the viscosity and electrical conductivity of the solution. This modification significantly reduced bead forming on the fibers and successfully countered the low viscosity characteristic of bleached shellac.

To summarize, the unique features of the electrospun fibers investigated in the present research, such as their diminished diameter and minimized bead formation, can be ascribed to the intentional application of bleached shellac and the inclusion of SA leaf extract. These adjustments not only addressed potential clogging problems during electrospinning process but also eased the achievement of the intended ultrafine fiber structure.

Table 17. Criteria for the Optimal Electrospinning Conditions (173).

Parameters	Goal	Lower Limit	Upper Limit
X_1: Shellac content (% w/w)	in range	35.00	45.00
X_2: Extract content (% w/w)	in range	1.00	4.00
X_3: Applied voltage (kV)	in range	9.00	24.00
X_4: Feed rate (mL/h)	equal to 0.8 mL/h	0.40	1.20
Fiber diameter (nm)	in range	250	500
Bead-to-fiber ratio	in range	0.02	0.30
Entrapment efficiency (%)	in range	95.00	105.00

Table 18. Optimal Conditions with Favorable Outcomes (173).

Applied Voltage (kV)	Feed Rate (mL/h)	Shellac Content (% *w/w*)	Extract Content (% *w/w*)	Fiber Diameter (nm)	Bead-to-Fiber Ratio	Entrapment Efficiency (%)	Desirability
23.99	0.80	38.50	3.80	335.36	0.30	95.07	1.00
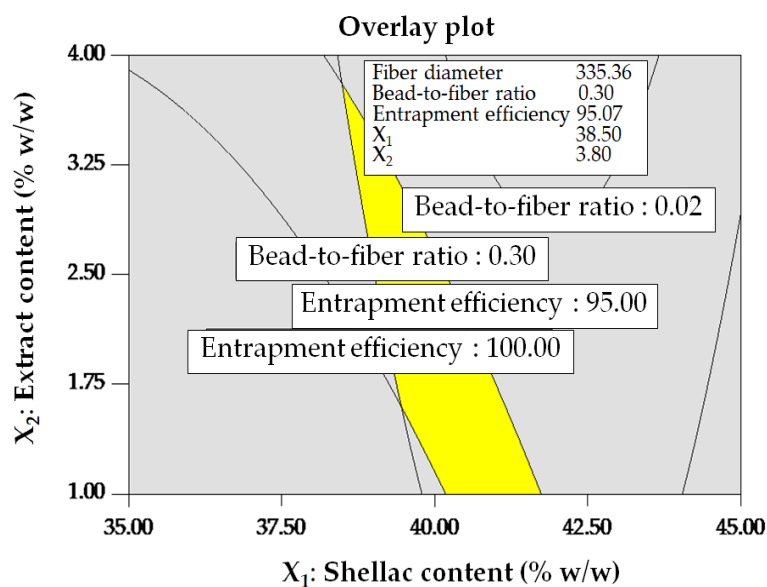
Figure 34. Contour Plot Overlay for Optimized Conditions. The region satisfying the criteria is highlighted in yellow, while the area not meeting the criteria is depicted in grey (173).

Table 19. Confirmation (173).

Response	Prediction	Experimental Value (n=3)	95% PI* Low	95% PI* High
Fiber diameter	335.36	305.77 ± 10.93	291.59	379.13
Bead-to-fiber ratio	0.30	0.29 ± 0.05	0.02	0.57
Entrapment efficiency	95.07	96.38 ± 1.42	86.11	104.03

PI*= Prediction interval

4.2.8. Assessment of solution properties

The morphological appearance of resultant fibers is notably affected by the properties of the fluids used in electrospinning. This research aimed to evaluate the influence of viscosity, surface tension, and electrical conductivity concerning different ratios of shellac to extract. Table 20 (173) presents a thorough summary of the conducted measurements, unveiling significant trends.

According to the findings, there was a consistent increase in viscosity observed with rising proportions of both shellac and extract. Particularly, increased amount of

both shellac and extract were associated with high viscosity. The conductivity of the shellac solution typically decreased with high shellac content. Interestingly, incorporating extract at the same level of shellac revealed a significant increase in conductivity as the extract percentage weight increased. Conversely, surface tension results were found to be slight fluctuations in different shellac-extract ratios. The consistency of surface tension is minimally affected by variations in shellac and extract content.

Table 20. Properties of Solutions at Various Shellac-Extract Ratios (173).

Shellac Content (% w/w)	SA leaf Extract Content (% w/w)	Viscosity (mPa. S) (Mean ± SD) (n=3)	Conductivity (µS) (Mean ± SD) (n=3)	Surface Tension (mN/m) (Mean ± SD) (n=3)
35.00	0.00	30.81 ± 1.74	94.17 ± 0.15	28.15 ± 0.15
40.00	0.00	59.49 ± 0.98	77.27 ± 0.31	28.56 ± 0.23
45.00	0.00	132.85 ± 1.22	71.50 ± 1.39	28.94 ± 0.06
35.00	1.00	35.89 ± 0.61	170.80 ± 3.36	27.64 ± 0.31
35.00	2.50	48.18 ± 2.82	178.50 ± 0.10	28.52 ± 0.08
35.00	4.00	52.71 ± 1.29	187.80 ± 1.01	30.23 ± 0.28
40.00	1.00	73.57 ± 1.22	160.10 ± 0.10	28.24 ± 0.16
40.00	2.50	91.89 ± 2.09	165.47 ± 1.29	28.64 ± 0.07
40.00	4.00	108.96 ± 4.36	179.17 ± 0.74	29.08 ± 0.05
45.00	1.00	159.41 ± 3.81	158.00 ± 0.56	30.60 ± 0.11
45.00	2.50	183.61 ± 1.42	160.40 ± 0.10	30.32 ± 0.09
45.00	4.00	267.98 ± 6.94	176.50 ± 1.18	32.05 ± 0.19
38.50 (Optimized)	3.80 (Optimized)	88.36 ± 3.15	180.20 ± 0.66	29.11 ± 0.09

In conclusion, this study highlighted the significant impact of electrospinning fluid characteristics on fiber morphology. Viscosity, conductivity, and surface tension emerge as crucial parameters in shaping the structure of electrospun fibers. These

observations provide valuable understanding into the complex interplay between the amounts of shellac extract and the attributes of electrospun fibers.

4.2.9. Entrapment efficiency of shellac electrospun fibers loaded with SA leaf extract

The measurement of rhein compound entrapped in the nanofibers was carried out utilizing a validated HPLC-DAD method specifically developed for rhein content quantification (143). Evaluating the amount of rhein in the fibers involved employing a linear regression equation and a coefficient determination ($R^2 = 0.9999$) obtained from the calibration curve of standard rhein. In Figure 35, the rhein peak was consistently observed at 23.5 min in the HPLC chromatograms of fibers loaded extract (a) and standard rhein (b) (173).
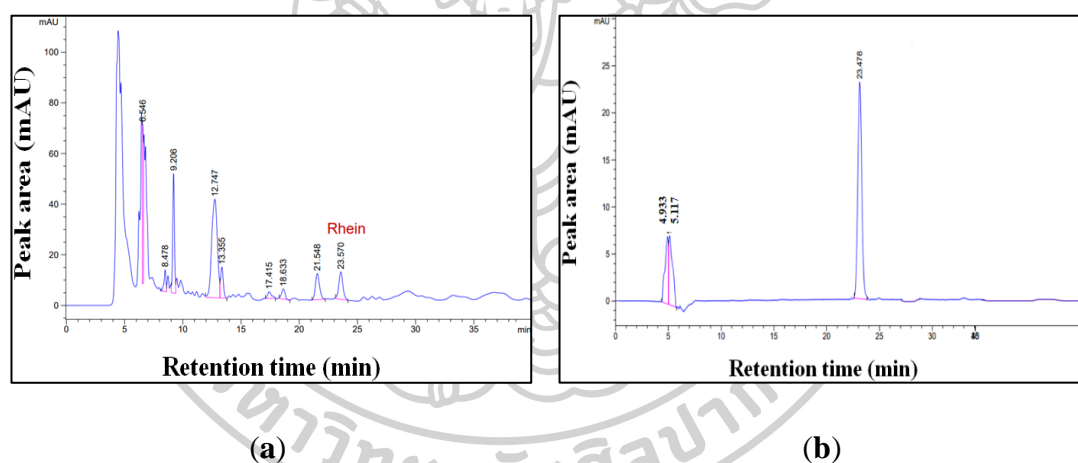
Figure 35. Chromatographic profiles of Shellac Fibers Loaded SA Leaf Extract (**a**), and Standard Rhein (**b**) Demonstrating a Consistent Retention Time for the Rhein Peak at 23.5 min (173).

As outlined in Table 15 (173), the entrapment efficiency, evaluated across different electrospinning conditions, ranges from 58.88% to 105.42%. The results underscore the ability of the extract to entrap in the fibers which can be influenced by various operating conditions. The clear identification of the rhein peak in the chromatograms further validates the precision of the HPLC-DAD method in

quantification of entrapped rhein, offering the deeper understanding into the effectiveness of the electrospinning procedure for encapsulating active ingredients within the nanofibers.

4.2.10. Conclusion

The concentration of shellac exerts the most significant influence on the morphological appearance of electrospun nanofibers, with applied voltage and extract content serving as secondary influencing factors. These findings underscore the effects of variations in applied voltage and shellac concentration on diameter of fiber, highlighting the intricate interactions among these variables and their implications for fiber characteristics. Electrospinning conditions characterized by high applied voltage, shellac, and extract contents efficiently minimize the bead formation.

Shellac content, extract content, and voltage were observed as key parameters affecting entrapment efficiency, with beneficial outcomes obtained under operating with increased voltage and minimal levels of shellac and extract. The optimal parameters, which included 38.5% w/w shellac content, 3.8% w/w extract content, and a 24 kV applied voltage, resulted in nanofibers with a smaller diameter (306 nm), a low bead-to-fiber ratio (0.29), and a remarkable 96% entrapment efficiency of extract into fibers.

4.3. Characterization and evaluation of optimized nanofibers
4.3.1. Scanning Electron Microscope (SEM)

Scanning electron microscopy (SEM) was employed to examine the morphological features of shellac fibers incorporated SA leaf extract. The fiber diameter and bead-to-fiber ratio, determined from SEM images, are presented in Table 15 (173). These findings were clearly supported by SEM images in Figure 36 and 37 (173). Specifically, Figures 36(a) and 36(b) display distinct forms of fibers at different proportion of shellac while the other factors remain constant in operating conditions, illustrating a discernible large fiber diameter with maximal shellac content.
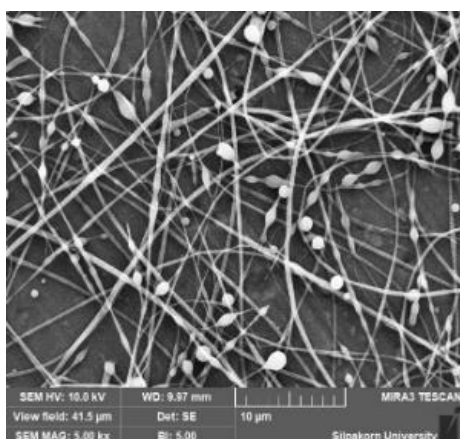
Diameter = 280.29 ± 21.53 nm

Conditions:

Shellac: Extract ratio - 35:4 (% w/w)

Voltage - 16.5 kV

Feed rate - 0.8 mL/h

(**a**)
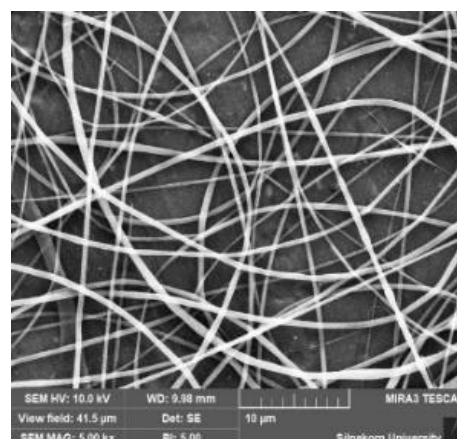
Diameter = 422.25 ± 22.60 nm

Conditions:

Shellac: Extract ratio - 45:4 (% w/w)

Voltage - 16.5 kV

Feed rate - 0.8 mL/h

(**b**)
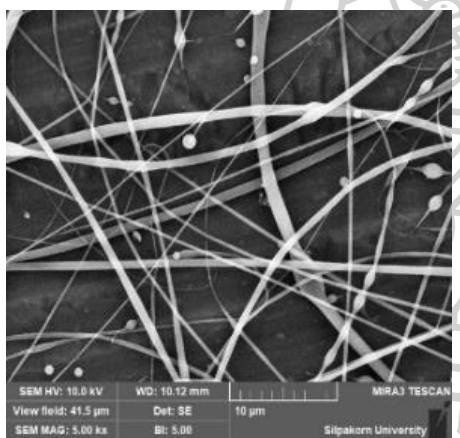
Diameter = 480.01 ± 8.57 nm

Conditions:

Shellac: Extract ratio - 40:4 (% w/w)

Voltage - 9 kV

Feed rate - 0.8 mL/h

(**c**)
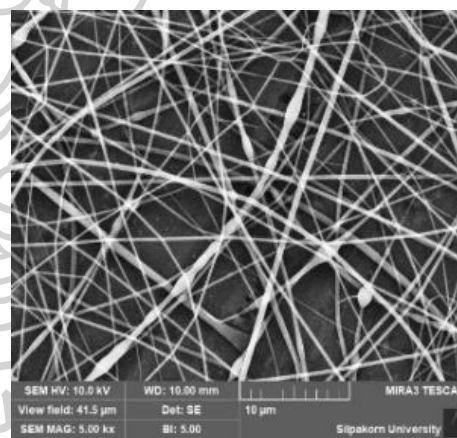
Diameter = 351.06 ± 20.18 nm

Conditions:

Shellac: Extract ratio - 40:4 (% w/w)

Voltage - 24 kV

Feed rate - 0.8 mL/h

(**d**)

Figure 36. SEM Images Illustrating the Individual Effect on Fiber Diameter: Low Shellac Content (**a**); High Shellac Content (**b**); Low Voltage (**c**); High Voltage (**d**) (173).

Figures 36(c) and 36(d) show that significant differences in fiber diameter were found under various applied voltages at constant shellac-to-extract ratios and flow rates. More specifically, compared to lower voltage levels, an increase in applied voltage caused a decrease in fiber diameter. This observation indicates that electrospinning at high voltage levels might be a favorable condition to achieve smaller and controllable fibers. The correlation of applied voltage and fiber diameter warrants additional investigation, as it may have complications for optimizing electrospinning techniques in the production of shellac fibers loaded with SA leaf extract.

Bead-to-fiber ratio = 2.37

Conditions:

Shellac: Extract ratio - 35:1 (% w/w)

Voltage - 16.5 kV

Feed rate - 0.8 mL/h

(**a**)

Bead-to-fiber ratio = 0.05

Conditions:

Shellac: Extract ratio - 45:1 (% w/w)

Voltage - 16.5 kV

Feed rate - 0.8 mL/h

(**b**)
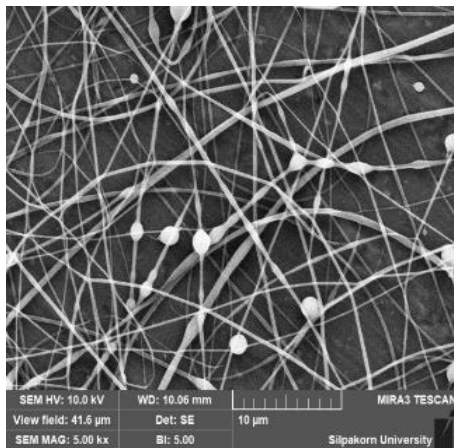
Bead-to-fiber ratio = 0.37

Conditions:

Shellac: Extract ratio - 40:1 (% w/w)

Voltage - 16.5 kV

Feed rate - 0.4 mL/h

(**c**)
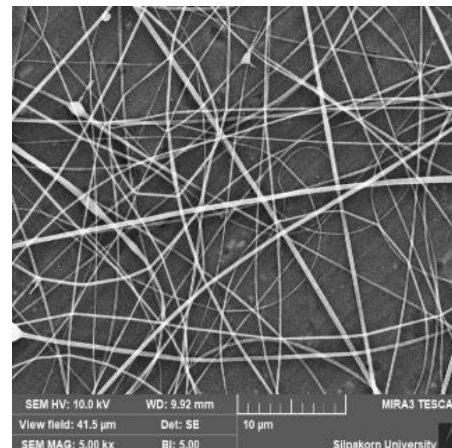
Bead-to-fiber ratio = 0.09

Conditions:

Shellac: Extract ratio - 40:4 (% w/w)

Voltage - 16.5 kV

Feed rate - 0.4 mL/h

(**d**)
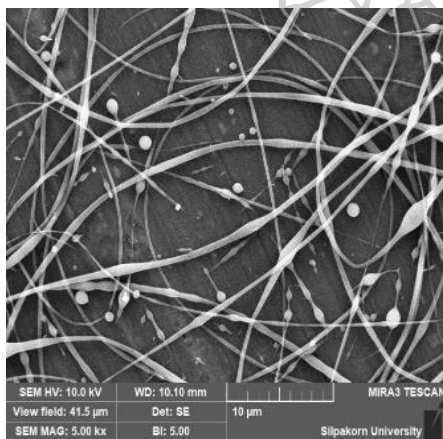
Bead-to-fiber ratio = 1.31

Conditions:

Shellac: Extract ratio - 40:2.5 (% w/w)

Voltage - 9 kV

Feed rate - 0.4 mL/h

(**e**)
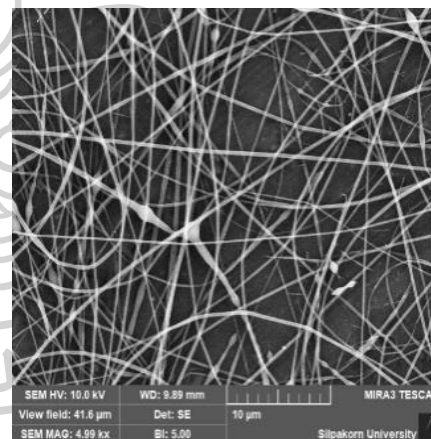
Bead-to-fiber ratio = 0.43
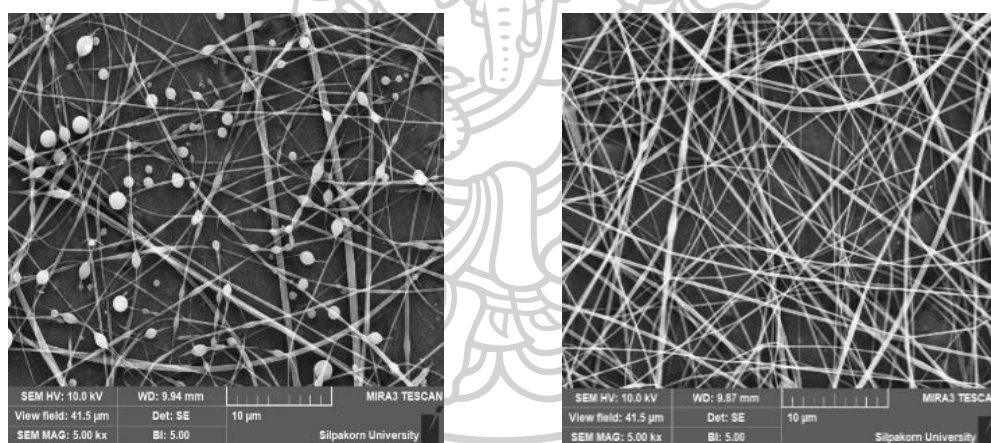
Conditions:

Shellac: Extract ratio - 40:2.5 (% w/w)

Voltage - 24 kV

Feed rate - 0.4 mL/h

(**f**)

Figure 37. SEM Images Illustrating the Individual Effect on Bead-to-Fiber Ratio: Low Shellac Content (**a**); High Shellac Content (**b**); Low Extract Content (**c**); High Extract Content (**d**); Low Voltage (**e**); High Voltage (**f**) (173).

In Figure 37(a) and 37(b), the SEM images provide a clear visual representation of the shellac concentrations (35% w/w and 45% w/w) influencing on the bead-to-fiber ratios under consistent electrospinning conditions. It is apparent that minimal shellac concentration promotes the beads generation on the strings of fibers. Additionally, Figures 37(c) and 37(d) emphasize the effect of different extract content on bead formation. In this case, a reduced extract content leads to fibers with a greater incidence of beads, highlighting the susceptibility of the electrospinning to the extract content

Examining the impact of voltage on the bead-to-fiber ratios, Figure 37(e) and 37(f) illustrates a significant disparity in the high and low level of applied voltage. Specifically, decreased voltage levels result in a higher bead amount compared to increase voltage settings. This observation suggests that the electric field strength during the electrospinning process plays a crucial role in influencing bead formation.

4.3.2. Fourier Transform Infrared (FTIR) spectroscopy

The investigation into the chemical components and interaction of shellac and SA leaf extract following the fabrication of electrospun fibers was conducted using FTIR. The presence of the carboxy group in both shellac and the extract were confirmed by detecting peaks at 1709 cm^{-1} and 1706 cm^{-1}, corresponding to C=O stretching vibrations, as well as peaks at 1463 cm^{-1}, 1374 cm^{-1}, and 1247 cm^{-1} for shellac, and 1448 cm^{-1}, 1361 cm^{-1}, and 1259 cm^{-1} for the extract, indicative of C−O stretching vibrations (Figure 38) (173). Additionally, prominent peaks at 3400 cm^{-1} and 3301 cm^{-1} for shellac and the extract, respectively, were observed, representing O−H stretching vibrations and confirming the presence of hydroxy groups. The absorption peaks of C−H stretching occurred at 2928 cm^{-1} and 2856 cm^{-1} of shellac, and 2919 cm^{-1} and 2850 cm^{-1} of extract. The recognition of specific peaks in the bleached shellac and extract aligned with previous research findings (30, 182-186).

The FTIR spectrum of the optimized extract is composed of wide bands related to OH groups (at 3301 cm^{-1}), moderate peaks linked to C−H stretching (at 2919 cm^{-1} and 2850 cm^{-1}), paired C=C−C stretching bands within aromatic rings (at 1600 cm^{-1} and 1448 cm^{-1}), distinctive peaks suggesting conjugated carbonyl (C=O) groups (at 1706 cm^{-1}), and moderate peaks associated with C−O groups (at 1039 cm^{-1}). These characteristic peaks in the SA leaf extract spectrum correlate with the rhein's structural characteristics (refer to Figure 1) and support prior research findings (143). This consistent pattern clearly indicates that rhein is a primary constituent of the extract.

Due to the significant proportion of shellac in the shellac to extract ratio, their physical mixtures displayed an FTIR spectrum almost identical to that of bleached shellac. However, a remarkable shift in most of the absorption peaks of extract towards larger frequencies was observed in the resultant fibers: 3301 cm^{-1} to 3381 cm^{-1}, 2919 cm^{-1} to 2928 cm^{-1}, 2850 cm^{-1} to 2856 cm^{-1}, 1706 cm^{-1} to 1710 cm^{-1}, 1600 cm^{-1} to 1635 cm^{-1}, and 1448 cm^{-1} to 1463 cm^{-1}. The rhein compound in the extract forms a hydrogen bond with the shellac, which leads to a shift in the spectrum of fiber.

The observed shift in the fiber spectrum indicates that SA leaf extract was successfully incorporated into the shellac matrix during the electrospun operating procedure, which may have consequences for the functional characteristics of the resultant fibers. These results demonstrate that controlled electrospinning procedures can be used to customize fiber compositions for particular applications, providing a fundamental step for future research in related fields and delivery of drugs, among other areas.
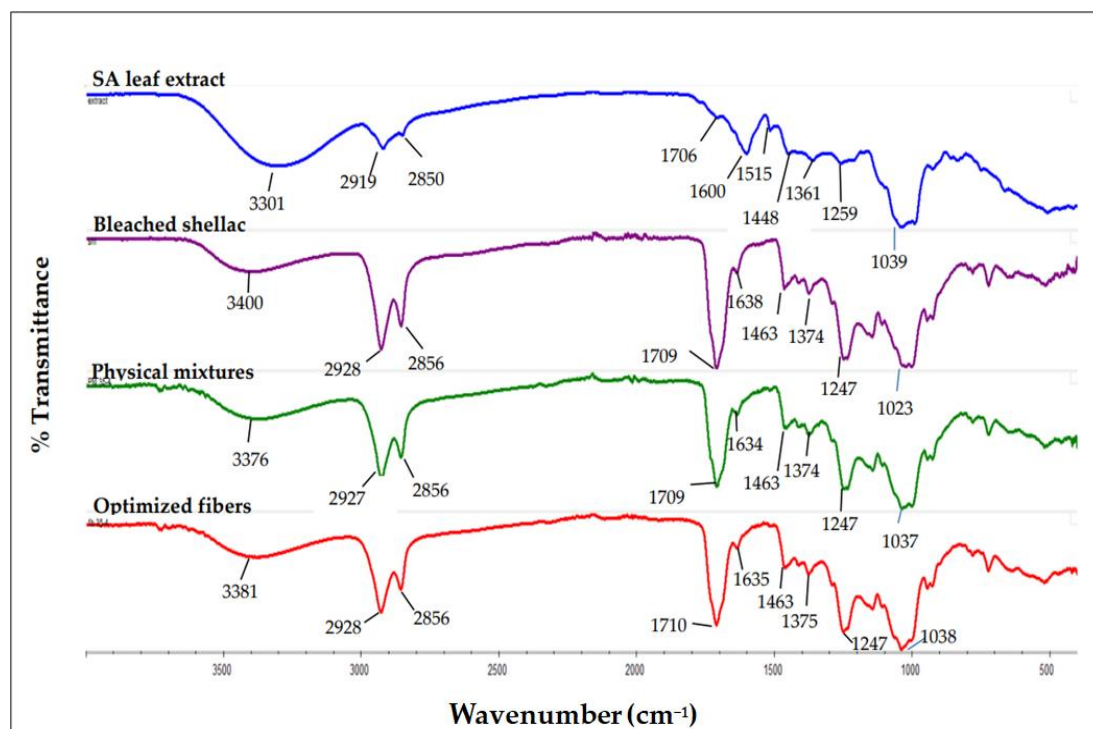
Figure 38. FTIR Spectrum of SA Leaf Extract, Bleached Shellac, their Physical Mixtures, and Optimized Fibers (173).

4.3.3. Powder X-ray Diffraction (PXRD)

The PXRD patterns of SA leaf extract, bleached shellac, and their physical mixture and optimized fiber are shown in Figure 39 (173). Broad peaks were seen at $2\theta^o$ angles of $9.90 \pm 0.3°$, $18.21 \pm 0.14°$, and $39.40 \pm 0.3°$ in the diffractograms of bleached shellac, with related intensities of 218 ± 19, 1288 ± 43, and 358 ± 30, respectively. The broad peaks, with intensities of 1186 ± 34 and 1209 ± 34, respectively, were seen at $2\theta°$ angles of $18.45 \pm 12°$ and $18.54 \pm 12°$ in the physical mixes and fibers. Remarkably, the diffractogram of SA leaf extract was ambiguous and did not yield precise data, indicating that it was an amorphous material. Given that shellac is a low-crystallinity, semi-crystalline polymer (187), the wide peaks seen in its PXRD pattern suggest an amorphous nature (30, 182). The diffraction pattern of the SA leaf extract likewise showed this amorphous quality, which was consistent with the general pattern. Crucially, there were no significant differences noticed between the electrospun shellac fibers loaded with SA leaf extract and the physical mixtures. SA leaf extract has been

successfully incorporated into the shellac matrix, as evidenced by the amorphous form of the electrospun fibers and physical mixtures. The fact that amorphous forms are frequently linked to improved solubility and bioavailability of active medicinal substances, this is crucial for potential applications. The PXRD study results demonstrate the electrospinning process's capacity for creating composite fibers with homogeneous and amorphous properties, highlighting its potential for use in controlled drug delivery systems.
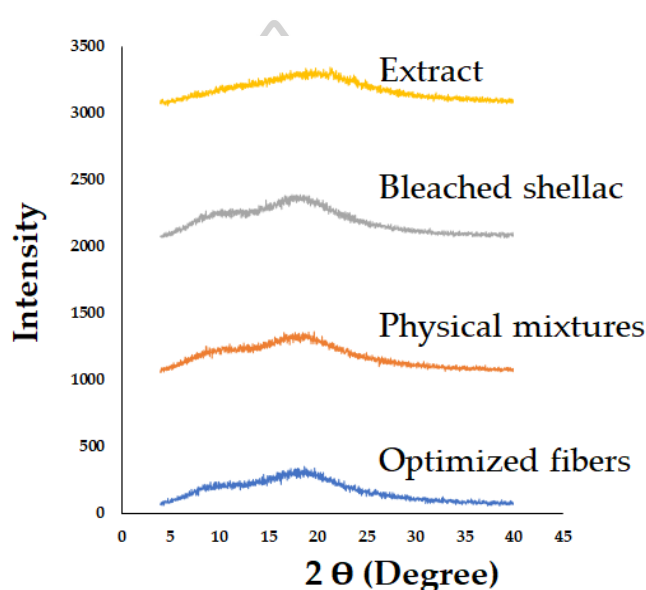
Figure 39. Diffractogram of SA Leaf Extract, Bleached Shellac, their Physical Mixtures, and Optimized Fibers (173).

4.3.4. Differential Scanning Calorimetry (DSC)

The results acquired from employing DSC to assess the thermal behaviors of the fibers are shown in Figure 40 (173). According to earlier research, the endothermic peak of bleached shellac was measured around 54 °C (30). Identical peaks were found at temperatures of 55.04 °C and 55.75 °C in fibers and physical mixtures, respectively.

It's interesting to note that DSC thermogram of SA leaf extract showed no obvious peak. Although the extract showed a large exothermic peak at 185.84 °C, the fiber thermogram did not show this feature. The existence of this peak could be explained by the extract's decomposition or by the SA leaf extract's full integration into the fibers. It presents interesting possibilities since the fiber thermogram around the

temperature of the SA leaf extract's exothermic peak does not show an apparent peak. It implies that the extract might have been effectively incorporated into the fibers through the electrospinning process, modifying the extract's thermal properties.
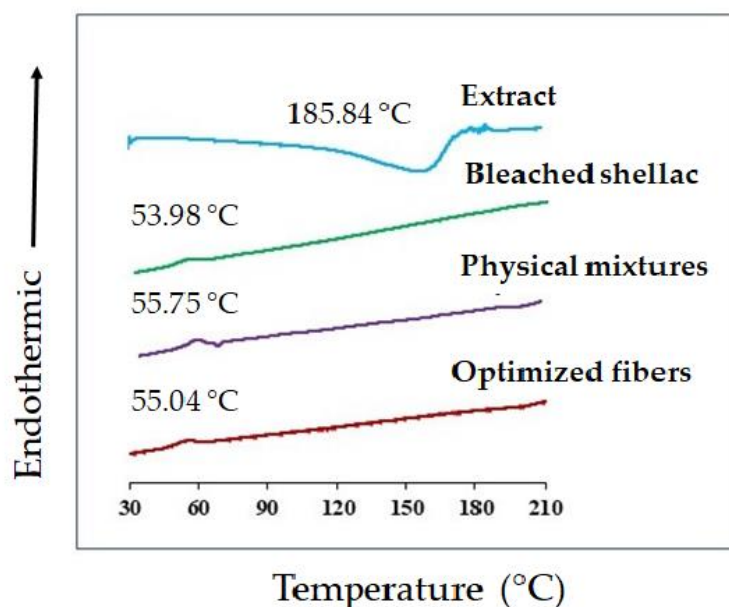
Figure 40. Thermal Analysis Diagrams of SA Leaf Extract, Bleached Shellac, their Physical Mixtures, and Optimized Fibers (173).

This finding emphasizes that the electrospinning process is transformative, which could have an impact on the thermal properties of composite fibers. Additional research on the interactions and structural alterations that take place during the electrospinning procedure could provide significant insights into the effective incorporation of SA leaf extract into the shellac matrix. The DSC findings highlight the future opportunity of electrospinning as a technique for customized drug delivery systems, where the final product's stability and functionality greatly depend on its thermal properties.

4.3.5. *In vitro* release study

As shown in Figure 41(a) (173), the release patterns of all fiber samples primarily coincide in the releasing media with a pH of 7.4. In the first hour, a preliminary release of rhein was seen in all fiber samples, with a range of 63% to 88%. The highest cumulative release observed for each sample was below: 90.95% for Run

3 (large-diameter fibers), 91.72% for Run 18 (large-diameter fibers), 88.94% for Run 19 (small-diameter fibers), 92.88% for Run 25 (small-diameter fibers), 94.50% for the optimized fibers, and 81.61% for the intact extract. The findings suggest that infusing the extract to the shellac fibers facilitated the release of rhein.

At a pH of 6.8, as demonstrated in Figure 41(b) (173), incomplete release of rhein was observed from all fibers. Consequently, at pH 7.4, compared to pH 6.8 media, a higher percentage of rhein was released cumulatively from all fiber samples. Following a 24-h incubation in each releasing medium, all fibers and the extract dissolved entirely at pH 7.4, whereas all fiber samples could not achieve full solubility at pH 6.8. The pH 6.8 medium retained undissolved fibers, as it is below the pH at which shellac dissolves. There were no significant variations in the cumulative release of the intact extract between the two pH levels.

(a) **(b)**
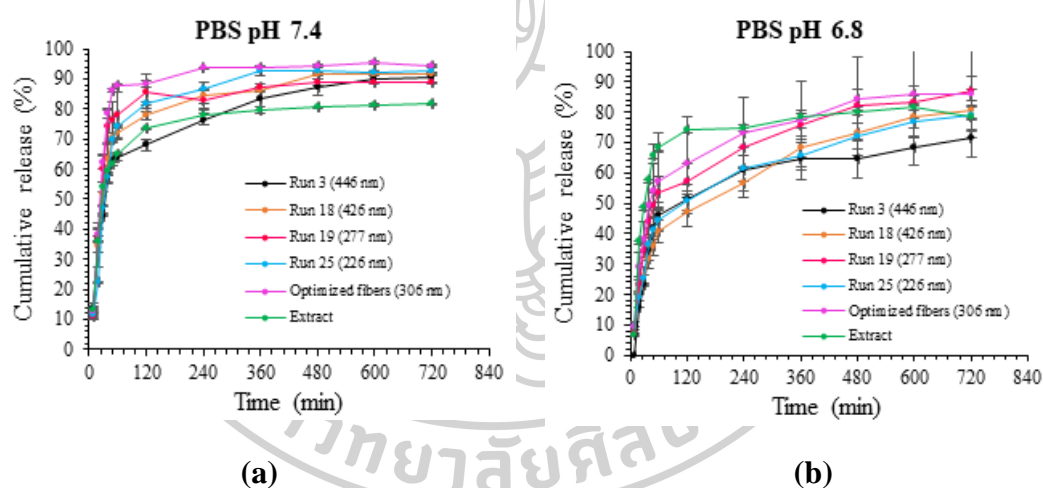
Figure 41. Overall Release Pattern of Rhein in Different Media at pH 7.4 **(a)**, and pH 6.8 **(b)** (173)**.**

The release of rhein from each run of fiber sample reached the maximum at 4 h and remained steady for the further 12 h, suggesting continuous release after the initial burst. Over the course of this prolonged duration, residual rhein molecules were consistently released at a relatively uniform rate. The continuous release was commonly ascribed to the drug or compound diffusing through the fiber matrix. The matrix

maintains a constant release rate as molecules continuously replenish and diffuse out of the fibers (188). Furthermore, the comparatively slow rate of shellac dissolution facilitates the emergence of continuous release profiles, which is affected by water uptake and swelling. This emphasizes the effectiveness of these fibers for applications involving controlled release of pharmaceuticals (189).

The optimized fibers exhibited a dual-phase release pattern in media with pH values of 7.4 and 6.8. This releasing profile consisted of an initial rapid release followed by a prolonged and steady release. The initial burst release is commonly observed when a portion of the substance is rapidly released from the surface or nearby regions of the fibers. This mechanism facilitates the immediate release of compounds and is often linked to molecules present on the surface of the fiber matrix or loosely bound to it (188).

The optimized fibers displayed superior rhein release compared to other fiber samples. Particularly noteworthy was the faster rhein release of the optimized fibers compared to small and large diameter of fibers, peaked release within 4 h. In contrast, smaller-diameter fibers reaching maximum release after 6 h, while larger-diameter fibers exhibited the highest cumulative percent of release at 8 h. These outcomes can be contributed to the effect of fiber diameter on drug release kinetics. Smaller-diameter fibers demonstrated accelerated release, achieving peak levels in a short duration of 6-h period. This behaviour is related to their heightened surface area-to-volume ratio, which promotes increased contact between drug-loaded fibers and the surrounding medium. The expanded surface area facilitates a more rapid rate of drug release (190).

Conversely, larger-diameter fibers, characterized by diminished porosity and a decreased surface area-to-volume ratio, exhibited a more gradual release profile. The extended diffusion path and restricted interaction with the surrounding medium led to a slow release of the drug. The optimization procedure employed to produce the optimized fibers especially targeted the enhancement of surface area and diffusion properties. This optimization is likely responsible for the relatively accelerated release observed in these fibers when compared to others. These results underscore the pivotal influence of fiber diameter on the dynamics of drug release in electrospun fibers, offering valuable insights for customized drug delivery system.

In comparison to pH 7.4, rhein release from all fiber samples was significantly reduced at pH 6.8 in case of pH-dependent release. Shellac exhibits a relatively high dissolution pH of approximately 7.3. This can be attributed to the limited solubility of shellac in aqueous solutions, resulting in incomplete rhein release in the pH 6.8 medium (191). Moreover, shellac displayed complete solubility at a pH of 7.4, surpassing its dissolution pH, leading to the greater rhein release (183, 192). The extract appeared to be fully dissolved in both pH conditions (pH 7.4 and pH 6.8). Nevertheless, the release of the extract was relatively slower compared to that of the fibers. Importantly, all fiber samples exhibited an enhanced cumulative release compared to the extract. The faster drug release from fibers could be attributed to accelerated polymer hydration, degradation, or facilitated drug diffusion processes (125).

The amorphous nature of the extract, coupled with the nanometer-sized diameters of the fibers, markedly elevated the rhein release in PBS solution (pH 7.4) compared to the release from the intact extract. Furthermore, it is important to highlight the presence of biphasic release profiles, characterized by an initial burst of release succeeded by a sustained and gradual release which has the potential to extend the duration of bacterial inhibition efficacy (98). This distinctive release pattern emphasizes the adaptability and favorable therapeutic outcomes of electrospun shellac fibers containing SA leaf extract.

The results highlight the significance of pH-dependent release patterns of rhein in electrospun fibers, indicating the significance of considering environmental conditions when developing drug delivery systems. This knowledge provides valuable perspectives for the advancement of controlled drug release and formulation design within the field.

4.3.6. Release kinetics

Various kinetic models, such as zero-order, first-order, Higuchi's, and Korsmeyer–Peppas models, were fitted with the release data acquired from the pH 7.4 and 6.8 medium to examine the release kinetics of fibers. The best fitting model was selected according to the lowest AIC, highest MSC, and highest Adj R^2 values (173, 193). Specifically, in Run 19 and Run 25, which involved small-diameter fibers, and in the case of optimized fibers, the zero-order release kinetics demonstrated high accuracy

in a pH 7.4 medium with the R^2 values of 0.9217, 0.9722, and 0.9604, respectively. On the other hand, for large-diameter fibers in Run 3 and Run 18, the first-order release kinetics were observed, with R^2 values of 0.9741 and 0.9558, respectively. The zero-order release pattern, characterized by a sustained and consistent release of the drug, is the preferred pattern to minimize explosive release and maintain a consistent level drug within the therapeutic range (189).

By applying different mathematical models to analyze the release data from PBS at pH 6.8, it was observed that the first-order kinetics model provided the most precise description for both optimal and small-diameter fibers. This indicates that the amount of drug remaining in the matrix is closely correlated with the rate of drug release (194).

Conversely, the Korsmeyer–Peppas model was demonstrated using large-diameter fibers. Run 3 showed a 1.279 release exponent (n), indicating the possibility of a Super Case II transport mechanism. Run 18 (large-diameter fibers) showed anomalous or non-Fickian behavior with a release exponent (n) of 0.730. This finding suggests that a combination of diffusion and erosion mechanisms affect drug release, indicating a complex drug release pattern (195).

This extensive investigation of release kinetics offers useful details on the different behaviors that different kinds of fiber exhibited in response to pH variations. Determining the appropriate release profiles for increased therapeutic efficacy involves customizing drug delivery systems, which requires an understanding of these mechanisms.

4.3.7. Antimicrobial activity of optimized nanofibers

The time-kill study is a well-established microbiological assessment method used to evaluate the bactericidal activity of antimicrobial substances by assessing their ability to eradicate bacteria. In this investigation, the time-varying antibacterial effects of the optimized fibers were evaluated in comparison to those of the extract alone. As depicted in Figure 42 (173), the time–kill profiles illustrate the antibacterial activity against three different microbes—*S. aureus*, *P. aeruginosa*, and *E. coli*. Each data point represents the percentage of survival bacterial cells at designated time intervals (n = 3). Following a 9-h incubation period, a notable decrease in living microbial cells was

revealed in both the optimized fibers and extract for all bacteria. Figure 43 illustrates the antibacterial activities of the optimized fibers (173).
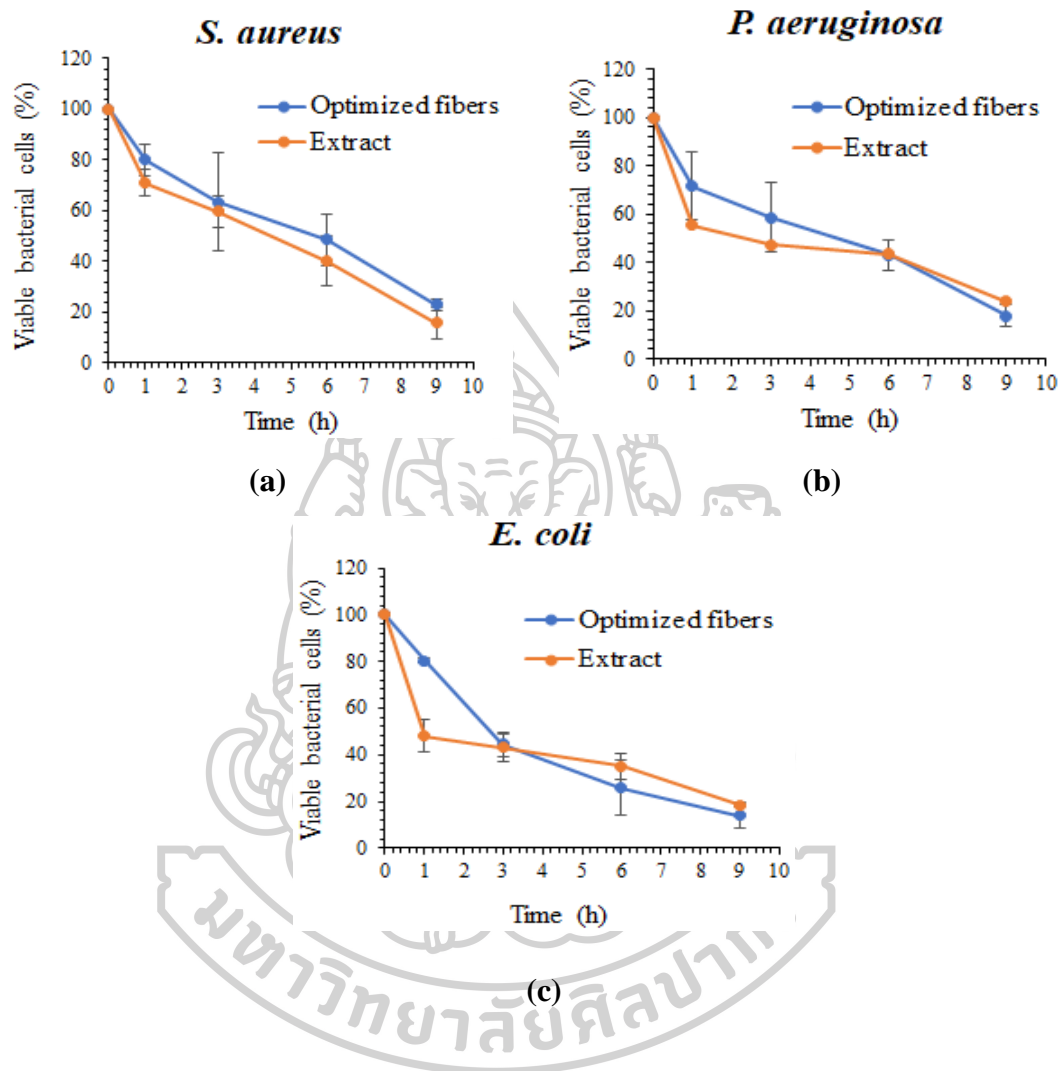
Figure 42. Time–Kill Kinetics of Optimized Fibers and SA Leaf Extract against *S. aureus* **(a)**, *P. aeruginosa* **(b)**, and *E. coli* **(c)** (173).
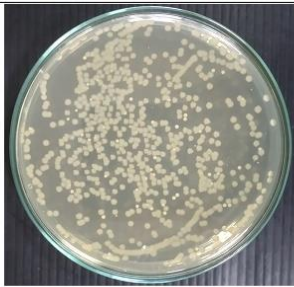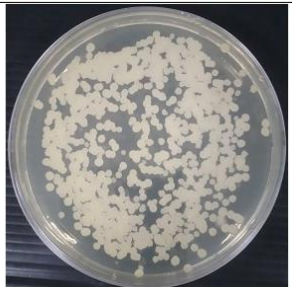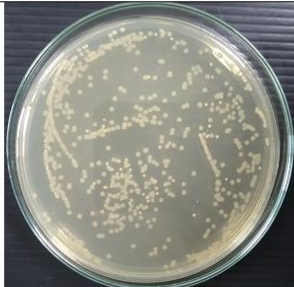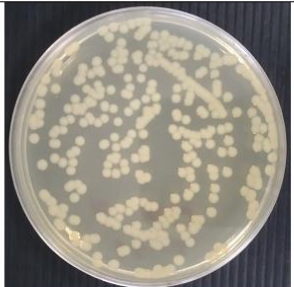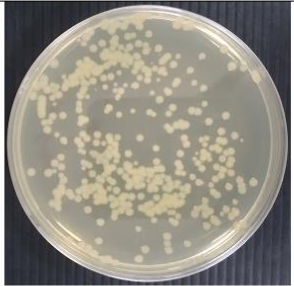
During a 9-h incubation period, the optimized fibers exhibited a significant reduction in microbial loads for *S. aureus*, resulting 23.01% compared to the controlled bacterial sample (Figure 42(a)). Notably, the optimized fibers demonstrated superior antimicrobial activity, evident in decreased viable bacterial cells for both *P. aeruginosa* (17.70%) and *E. coli* (13.88%) in comparison to the extract after 9-h of incubation (Figure 42(b, c)). The results of this investigation underscore that the optimized fibers

exhibited enhanced bacteriostatic effects against *P. aeruginosa* and *E. coli* after a 9-h incubation period when compared to the SA leaf extract alone.

In the initial hour following the administration of the fiber-loaded extract, a rapid release of rhein was noted, as depicted in Figure 41. This observation is consistent with the results obtained from the optimized fibers, indicating a markedly enhanced decrease in viable cell number against each pathogen after 1 h of incubation. Moreover, with the extension of the incubation period to 9 h, a progressive decline in the proportion of viable bacterial cells was observed (Figure 42 and 43). These findings collectively suggest that optimized fibers loaded with SA leaf extract have the potential to serve as an efficacious wound dressing product, exhibiting prolonged and strong antimicrobial activity against a diverse array of bacterial strains.

The time–kill effects of both fibers and extract consistently showed a significant reduction in living bacterial cells at every designated time interval, although notable differences in bacterial survival rates were observed between these two samples. Particularly within the initial hour, it is evident that the SA leaf extract exhibited a quicker reduction in bacterial count compared to the optimized fibers, possibly due to disparities in release characteristics.

Earlier research has suggested a possible connection of the antimicrobial properties of electrospun fibers and their drug release behaviours (190). The findings of this research suggest that the optimized fibers effectively regulate the gradual release of antibacterial compounds from the matrix during the incubation period. One possible explanation for the swift reduction in microbial growth in the early period is that the extract may have direct contact with the microorganisms, whereas the optimized fibers possess the ability to sustain an antibacterial effect for a more extended duration.

Times	*S. aureus*	*P. aeruginosa*	*E. coli*
0 min			
Microbial load (CFU/mL)	3.46×10^8 (100% viable microorganisms)	10.50×10^8 (100% viable microorganisms)	7.20×10^8 (100% viable microorganisms)
1 h			
Microbial load (CFU/mL)	2.9×10^8 (80.02% viable microorganisms)	9.12×10^8 (71.53% viable microorganisms)	5.84×10^8 (80.36% viable microorganisms)
3 h			
Microbial load (CFU/mL)	2.42×10^8 (63.39% viable microorganisms)	7.54×10^8 (58.61% viable microorganisms)	3.46×10^8 (44.42% viable microorganisms)
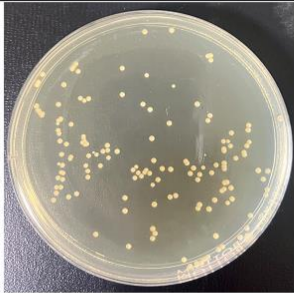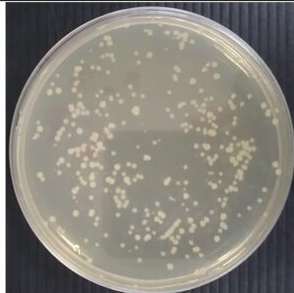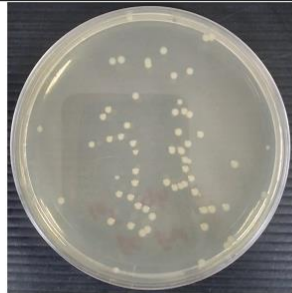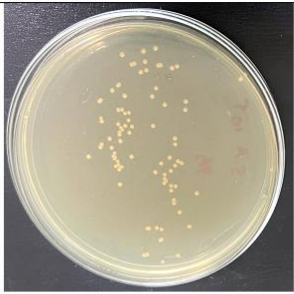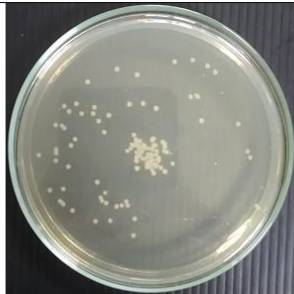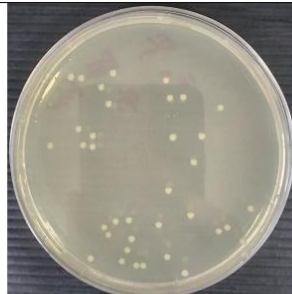
Times	*S. aureus*	*P. aeruginosa*	*E. coli*
6 h			
Microbial load (CFU/mL)	1.76×10^8 (48.50% viable microorganisms)	5.26×10^8 (43.12% viable microorganisms)	1.26×10^8 (25.74% viable microorganisms)
9 h			
Microbial load (CFU/mL)	7.00×10^7 (23.01% viable microorganisms)	2.20×10^8 (17.70% viable microorganisms)	7.40×10^7 (13.88% viable microorganisms)

Figure 43. Antimicrobial Activities of Optimized Fibers (173).

The incorporation of controlled release mechanisms may prolong the exposure of the bacteria to antibacterial substances, potentially leading to a steady yet continuous decrease in the living bacterial count. Moreover, divergence of antimicrobial efficacy against diverse microbes observed in the research can be linked to factors such as the contribution and quantity of active substances in the extract, along with specific interactions between the fiber matrix and bacteria.

At the end of the incubation period, the optimized fibers exhibited higher rhein release, leading to a more effective reduction in microbial loads. This may be attributed to the fibbers' capacity to promote air circulation, thus aiding in optimal wound healing. Further research is needed to clarify the underlying mechanisms and practical implications of these materials in antimicrobial treatment. Additionally, exploring

broader applications in wound care is essential to maximize their effectiveness in clinical settings.

4.3.8. Stability study

The optimized fibers and extract were subjected to controlled storage conditions, with normal conditions maintained at 25 °C and stress conditions at 40 °C with 75% RH, over a 90-day period. Figure 44 graphically represents the percentage of retained rhein content in the samples at initial, 30, 60, and 90 days after storage in these distinct environments. After 90 days in normal storage conditions, there were no observable changes in the physical appearance of both the fiber and extract. However, within the stability chamber, the fibers exhibited alterations in colour and texture, turning brown and sticky after 30 days, while the extract maintained its original characteristics.

The average retaining rhein content (%) in the SA leaf extract remained consistently stable during storage under both normal and stress conditions, with no statistically significant differences noted. The rhein content in the extract demonstrated sustained stability throughout the entire 90-day period under both storage conditions. These findings align with a prior study where the stability of SA leaf extract was successfully demonstrated over a 4-month period under accelerated conditions at 45°C and 75% RH (43).

Under normal conditions at 25°C, the amount of rhein content in the fibers exhibited no decline over the entire 90-day period. In contrast, under accelerated conditions in the stability chamber, the retained rhein in the fiber mats remained stable up to 60 days, after which a slight decrease was observed, reducing from 98% to 91% after the full 90 days. The outcomes of this stability study suggest that the stability of SA leaf extract-loaded fiber mats is better preserved under lower temperature storage conditions.
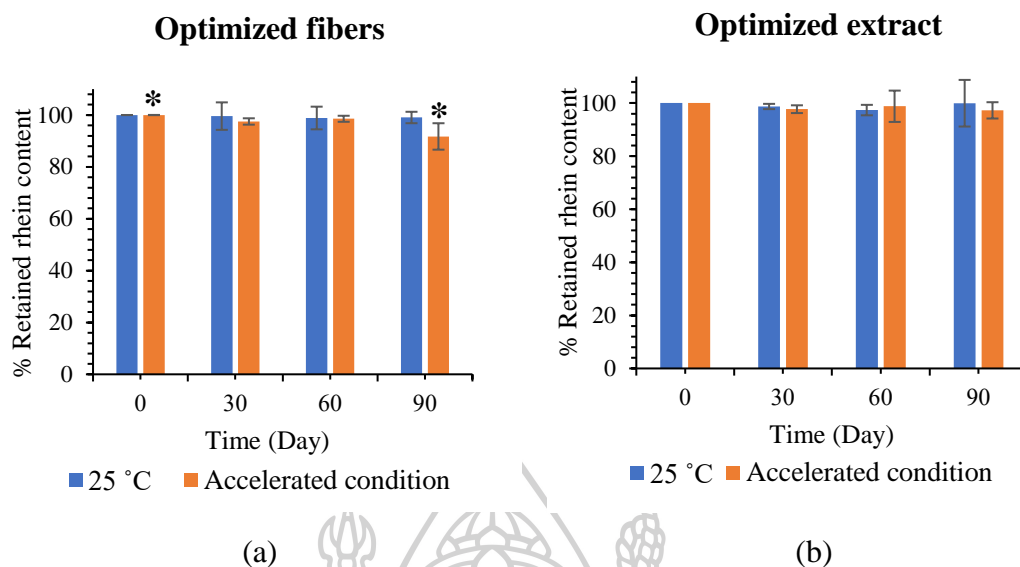
* Statistically significant differences at p-value <0.05

Results are shown as mean ± SD. Data were analyzed by SPSS software to estimate significant difference between the values at each time point.

Figure 44. Percentage of Retained Rhein contents at each Time Point under Different Storage Conditions; Optimized fibers (a), Extract (b).

4.3.9. Conclusion

In conclusion, the physicochemical characterization of shellac, SA leaf extract, their mixtures, and nanofibers, along with SEM analysis, highlight the critical role of precise control over processing parameters. The effective integration of SA leaf extract into shellac matrix was confirmed through FTIR and PXRD studies, revealing a notable shift in absorption peaks, indicating substantial interaction between rhein and shellac within the fibers. The DSC results emphasize the transformative character of the electrospinning procedure, offering insights into effective bioactive compound incorporation. The biphasic pattern observed in the *in vitro* release study of optimized nanofibers, coupled with demonstrated antimicrobial effectiveness against various pathogens, highlights the potential of electrospun fibers incorporated with SA leaf extract for applications in controlled release and antimicrobial strategies.

Chapter 5
Summary and general conclusion

This study successfully validated the rhein assay method in accordance with the ICH Q2 (R1) guideline, employing a meticulously developed HPLC–DAD method. The validated HPLC conditions include acetonitrile and 0.1% v/v of aqueous phosphoric acid (65:35) as mobile phase, at a flow rate of 1 mL/min with a detection wavelength 254 nm. These parameters significantly reduced the duration and solvent consumption for analysis while ensuring a high degree of purity (996 to 999), good resolution (7.34 to 7.87), and a short retention time for rhein.

The optimized conditions for preparation of a rhein-rich extract using the UAE technique were identified as 95% v/v ethanol, a solvent-to-solid ratio of 25:1 (mL/g), a temperature of 60 °C, and an extraction time of 18 min. The extraction temperature, duration, and the solvent-to-solid ratio were observed to be the main factors affecting the UAE method. RSM incorporated within the BBD demonstrated its effectiveness in optimizing extraction conditions to enhance the rhein content in SA leaf extracts.

Under the established optimal conditions, the rhein-rich extract exhibited a maximum yield of 10.36 ± 0.27 mg/g extract, showcasing potent antibacterial activity against *S. aureus*, *E. coli*, and *P. aeruginosa*.

The findings of this study not only support the efficacy of SA leaf extracts containing rhein for pharmaceutical preparations but also establish the foundation for the development of herbal cosmeceuticals and pharmaceuticals. The optimized rhein-rich SA leaf extracts, with their antibacterial and anti-inflammatory activities, hold promise for future applications in the field of skincare and pharmaceutical industries. This comprehensive study contributes valuable insights into the potential therapeutic benefits and safety of utilizing SA leaf extract in various formulations.

Due to its exceptional characteristics, shellac finds extensive applications in the food, pharmaceutical, and agricultural sectors, and it has been increasingly utilized in drug delivery systems. Medicated nanofibers are produced by combining a carrier polymer and desired active ingredients in a mixed solution or melt, often processed using single-fluid electrospinning. The electrospinning technique has gained prominence for efficiently generating fibers with diverse applications. This study

employed fractional factorial design to assess the significant effects of various factors on the morphological features of electrospun fibers, specifically focusing on fiber diameter and bead-to-fiber ratio. The BBD was employed to establish the optimal conditions conducive to achieving the desired morphology and properties of the fibers. The key parameter influencing fiber appearance was identified as shellac content. Optimal process and solution parameters were determined to produce nanofibers with reduced diameter (306 nm), a minimal bead-to-fiber ratio (0.29), and an impressive 96% entrapment efficiency of the extract within the fibers.

Furthermore, physicochemical characterization of shellac, SA leaf extract, their physical mixtures, and nanofibers was carried out using techniques such as DSC, PXRD, and FTIR spectroscopy. The morphological appearance of fibers, as indicated by SEM results, underscores the essential significance of careful management of processing variables. These parameters include the proportions of shellac and extract, along with voltage settings, and are pivotal in attaining the intended fiber morphology. A thorough comprehension of these interdependencies is vital for tailoring electrospinning conditions, enabling the production of fibers with distinct characteristics.

The characterization studies revealed effective incorporation of SA leaf extract into shellac fibers. FTIR spectra exhibited distinct characteristic bands for both the extract and shellac, confirming their presence. Notably, the fabrication of electrospun fibers loaded with SA leaf extract resulted in a significant shift in the absorption peaks of the extract towards higher frequencies. This shift, particularly in key functional groups like OH stretching, C−H stretching, C=O stretching, and C=C−C stretching within aromatic rings, suggests a substantial interaction between rhein (the primary extract component) and shellac within the fibers. This engagement is pivotal, signifying the harmony and fusion of the extract within the polymeric matrix, potentially impacting release patterns and overall fiber functionality.

In PXRD analysis, no significant differences were observed in diffractograms between electrospun shellac fibers loaded with SA leaf extract and physical mixtures indicating the compatibility of extract and shellac matrix, evident from the amorphous nature of the electrospun fibers and physical mixtures.

The DSC results highlight the transformative nature of the electrospinning process, providing insights into the effective incorporation of bioactive compounds into the fibers. In summary, these findings enhance the understanding of herbal extract optimization and contribute to the development of functional nanofiber-based materials.

A biphasic pattern was identified in the *in vitro* release study of the optimized nanofibers, with an initial rapid release that accounted for 88% within the first hour followed by a sustained release exceeding 90% for up to 12 h. Additionally, the antimicrobial effectiveness of the optimized fibers incorporated with SA leaf extract against *S. aureus*, *P. aeruginosa*, and *E. coli* was demonstrated. These fibers displayed remarkable control over the gradual release of rhein, leading to sustained reduction in viable bacterial count throughout the entire 9-hour incubation period. In stability testing, it was found that the SA leaf extract-loaded fiber mats remained stable for up to 60 days at 40°C with 75% RH. These results highlight the potential synergies achievable through the combination of electrospun shellac fibers with SA extract for antimicrobial applications. Further exploration into the mechanisms and modifications these materials show potential for developing creative and effective approach in the continuous battle against bacterial infections.

Suggestions for further studies

Based on the extraction of rhein from SA leaves and the optimization of extraction conditions, the scalability of the optimized extraction process can be investigated by assessing the conditions identified in this study when applied to larger volumes or batches, addressing practical considerations for industrial-scale production. The different formulations incorporating the rhein-rich extract should be explored for the development of novel pharmaceutical or cosmeceutical formulations, considering factors like stability, dosage forms, and potential combination with other active ingredients. By exploring these suggested areas for further studies, researchers can deepen their understanding of rhein extraction from SA leaves, optimize the process, and contribute to the development of practical applications in pharmaceuticals, cosmeceuticals, and related industries.

The release profiles of nanofibers should be further optimized by investigating additional factors, such as polymer blending or incorporation of other natural extracts. This could enhance the control and duration of the release, catering to diverse applications like sustained drug delivery or wound healing. The comprehensive biocompatibility assessments should be conducted to ensure the safety and compatibility of the electrospun nanofibers for various biological applications. This includes *in vivo* studies to validate the materials' efficacy and safety in living systems.

The antimicrobial studies including fungal strains should be conducted to encompass a broader spectrum of microorganisms. This would provide a more comprehensive understanding of the potential applications of the electrospun nanofibers in combating various types of microbial infections.

The scalable manufacturing processes should be explored for producing electrospun nanofibers with consistent quality on a larger scale. This step is crucial for transforming laboratory findings into practical applications and commercial products. By addressing these areas in future studies, researchers can contribute to the advancement of knowledge in the field of electrospun nanofibers, potentially paving the way for innovative applications in drug delivery, wound healing, and antimicrobial interventions.

Appendix

$$y = 22.4138x + 13.2070$$
$$R^2 = 0.9990$$
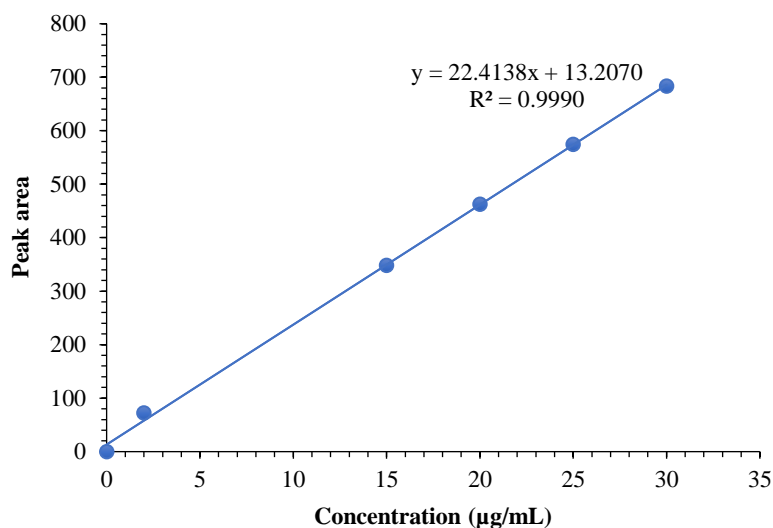
Figure 45. Calibration Curve of Standard Rhein

Table 21. Cumulative Rhein Release (%) of all Samples in PBS pH 6.8 (n=3).

Time (min)	Cumulative Release (%) (Mean ± SD)					
	Run 3 (446 nm)	Run 18 (426 nm)	Run 19 (277 nm)	Run 25 (226 nm)	Optimized fibers (306 nm)	Extract
10	0 ± 0.00	9.35 ± 0.00	7.01 ± 0.00	9.50 ± 0.00	9.59 ± 1.22	6.90 ± 0.00
20	15.77 ± 0.00	20.59 ± 0.00	23.31 ± 2.30	18.97 ± 0.99	29.22 ± 4.58	37.63 ± 0.00
30	23.40 ± 0.00	25.69 ± 3.10	34.54 ± 2.45	25.08 ± 1.45	38.22 ± 5.80	48.63 ± 0.00
40	34.18 ± 3.05	31.56 ± 2.93	44.12 ± 4.61	36.57 ± 1.85	49.22 ± 7.48	57.77 ± 0.00
50	41.81 ± 3.95	36.02 ± 3.13	49.32 ± 4.32	41.14 ± 1.91	53.99 ± 9.21	65.83 ± 3.36
60	45.91 ± 4.54	40.54 ± 3.80	53.57 ± 5.05	44.47 ± 3.56	57.10 ± 9.46	68.29 ± 4.61

120	51.41 ± 4.97	47.04 ± 4.63	57.36 ± 5.56	50.82 ± 3.36	62.90 ± 10.22	73.98 ± 4.55
240	61.18 ± 7.03	56.67 ± 5.00	68.40 ± 6.16	61.43 ± 4.29	73.33 ± 11.64	74.92 ± 1.14
360	64.87 ± 7.38	68.32 ± 6.53	75.84 ± 4.97	65.53 ± 4.49	77.64 ± 12.30	78.28 ± 1.14
480	64.42 ± 6.28	73.09 ± 7.54	81.96 ± 5.60	71.98 ± 4.39	84.36 ± 13.55	80.26 ± 1.14
600	68.57 ± 6.32	78.67 ± 6.81	83.08 ± 5.36	76.75 ± 5.22	86.09 ± 14.38	81.42 ± 1.14
720	71.62 ± 6.53	80.76 ± 6.89	87.01 ± 4.80	78.89 ± 4.63	85.83 ± 14.32	78.34 ± 3.07

Table 22. Cumulative Rhein Release (%) of all Samples in PBS pH 7.4 (n=3).

Time (min)	Cumulative Release (%) (Mean ± SD)					
	Run 3 (446 nm)	Run 18 (426 nm)	Run 19 (277 nm)	Run 25 (226 nm)	Optimized fibers (306 nm)	Extract
10	13.64 ± 0.55	11.82 ± 1.84	10.97 ± 0.91	11.31 ± 0.29	12.48 ± 0.22	13.13 ± 2.51
20	36.82 ± 1.01	34.63 ± 7.42	36.73 ± 1.08	22.32 ± 0.003	38.16 ± 2.33	36.25 ± 3.74
30	44.43 ± 0.08	51.59 ± 3.88	59.86 ± 4.41	46.93 ± 1.39	62.43 ± 2.35	54.24 ± 1.66
40	56.71 ± 1.56	63.25 ± 5.28	74.20 ± 5.83	57.36 ± 1.68	78.42 ± 1.30	59.34 ± 1.68
50	62.58 ± 1.25	70.46 ± 1.39	76.12 ± 6.24	69.68 ± 0.73	86.17 ± 0.31	61.86 ± 0.51
60	63.80 ± 0.99	71.98 ± 2.33	77.96 ± 7.53	74.19 ± 0.35	88.00 ± 0.24	64.85 ± 0.41

120	68.06 ± 1.79	77.74 ± 1.49	85.77 ± 5.61	81.68 ± 0.65	88.58 ± 1.09	73.38 ± 0.11
240	76.57 ± 1.92	84.25 ± 4.41	83.16 ± 3.21	86.63 ± 0.01	93.65 ± 0.39	78.20 ± 3.69
360	83.26 ± 3.77	86.38 ± 0.75	87.01 ± 1.05	92.67 ± 1.55	94.04 ± 0.11	79.62 ± 1.20
480	87.10 ± 2.78	91.67 ± 0.51	88.78 ± 0.92	92.83 ± 1.06	94.35 ± 0.28	80.61 ± 0.06
600	90.04 ± 1.38	91.47 ± 0.67	88.80 ± 0.05	92.22 ± 0.45	95.35 ± 0.52	81.44 ± 0.46
720	90.59 ± 1.58	91.72 ± 0.32	88.94 ± 0.14	92.88 ± 1.59	94.50 ± 0.50	81.61 ± 0.18
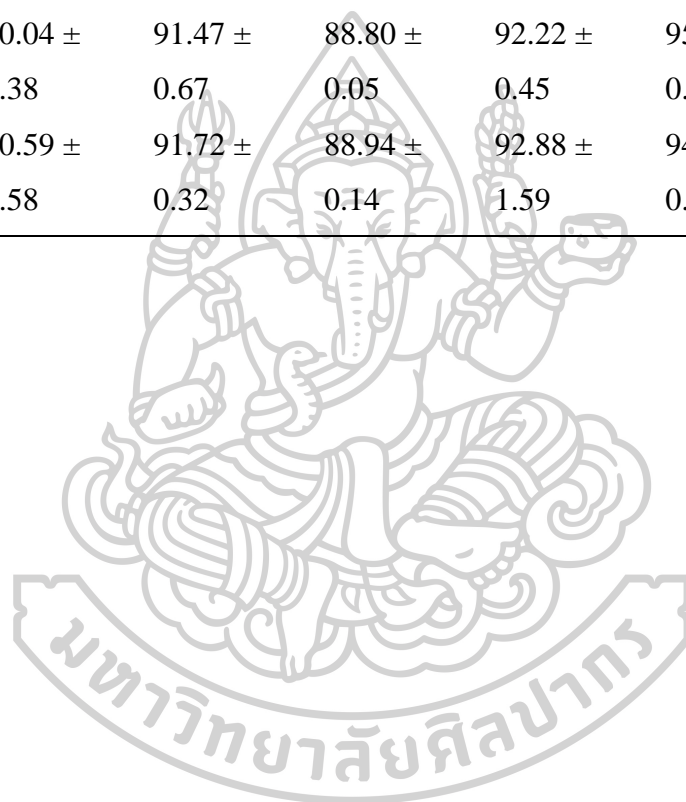
Table 23. Release Kinetic Model of Different Samples in pH 7.4.

Sample	Parameter	Model			
		Zero order	First order	Higuchi's	Korsmeyer-Peppas
Run 3 (Large fibers)	Adj R^2	0.9066	**0.9741**	0.8693	0.9466
	AIC	26.6231	**20.2000**	28.3012	24.3889
	MSC	1.9706	**3.2552**	1.6349	2.4174
		k0 - 1.382	**k1- 0.020**	kH - 8.349	kKP - 3.278
	n	-	-	-	0.764
Run 18 (Large fibers)	Adj R^2	0.9544	**0.9558**	0.8216	0.9534
	AIC	25.0948	**24.9385**	31.9180	25.7682
	MSC	2.6882	**2.7195**	1.3236	2.5535
	k	k0 - 1.529	**k1- 0.023**	kH - 9.154	kKP - 2.373
	n	-	-	-	0.880
Run 19 (Small fibers)	Adj R^2	**0.9217**	0.9104	0.7846	0.9062
	AIC	**29.3787**	30.0540	34.4412	30.8460
	MSC	**2.1476**	2.0125	1.1351	1.8541
	k	**k0 - 1.712**	k1- 0.028	kH - 10.229	kKP - 2.525
	n	-	-	-	0.894
Run 25 (Small fibers)	Adj R^2	**0.9722**	0.9107	0.7499	0.9676
	AIC	**22.9034**	28.7419	33.8908	24.2397
	MSC	**3.1835**	2.0158	0.9860	2.9162
	k	**k0 - 1.408**	k1- 0.020	kH - 8.320	kKP - 1.037
	n	-	-	-	1.083
Optimized fibers	Adj R^2	**0.9604**	0.8969	0.7893	0.9494
	AIC	**26.8842**	31.6741	35.2465	28.6763
	MSC	**2.8298**	1.8718	1.1573	2.4714
		k0 - 1.856	k1- 0.031	kH - 11.049	kKP - 2.232
	n	-	-	-	0.950

Table 24. Release Kinetic Model of Different Samples in pH 6.8.

Sample	Parameter	Model			
		Zero order	First order	Higuchi's	Korsmeyer-Peppas
Run 3 (Large fibers)	Adj R^2	0.9326	0.8983	0.6726	**0.9475**
	AIC	23.3433	25.4045	31.2487	**22.6540**
	MSC	1.6039	1.1916	0.0228	**1.7417**
	k	k0 - 0.814	k1- 0.010	kH - 4.735	**kKP - 0.291**
	n	-	-	-	**1.279**
Run 18 (Large fibers)	Adj R^2	0.9039	0.9655	0.9049	**0.9754**
	AIC	20.5897	15.4610	20.5368	**14.3343**
	MSC	1.9424	2.9682	1.9530	**3.1935**
	k	k0 - 0.789	k1- 0.010	kH - 4.778	**kKP - 2.117**
	n	-	-	-	**0.730**
Run 19 (Small fibers)	Adj R^2	0.9643	**0.9666**	0.7992	0.9559
	AIC	20.5888	**20.2472**	29.2210	22.2032
	MSC	2.9321	**3.0004**	1.2056	2.6092
	k	k0 - 1.055	**k1- 0.014**	kH - 6.289	kKP - 1.331
	n	-	-	-	0.937
Run 25 (Small fibers)	Adj R^2	0.9810	**0.9864**	0.8332	0.9837
	AIC	14.6579	**13.0036**	25.5285	14.4748
	MSC	3.5653	**3.8961**	1.3912	3.6019
	k	k0 - 0.863	**k1- 0.011**	kH - 5.163	kKP - 1.234
	n	-	**-**	-	0.902
Optimized fibers	Adj R^2	0.9410	**0.9716**	0.8353	0.9481
	AIC	23.4922	**19.8282**	28.6236	23.4099
	MSC	2.4301	**3.1629**	1.4038	2.4466
	k	k0 - 1.181	**k1- 0.016**	kH - 7.089	kKP - 2.111
	n	-	**-**	-	0.841

Table 25. Percentage of Viable Bacterial Cells at each Time Point (n=3).

Time (h)	*S. aureus*		*P. aeruginosa*		*E. coli*	
	Fibers	Extract	Fibers	Extract	Fibers	Extract
0	100 ± 0.00	100 ± 0.00	100 ± 0.00	100 ± 0.00	100 ± 0.00	100 ± 0.00
1	80.02 ± 6.16	70.94 ± 5.23	71.53 ± 14.15	55.26 ± 0.00	80.36 ± 1.06	47.92 ± 6.87
3	63.39 ±19.30	59.62 ± 6.06	58.61 ± 14.20	47.37 ± 0.00	44.42 ± 5.15	43.06 ± 5.89
6	48.50 ±10.30	40.14 ± 9.70	43.12 ± 6.37	43.42 ± 0.00	25.74 ± 11.65	35 ± 5.50
9	23.01 ± 2.48	15.72 ± 6.05	17.70 ± 4.55	23.68 ± 0.00	13.88 ± 5.09	18.61 ± 1.18

Table 26. Percentage of Retained Rhein contents at each Time Point (n=3).

Time (Day)	Optimized fibers		Extract	
	25ºC	Accelerated conditions (40 ºC, 75% RH)	25ºC	Accelerated conditions (40 ºC, 75% RH)
0	100 ± 0.00	100 ± 0.00 *	100 ± 0.00	100 ± 0.00
30	99.59 ± 5.30	97.52 ± 1.22	98.72 ± 0.99	97.71 ± 1.46
60	98.85 ± 4.37	98.56 ± 1.16	97.37 ± 1.97	98.82 ± 5.90
90	99.05 ± 2.20	91.74 ± 5.10 *	99.96 ± 8.79	97.27 ± 3.07

* Statistically significant differences at p-value <0.05

Results are shown as mean ± SD. Data were analyzed by SPSS software to estimate significant difference between the values at each time point.

REFERENCES

1.   Oladeji OS, Adelowo FE, Oluyori AP, Bankole DT. Ethnobotanical description and biological activities of *Senna alata*. Evidence-Based Complementary and Alternative Medicine. 2020;2020:2580259.

2.   Palanichamv S, Nagarajan S. Analgesic activity of *Cassia alata* leaf extract and Kaemferol 3-*O*-sophoroside Journal of Ethnopharmacology. 1990;29:73-8.

3.   Elujoba AA, Ajulo OO, Iweibo GO. Chemical and biological analyses of Nigerian *Cassia* species for laxative activity. Journal of Pharmaceutical & Biomedical Analysis. 1989;7(12):1453-7.

4.   Sagnia B, Fedeli D, Casetti R, Montesano C, Falcioni G, Colizzi V. Antioxidant and anti-inflammatory activities of extracts from *Cassia alata*, *Eleusine indica*, *Eremomastax speciosa*, *Carica papaya* and *Polyscias fulva* medicinal plants collected in Cameroon. PLOS One. 2014;9(8):e103999.

5.   Somchit MN, Reezal I, Elysha Nur I, Mutalib AR. *In vitro* antimicrobial activity of ethanol and water extracts of *Cassia alata*. Journal of Ethnopharmacology 2003;84:1-4.

6.   Kasiama GN, Ikey A, Kabengele CN, Kilembe JT, Matshimba EN, Bete JM, et al. Anthelmintic and antioxidant activities, phytochemical profile and microscopic features of *Senna alata* collected in the Democratic Republic of Congo. Annual Research & Review in Biology. 2022;37(6):28-36.

7.   Roy S, Ukil B, Lyndem LM, El-Nezami H. Acute and sub-acute toxicity studies on the effect of *Senna alata* in Swiss Albino mice. Cogent Biology. 2017;2(1):1-11.

8.   Léonard DF, Youssoufou O, Abel SA, Aimée ST, Paténéma S, Balé B. Toxicity studies on the leaves of *Senna alata*, a medicinal plant from Burkina Faso, in mice and rats World Journal of Pharmacy and Pharmaceutical Sciences 2020;9:85-95.

9.   Senou M, Dehou R, Agbogba F, Tchogou P, Abissi Y, Houngbeme A, et al. Safety of the aqueous extract of the leaves of *Senna alata* (L.) Roxb. (Leguminosae-Caesalpinioideae), a plant used in Benin to treat infections. Journal of Biosciences and Medicines. 2022;10(12):86-95.

10.   Alalor CA, Igwilo CI, Azubuike CP. Evaluation of the antibacterial activity of herbal ointments formulated with methanolic extract of *Cassia alata*. Asian Journal of Biomedical & Pharmaceutical Sciences. 2012; 2 (13):15-9.

11.   Misal G, Dixit G, Gulkari V. Formulation and evaluation of herbal gel. Indian Journal of Natural Products and Resources (IJNPR). 2012;3 (4):501-5.

12.   Oyedele AO, Akinkunmi EO, Fabiyi DD, Orafidiya LO. Physicochemical properties and antimicrobial activities of soap formulations containing *Senna alata* and *Eugenia uniflora* leaf preparations. Journal of Medicinal Plants Research. 2017;11(48):778-87.

13.   Alalor C. Evaluation of the antifungal properties of *Cassia alata* based herbal ointments formulated in different ointment bases. Scholars International Journal of Traditional and Complementary Medicine. 2018;1 (3):38-42.

14.   Iraqui P, Chakraborty T, Das MK, Yadav RNS. Herbal antimicrobial gel with leaf extract of *Cassia alata* L. Journal of Drug Delivery and Therapeutics. 2019;9(3):82-94.

15.   Karthika C, Mohamed RK, Manivannan S. Phytochemical analysis and evaluation of antimicrobial potential of *S. alata* Linn. leaves extract. Asian Journal of Pharmaceutical and Clinical Research. 2016;9(2):253-7.

16.   Panichayupakaranant P, Intaraksa N. Distribution of hydroxyanthracene derivatives in *Cassia alata* and the factors affecting the quality of the raw material. Songklanakarin Journal of Science and Technology. 2003;25:498-502.

17.   Ghafoor K, Choi YH. Optimization of ultrasound assisted extraction of phenolic compounds and antioxidants from Grape peel through response surface methodology. Journal of the Korean Society for Applied Biological Chemistry. 2009;52(3):295-300.

18.   Fang X, Wang J, Wang Y, Li X, Zhou H, Zhu L. Optimization of ultrasonic-assisted extraction of wedelolactone and antioxidant polyphenols from *Eclipta prostrate* L using response surface methodology. Separation and Purification Technology. 2014;138:55-64.

19.   Zhou Y-X, Xia W, Yue W, Peng C, Rahman K, Zhang H. Rhein: A review of pharmacological activities. Evidence-Based Complementary and Alternative Medicine. 2015;2015:578107.

20. Lin C-F, Chuang S-Y, Huang T-H, Nguyen TMH, Wang P-W, Alalaiwe A, et al. A systematic comparison of the effect of topically applied anthraquinone aglycones to relieve psoriasiform lesion: The evaluation of percutaneous absorption and anti-inflammatory potency. Biomedicine & Pharmacotherapy. 2022;145:112482.

21. Lee J-H, Kim JM, Kim C. Pharmacokinetic analysis of rhein in *Rheum undulatum* L. Journal of Ethnopharmacology. 2003;84 5-9.

22. Krumbiegela G, HU S. Rhein and aloe-emodin kinetics from Senna laxatives Pharmacology. 1993;47 (1):120-4.

23. Lu C, Xu P, Zhu J, Lou Z, Wang H, Xie J, et al. Antibacterial properties of anthraquinones extracted from rhubarb against *Aeromonas hydrophila*. Fisheries Science. 2011;77(3):375-84.

24. Guo L, Guo J, Xu F. Optimized extraction process and identification of antibacterial substances from Rhubarb against aquatic pathogenic *Vibrio harveyi*. 3 Biotech. 2017;7(6):377.

25. Fouillaud M, Venkatachalam M, Girard-Valenciennes E, Caro Y, Dufossé L. Anthraquinones and derivatives from marine-derived fungi: structural diversity and selected biological activities. Marine Drugs. 2016;14(4):1-64.

26. Thombare N, Kumar S, Kumari U, Sakare P, Yogi RK, Prasad N, et al. Shellac as a multifunctional biopolymer: A review on properties, applications and future potential. International Journal of Biological Macromolecules. 2022;215:203-23.

27. Liu L, Li X, Dong G, Zhang H, Tao Y-F, He R, et al. Bioinspired natural shellac dressing for rapid wound sealing and healing. ACS Applied Material & Interfaces. 2023;15(37):43294-308.

28. Thammachat T, Sriamornsak P, Luangtana-Anan M, Nunthanid J, Limmatvapirat C, Limmatvapirat S. Preparation and characterization of shellac fiber as a novel material for controlled drug release. Advanced Materials Research. 2010;152-153:1232-5.

29. Wu YH, Yu DG, Huang SM, Zha DP, Wang ML, Wang SJ. Ultra-thin shellac fibers fabricated using two different electrospinning processes. Advanced Materials Research. 2014;1015:51-5.

30.   Luangtana-anan M, Saengsod S, Limmatvapirat S. Improvement of bleached shellac as enteric coating by composite formation. American Association of Pharmaceutical Scientists PharmSciTech. 2021;22(7):241.

31.   Chauhan OP, Nanjappa C, Ashok N, Ravi N, Roopa N, Raju PS. Shellac and aloe vera gel based surface coating for shelf life extension of tomatoes. Journal of Food Science and Technology. 2013;52(2):1200-5.

32.   Phaechamud T, Setthajindalert O. Antimicrobial in-situ forming gels based on bleached shellac and different solvents. Journal of Drug Delivery Science and Technology. 2018;46:285-93.

33.   Weng L, Xie J. Smart electrospun nanofibers for controlled drug release: recent advances and new perspectives. Current Pharmaceutical Design. 2015;21(15):1944-59.

34.   Azimi B, Maleki H, Zavagna L, Ossa JGDl, Linari S, Lazzeri A, et al. Bio-based electrospun fibers for wound healing. Journal of Functional Biomaterials. 2020;11(3):67-103.

35.   Donkor A-M, Suurbaar J, Mosobil R. *In vitro* bacteriostatic and bactericidal activities of *Senna alata*, *Ricinus communis* and *Lannea barteri* extracts against wound and skin disease causing bacteria. Journal of Analytical & Pharmaceutical Research. 2016;3(1):1-6.

36.   Nayak BK, Mukilarasi V, Nanda A. Antibacterial activity of leaf extract of *Cassia alata* separated by soxhlet extraction method. Der Pharmacia Lettre. 2015;7(4):254-7.

37.   Muhammad SL, Wada Y, Mohammed M, Ibrahim S, Musa KY, Olonitola OS, et al. Bioassay-guided identification of bioactive compounds from *Senna alata* L. against Methicillin-resistant *Staphylococcus aureus*. Applied Microbiology. 2021;1(3):520-36.

38.   Anibijuwon II, Gbala ID, Nnadozie BI, Ifayefumi O. Susceptibility of selected multi-drug resistant clinical isolates to different leaf extracts of *Senna alata*. Notulae Scientia Biologicae. 2018;10(1):26-32.

39.   Mordi RM, Osula AN, Igeleke CL, Odjadjare EE, Oboh FOJ, Uwadiae EO. The evaluation of the antimicrobial property of *Cassia alata* leaves in Benin city, Nigeria. Journal of Bio-medicine and Nursing. 2016;22:14-23.

40.   Sangkaew S, Wanmasae S, Bunluepeuch K, Ongtanasup T, Srisang S, Manaspon C, et al. Development of nanoemulsions for wound dressings containing *Cassia alata* L. leaf extraction. Evidence-Based Complementary and Alternative Medicine. 2022;2022:4282678.

41.   Grosvenor PW, Gothard PK, McWdham NC, Suprlono A, Gray DO. Medicinal plants from Riau Province, Sumatra, Indonesia. Part 1: Uses. Journal of Ethnopharmacology 1995;45:75-95.

42.   Khare CP. Indian medicinal plants. London, UK: Springer Press; 2007. 126-7 p.

43.   Sakunpak A, Sirikatitham A, Panichayupakaranant P. Preparation of anthraquinone high-yielding *Senna alata* extract and its stability. Pharmaceutical Biology. 2009;47(3):236-41.

44.   Akporhuarho AA, Onoriode A, Jonathan AO, John TN. Evaluation of bio-active constituents and In vitro antioxidant potentials of the ethanolic leaf extracts of *Dracaena mannii*, *Euphorbia hirta* and *Senna alata*. Journal of Biological Research & Biotechnology. 2022;20(3):1753-62.

45.   Cavalcante MdA, Oliveira JdS, Barreto MSdS, Cantuária PdC, Borges WL, Silva GAd, et al. An HPLC method to determine phenolic compounds of plant extracts: Application to *Byrsonima crassifolia* and *Senna alata* leaves. Pharmacognosy Research. 2022;14(4):395-404.

46.   Igara CE, Ndukwe MK, Ahuchaogu AA, Nwali IU, Okpani CG. Chemical composition by gas chromatography and mass spectrometry and antioxidant activity of *Cassia alata* plant leaf. Journal of Medicinal Plants Studies. 2023;11(1):1-6.

47.   Saito ST, Trentin DdS, Jos´eMacedo A, Pungartnik C, Gosmann G, Silveira JdD, et al. Bioguided fractionation shows *Cassia alata* extract to inhibit *Staphylococcus epidermidis* and *Pseudomonas aeruginosa* growth and biofilm formation. Evidence-Based Complementary and Alternative Medicine. 2012;2012:1-13.

48.   Damodaran S, Venkataraman S. A study on the therapeutic efficacy of *Cassia alata*, Linn. leaf extract against *Pityriasis versicolor*. Journal of Ethnopharmacology. 1994;42(1):19-23.

49.	Villasen~or IM, Canlas AP, Pascua MPI, Sabando MN, Soliven LAP. Bioactivity studies on *Cassia alata* Linn. leaf extracts. Phytotherapy Research. 2002;16 Suppl 1:S93-S6.

50.	Vo Thi Dieu Hoa, Pham Hong Ngoc, Tran Chieu An, Pham Ngoc Truc, Tran Phan Huynh Nhu, Phan Thi Thanh Tam, et al. Isolation, characterization, and simultaneous quantification of main chemical constituents from *Cassia alata* Linn. Leaves. Journal of Science and Technology Development [Internet]. 2021;24 (4):2187-92.

51.	Ndukwe GI, G. TJ, Clark PD. Phytochemical screening and *in vitro* antioxidant assessment of *Cassia alata* (Linn) leaf extracts. ChemSearch Journal. 2020;11 (2):64-72.

52.	Suriya S, Uthirapandi V, Chelladurai I, Jeyaprakash K. A preliminary phytochemical and antimicrobial analysis on *Senna alata* (L.) Roxb. (Leguminosae). International Journal of Botany Studies. 2023;8(6):10-5.

53.	Bassey E, Alaribe A, Ikpi E, Thomas P. Studies on the antibacterial susceptibility of uropathogens to *Senna alata* extracts in Calabar, Cross River State, Nigeria. Annual Research & Review in Biology. 2022;37(12):39-60.

54.	Nkundineza JC, Ntandou N, Gelase Fredy NN, Bassoueka D AJ. Anticonvulsant and sedative effects of *Cassia alata* (Fabaceae) in mice. International Journal of Medical Research & Health Sciences. 2020;5(1):28-37.

55.	Mohanasundaram S, Rangarajan N, Sampath V, Porkodi K, Pennarasi M. GC–MS and HPLC analysis of antiglycogenolytic and glycogenic compounds in kaempferol 3–O–gentiobioside containing *Senna alata* L leaves in experimental rats. Translational Metabolic Syndrome Research. 2021;4:10-7.

56.	Edegbo E, Okolo M-LO, Adegoke AS, Omatola CA, Idache BM, Abraham JO, et al. Phytochemical screening and antifungal activity of *Cassia alata* (Linn.) crude leaf extracts. African Journal of Microbiology Research. 2023;17:176-83.

57.	Bhat A, Rajesh KS, Raghavan R. Evaluation of antivenom activity of *Cassia alata* leaf extract against *Daboia Russelii* venom. Journal of Pharmaceutical Research International. 2021;33(38A):288-98.

58.   Kittiwattanokhun A, Samosorn S, Innajak S, Watanapokasin R. Inhibitory effects on chondrosarcoma cell metastasis by *Senna alata* extract. Biomedicine & Pharmacotherapy. 2021;137:111337.

59.   Atanu FO, Rotimi D, Ilesanmi OB, Malki JSA, Batiha GE, Idakwoji PA. Hydroethanolic extracts of *Senna alata* leaves possess antimalarial effects and reverses haematological and biochemical pertubation in *Plasmodium berghei*-infected mice. Journal of Evidence-Based Integrative Medicine. 2022;27:1-7.

60.   Nwankwo OL, Bunu SJ, Aziakpono OM. Hypoglycemic activity of endophytic extract of *Senna alata* in STZ-induced diabetic mice model. Journal of Integrated Health Sciences. 2021;9(2):75-80.

61.   Angelina M, Mardhiyah A, Ekapratiwi Y, Dewijanti ID, Dewi RT, Sukirno, et al. Physicochemical and phytochemical standardization, and antibacterial evaluation of *Cassia alata* leaves from different locations in Indonesia. Pharmacia. 2021;68(4):947-56.

62.   Rahmawati F, Prihantini NN, Hady BC. *In vitro* bioactivity test of *Senna alata* (L.) Roxb leaves extract. International Journal of Health Sciences and Research. 2022;12(2):304-17.

63.   James OO, Emmanuel OO, Saanumi GA, Akinkunmi OO, Adekanmi AA. *Senna alata* leaf and stem: Phytochemical screening, nutritional content, and antimicrobial activities. Journal of Environmental Impact and Management Policy. 2022;2(26):1-11.

64.   Ahmed S, Rahman F, Shohael A. *In vitro* analysis of phytoconstituents and bioactivities of *Senna alata* L. leaf extracts. Discovery Phytomedicine. 2021;8:167-74.

65.   Anandan R, Jayakar B, Karar, Babuji S, Manavalan R, Kumar RS. Protective effect of leaves of *Cassia alata* Linn. in CCl4 Induced Hepatotoxicity in rats. Biosciences, Biotechnology Research Asia. 2008;5:487-90.

66.   Subuki I, Malek ANA, Saidin SH, Pisar MM. Optimization of supercritical extraction conditions of *Senna alata* and evaluation of biological activity. International Journal of Engineering & Technology. 2018;7 (3.11):94-100.

67.   Le PTQ. Phytochemical screening and antimicrobial activity of extracts of *Cassia alata* L. leaves and seeds. Bulgarian Chemical Communications. 2019;51(3):378-83.

68.   Yeong YL, Pang SF, Gimbun J. The effect of auxiliary energy on rhein, kaempferol and astragalin extraction from *Cassia alata*. MATEC Web of Conferences. 2017;111.

69.   Handa SS, Khanuja SPS, Longo G, Rakesh DD. Extraction technologies for medicinal and aromatic plants: International centre for science and high technology; 2008. 266 p.

70.   Zhang QW, Lin LG, Ye WC. Techniques for extraction and isolation of natural products: a comprehensive review. Chinese Medicine. 2018;13:1-26.

71.   Picot-Allain C, Mahomoodally MF, Ak G, Zengin G. Conventional versus green extraction techniques — a comparative perspective. Current Opinion in Food Science. 2021;40:144-56.

72.   Ling YY, Fun PS, Yeop A, Yusoff MM, Gimbun J. Assessment of maceration, ultrasonic and microwave assisted extraction for total phenolic content, total flavonoid content and kaempferol yield from *Cassia alata* via microstructures analysis. Materials Today: Proceedings. 2019;19:1273-9.

73.   Gritsanapan W, Mangmeesri P. Standardized *Senna alata* leaf extract Journal of Health Research. 2009;23(2):59-64.

74.   Poole C, Mester Z, Miró M, Pedersen-Bjergaard S, Pawliszyn J. Extraction for analytical scale sample preparation (IUPAC Technical Report). Pure and Applied Chemistry. 2016;88(7):649-87.

75.   Rasul MG. Extraction, isolation and characterization of natural products from medicinal plants. International Journal of Basic Sciences and Applied Computing (IJBSAC). 2018;2(6):1-6.

76.   Rasul MG. Conventional extraction methods use in medicinal plants, their advantages and disadvantages. International Journal of Basic Sciences and Applied Computing (IJBSAC). 2018;2(6):10-4.

77.   Frosi I, Montagna I, Colombo R, Milanese C, Papetti A. Recovery of chlorogenic acids from agri-food wastes: updates on green extraction techniques. Molecules. 2021;26(15).

78.   Mukherjee PK. Extraction and other downstream procedures for evaluation of herbal drugs. Quality Control and Evaluation of Herbal Drugs2019. p. 195-236.

79.   Miralrio A, Vázquez AE. Plant extracts as green corrosion inhibitors for different metal surfaces and corrosive media: a review. Processes. 2020;8(8).

80.   Tušek AJ, Šamec D, Šali´c A. Modern techniques for flavonoid extraction—To optimize or Not to optimize? Applied Sciences. 2022;12(22).

81.   Bachtler S, Bart HJ. Increase the yield of bioactive compounds from elder bark and annatto seeds using ultrasound and microwave assisted extraction technologies. Food and Bioproducts Processing. 2021;125:1-13.

82.   Yeong YL, Pang SF, Putranto A, Gimbun J. Optimisation of microwave-assisted extraction (MAE) of anthraquinone and flavonoids from *Senna alata* (L.) Roxb. Natural Product Research. 2022;36(14):3756-60.

83.   Doughari JH. Phytochemicals: extraction methods, basic structures and mode of action as potential chemotherapeutic agents. Phytochemicals – A global perspective of their role in nutrition and health2012.

84.   Moradi-kheibari N, Ahmadzadeh H, Talebi AF, Hosseini M, Murry MA. Recent advances in lipid extraction for biodiesel production. Advances in Feedstock Conversion Technologies for Alternative Fuels and Bioproducts2019. p. 179-98.

85.   Loa TC-T, Nianb H-C, Chiuc K-H, Wangd A-Y, Wuc B-Z. Rapid and efficient purification of chrysophanol in *Rheum Palmatum* Linn by supercritical fluid extraction coupled with preparative liquid chromatography in tandem. Journal of Chromatography B. 2012;893-894:101-6.

86.   Lonˇcari´c A, Celeiro M, Joki´c S, Jozinovi´c A, Jelini´c J, Kovaˇc T, et al. Green extraction methods for extraction of polyphenolic compounds from Blueberry Pomace. Foods. 2020;9(11).

87.   Yusoff IM, Taher ZM, Rahmat Z, Chua LS. A review of ultrasound-assisted extraction for plant bioactive compounds: Phenolics, flavonoids, thymols, saponins and proteins. Food Research International. 2022;157:111268.

88.   Carreira-Casais A, Otero P, Garcia-Perez P, Carpena M, Garcia-Oliveira P, Pereira AG, et al. Benefits and drawbacks of ultrasound-assisted extraction for the recovery of bioactive compounds from marine algae. International Journal of Environmental Research and Public Health. 2021;18(17).

89.   Fu X, Belwal T, Cravotto G, Luo Z. Sono-physical and sono-chemical effects of ultrasound: Primary applications in extraction and freezing operations and influence on food components. Ultrasonics Sonochemistry. 2020;60:104726.

90.   Alam P, Noman OM, Herqash RN, Almarfadi OM, Alqahtani AS. Response surface methodology (RSM)-based optimization of ultrasound-assisted extraction of sennoside A, sennoside B, aloe-emodin, emodin, and chrysophanol from *Senna alexandrina* (aerial parts): HPLC-UV and antioxidant analysis. Molecules. 2022;27(1).

91.   Yingngam B, Zhao H, Baolin B, Pongprom N, Brantner A. Optimization of ultrasonic-assisted extraction and purification of rhein from *Cassia fistula* Pod pulp. Molecules. 2019;24(10).

92.   Qua X, Wub CFJ-. One-factor-at-a-time designs of resolution V. Journal of Statistical Planning and Inference. 2005;131(2):407-16.

93.   Bakar FIA, Bakar MFA, Abdullah N, Endrini S, Fatmawati S. Optimization of extraction conditions of phytochemical compounds and anti-gout activity of *Euphorbia hirta* L. (Ara Tanah) using response surface methodology and liquid chromatography-mass spectrometry (LC-MS) analysis. Evidence-Based Complementry and Alternative Medicine. 2020;2020:4501261.

94.   Nangare S, Jadhav N, Ghagare P, Muthane T. Pharmaceutical applications of electrospinning. Annales Pharmaceutiques Françaises. 2020;78(1):1-11.

95.   Ponphaiboon J, Krongrawa W, Aung WW, Chinatangkul N, Limmatvapirat S, Limmatvapirat C. Advances in natural product extraction techniques, electrospun fiber fabrication, and the integration of experimental design: A comprehensive review. Molecules. 2023;28(13).

96.   Gao C, Zhang L, Wang J, Jin M, Tang Q, Chen Z, et al. Electrospun nanofibers promote wound healing: theories, techniques, and perspectives. Journal of Materials Chemistry B. 2021;9(14):3106-30.

97.   Ramakrishna S, Fujihara K, Teo W-E, Lim T-C, Ma Z. An introduction to electrospinning and nanofibers: World Scientific Publishing Co. Pte. Ltd. 396 p.

98.   Ye P, Wei S, Luo C, Wang Q, Li A, Wei F. Long-term effect against methicillin-resistant *Staphylococcus aureus* of emodin released from coaxial electrospinning nanofiber membranes with a biphasic profile. Biomolecules. 2020;10(3):362-78.

99. Balogh A, Farkas B, KornélFaragó, Farkas A, Wagner I, assche IV, et al. Melt-blown and electrospun drug-loaded polymer fiber mats for dissolution enhancement: A comparative study. Journal of Pharmaceutical Sciences. 2015;104(5):1767-76.

100. Yao C-H, Yeh J-Y, Chen Y-S, Li M-H, Huang C-H. Wound-healing effect of electrospun gelatin nanofibres containing *Centella asiatica* extract in a rat model. Journal of Tissue Engineering and Regenerative Medicine. 2017;11(3):905-15.

101. Sadri M, Arab-Sorkhi S, Vatani H, Bagheri-Pebdeni A. New wound dressing polymeric nanofiber containing green tea extract prepared by electrospinning method. Fibers and Polymers. 2015;16(8):1742-50.

102. Charernsriwilaiwat N, Rojanarata T, Ngawhirunpat T, Sukma M, Opanasopit P. Electrospun chitosan-based nanofiber mats loaded with *Garcinia mangostana* extracts. International Journal of Pharmaceutics. 2013;452(1-2):333-43.

103. Nootem J, Santiwat T, Srisuwannaket C, Pratumyot K, Lin W-C, Mingvanish W, et al. Enhanced stability and bioactivity of *Curcuma comosa* Roxb. extract in electrospun gelatin nanofibers. Fibers. 2019;7(9):76-88.

104. Limmatvapirat S, Limmatvapirat C, Luangtana-anan M, Nunthanid J, Oguchib T, Tozukab Y, et al. Modification of physicochemical and mechanical properties of shellac by partial hydrolysis. International Journal of Pharmaceutics. 2004;278(1):41-9.

105. Goswami D, Saha S. An investigation of the melting properties of different forms of lac by differential scanning calorimeter. Surface Coatings International. 2000;83:334-6.

106. Yuan Y, He N, Xue Q, Guo Q, Dong L, Haruna MH, et al. Shellac: A promising natural polymer in the food industry. Trends in Food Science & Technology. 2021;109:139-53.

107. Yuan Y, He N, Dong L, Guo Q, Zhang X, Li B, et al. Multiscale Shellac-Based Delivery Systems: From Macro- to Nanoscale. ACS Nano. 2021;15(12):18794-821.

108. Limmatvapirat S, Limmatvapirat C, Puttipipatkhachorn S, Nuntanid J, Luangtana-anan M. Enhanced enteric properties and stability of shellac films through composite salts formation. European Journal of Pharmaceutics and Biopharmaceutics. 2007;67(3):690-8.

109. Pandey SK, Yadav SKS, Prasad N, Sharma SC. Chouri-parta method of estimating seedlac yield. Journal of AgriSearch. 2018;5(04):260-4.

110. Wang X, Yu D-G, Li X-Y, Bligh SWA, Williams GR, Wang X, et al. Electrospun medicated shellac nanofibers for colon-targeted drug delivery. International Journal of Pharmaceutics. 2015;490(1):384-90.

111. Chinatangkul N, Limmatvapirat C, Nunthanid J, Luangtana-Anan M, Sriamornsak P, Limmatvapirat S. Design and characterization of monolaurin loaded electrospun shellac nanofibers with antimicrobial activity. Asian Journal of Pharmaceutical Sciences. 2018;13(5):459-71.

112. Xue J, Wu T, Dai Y, Xia Y. Electrospinning and electrospun nanofibers: Methods, materials, and applications. Chemical Reviews. 2019;119(8):5298-415.

113. Abbasipour M, Khajavi R. Controlling nanofiber morphology by the electrospinning process. 2017. p. 109-23.

114. Das AK, Dewanjee S. Chapter 3 - Optimization of extraction using mathematical models and computation. In: Sarker SD, Nahar L, editors. Computational Phytochemistry: Elsevier; 2018. p. 75-106.

115. Sahraee S, Ghanbarzadeh B, Falcone PM. Application of mixture design methodology for development of high antioxidant fruity functional beverage. Food Science & Nutrition. 2022;10(7):2245-54.

116. Gunst RF, Mason RL. Fractional factorial design. WIREs Computational Statistics. 2009;1(2):234-44.

117. Wagner JR, Mount EM, Giles HF. 25 - Design of Experiments. In: Wagner JR, Mount EM, Giles HF, editors. Extrusion (Second Edition). Oxford: William Andrew Publishing; 2014. p. 291-308.

118. Yuangyai C, Nembhard HB. Chapter 8 - Design of Experiments: A Key to Innovation in Nanotechnology. In: Ahmed W, Jackson MJ, editors. Emerging Nanotechnologies for Manufacturing. Boston: William Andrew Publishing; 2010. p. 207-34.

119. Sahoo P, Barman TK. 5 - ANN modelling of fractal dimension in machining. In: Davim JP, editor. Mechatronics and Manufacturing Engineering: Woodhead Publishing; 2012. p. 159-226.

120.   Bhattacharya S. Central Composite Design for response surface methodology and its application in pharmacy. In: Palanikumar K, editor. Response Surface Methodology in Engineering Science. Rijeka: IntechOpen; 2021. p. Ch. 5.

121.   International conference on harmonization of technical requirements for the registration of pharmaceuticals for human use (ICH) Guideline for validation of analytical procedures: Methodology Q2 (R1). Switzerland.2005.

122.   Horwitz W, Albert R. The Horwitz Ratio (HorRat): A useful index of method performance with respect to precision. Journal of AOAC International. 2006;89(4):1095-109.

123.   Rick-Leonid N-M-M, Cédric S-O, Croix NJDL, Privat OJ, Felix OA, Louis-Clément O-E. Phytochemical screening, antioxidant, anti-inflammatory and antiangiogenic activities of *Lophira procera* A. Chev. (*Ochnaceae*) medicinal plant from Gabon. Egyptian Journal of Basic and Applied Sciences. 2019;5(1):80-6.

124.   Arampatzis AS, Kontogiannopoulos KN, Theodoridis K, Aggelidou E, Rat A, Willems A, et al. Electrospun wound dressings containing bioactive natural products: physico-chemical characterization and biological assessment. Biomaterials Research. 2021;25(1):1-21.

125.   Gupta R, Chen Y, Sarkar M, Xie H. Surfactant mediated accelerated and discriminatory *in vitro* drug release method for PLGA nanoparticles of poorly water-soluble drug. Pharmaceuticals (Basel). 2022;15(12):1489-509.

126.   Krongrawa W, Limmatvapirat S, Vollrath MK, Kittakoop P, Saibua S, Limmatvapirat C. Fabrication, optimization, and characterization of antibacterial electrospun shellac fibers loaded with *Kaempferia parviflora* extract. Pharmaceutics. 2022;15(1):123-47.

127.   International conference on harmonisation of technical requirements for registration of pharmaceuticals for human uses, Stability testing of new drug substances and products Q1A (R2), current step2003.

128.   Kumara K, Srivastava S, Sharanagat VS. Ultrasound assisted extraction (UAE) of bioactive compounds from fruit and vegetable processing by-products: A review. Ultrasonics - Sonochemistry. 2021;70.

129.   Chemat F, Rombaut N, Sicaire A-G, Meullemiestre A, Fabiano-Tixier A-S, Abert-Vian M. Ultrasound assisted extraction of food and natural products. Mechanisms, techniques, combinations, protocols and applications. A review. Ultrasonics Sonochemistry. 2017;34:540-60.

130.   Vinatoru M, Mason TJ, Calinescu I. Ultrasonically assisted extraction (UAE) and microwave assisted extraction (MAE) of functional compounds from plant materials. Trends in Analytical Chemistry. 2017;97:159-78.

131.   Singh B, Nadkarni JR, Vishwakarma RA, Bharate SB, Nivsarkar M, Anandjiwala S. The hydroalcoholic extract of *Cassia alata* (Linn.) leaves and its major compound rhein exhibits antiallergic activity via mast cell stabilization and lipoxygenase inhibition. Journal of Ethnopharmacology. 2012;141(1):469-73.

132.   Pham DQ, Pham HT, Han JW, Nguyen TH, Nguyen HT, Nguyen TD, et al. Extracts and metabolites derived from the leaves of *Cassia alata* L. exhibit *in vitro* and *in vivo* antimicrobial activities against fungal and bacterial plant pathogens. Industrial Crops and Products. 2021;166.

133.   Aung WW, Krongrawa W, Ponphaiboon J, Kulpicheswanich P, Limmatvapirat C. Yields, phytochemicals, and biological activities of different solvent extracts of *Senna alata* Leaves. Key Engineering Materials. 2022;914:135-40.

134.   Silva BN, Cadavez V, Ferreira-Santos P, Alves MJ, Ferreira ICFR, Barros L, et al. Chemical profile and bioactivities of extracts from edible plants readily available in Portugal Foods. 2021;10(3).

135.   Limmatvapirat C, Nateesathittarn C, Dechasathian K, Moohummad T, Chinajitphan P, Limmatvapirat S. Phytochemical analysis of baby corn silk extracts. Journal of Ayurveda and Integrative Medicine. 2020;11(3):344-51.

136.   Wei S-y, Yao W-x, Ji W-y, Wei J-q, Peng S-q. Qualitative and quantitative analysis of anthraquinones in rhubarbs by high performance liquid chromatography with diode array detector and mass spectrometry. Food Chemistry. 2013;141(3):1710-5.

137.   Nag M, Kar A, Chanda J, Mukherjee PK. RP-HPLC analysis of methanol extract of *Viscum articulatum*. Journal of Ayurveda and Integrative Medicine. 2020;11(3):277-80.

138.   Chewchinda S, Sakulpanich A, Sithisarn P, Gritsanapan W. HPLC Analysis of laxative rhein content in *Cassia fistula* Fruits of different provenances in Thailand Thai Journal of Agricultural Science 2012;2(45):121-5.

139.   Panichayupakaranant P, Sakunpak A, Sakunphueak A. Quantitative HPLC determination and extraction of anthraquinones in *Senna alata* leaves. Journal of Chromatographic Science. 2009;47:197-200.

140.   Papadoyannis IN, Gika HG. Peak purity determination with a diode array detector. Journal of Liquid Chromatography & Related Technologies. 2007;27(6):1083-92.

141.   Wu J, Zhang J, Yu X, Shu Y, Zhang S, Zhang Y. Extraction optimization by using response surface methodology and purification of yellow pigment from *Gardenia jasminoides* var. *radicans* Makikno. Food Science & Nutrition. 2021;9(2):822-32.

142.   Krongrawa W, Limmatvapirat S, Saibua S, Limmatvapirat C. Optimization of ultrasound-assisted extraction of yields and total methoxyflavone contents from *Kaempferia parviflora* rhizomes. Molecules. 2022;27(13).

143.   Aung WW, Panich K, Watthanophas S, Naridsirikul S, Ponphaiboon J, Krongrawa W, et al. Preparation of bioactive de-chlorophyll rhein-rich *Senna alata* extract. Antibiotics (Basel). 2023;12(1).

144.   The United States Pharmacopeial Convention <621> Chromatography, in the United States Pharmacopeia 43 and the National Formulary 38. . The United States Pharmacopeial Convention: Rockville, MD, USA2020.

145.   Association of Official Agricultural Chemists (AOAC) Official methods of analysis. Guidelines for standard method performance requirements. AOAC International: Rockville, MD, USA,2016.

146.   Zhao L-C, Liang J, Li W, Cheng K-M, Xia X, Deng X, et al. The use of response surface methodology to optimize the ultrasound-assisted extraction of five anthraquinones from *Rheum palmatum* L. Molecules. 2011;16(7):5928-37.

147.   Wu YC, Wu P, Li YB, Liu TC, Zhang L, Zhou YH. Natural deep eutectic solvents as new green solvents to extract anthraquinones from *Rheum palmatum* L. RSC Advances. 2018;8(27):15069-77.

148.   Guo L, Guo J, Zhu W, Jiang X. Optimized synchronous extraction process of tea polyphenols and polysaccharides from Huaguoshan Yunwu tea and their antioxidant activities. Food and Bioproducts Processing. 2016;100:303-10.

149.   Cacace JE, Mazza G. Mass transfer process during extraction of phenolic compounds from milled berries. Journal of Food Engineering. 2003;59(4):379-89.

150.   Pinelo M, Rubilar M, Jerez M, Sineiro J, Núñez MJ. Effect of solvent, temperature, and solvent-to-solid ratio on the total phenolic content and antiradical activity of extracts from different components of Grape Pomace. Journal of Agricultural and Food Chemistry. 2005;53(6):2111-7.

151.   Yeong YL, Pang SF, Chong SY, Gimbun J. Comparison of microwave and ultrasonic assisted extraction of Kaempferol from *Cassia alata*. International Journal of Engineering & Technology. 2018;7(3.13):84-9.

152.   Pouget C, Gustave C-A, Ngba-Essebe C, Laurent F, Lemichez E, Tristan A, et al. Adaptation of *Staphylococcus aureus* in a medium mimicking a diabetic foot environment. Toxins (Basel). 2021;13(3).

153.   Hamuel JD, Okafor B. Antimicrobial activity of *Senna alata* Linn. East and Central African Journal of Pharmaceutical Sciences. 2008;10(1):17-21.

154.   Ehiowemwenguan G, Inetianbor JE, Yakubu JM. Antimicrobial qualities of *Senna alata*. IOSR Journal of Pharmacy and Biological Sciences. 2014;9(2):47-52.

155.   Ding X, Tang Q, Xu Z, Xu Y, Zhang H, Zheng D, et al. Challenges and innovations in treating chronic and acute wound infections: from basic science to clinical practice. Burns & Trauma. 2022;10:tkac014.

156.   Antonisamy P, Agastian P, Kang C-W, Kim NS, Kim J-H. Anti-inflammatory activity of rhein isolated from the flowers of *Cassia fistula* L. and possible underlying mechanisms. Saudi Journal of Biological Sciences. 2019;26(1):96-104.

157.   Wadkhien K, Chinpaisal C, Satiraphan M, Wetwitayaklung P, Pongnimitprasert N. Anti-inflammatory effects of rhein and crude extracts from *Cassia alata* L. in HaCaT cells. Science, Engineering and Health Studies. 2018;12 (1):19-32.

158.   Umapathy EU, Ndebia E, Meeme A, Menziwa P, Nkeh-Chungag B, Iputo J. An experimental evaluation of *Albuca setosa* aqueous extract on membrane stabilization,

protein denaturation and white blood cell migration during acute inflammation. Journal of Medicinal Plants Research. 2010;4:789-95.

159.   Ahmed S, Shohael AM. In Silico Studies of four anthraquinones of *Senna alata* L. as potential antifungal compounds. Pharmacology Online. 2019;2:259-68.

160.   Saengsod S, Limmatvapirat S, Luangtana-Anan M. A new approach for the preparation of bleached shellac for pharmaceutical application: solid method. Advanced Materials Research. 2012;506:250-3.

161.   Chuenbarn T, Tuntarawongsa S, Janmahasatian S, Phaechamud T. Bleached shellac in situ forming micro-particle fabricated with different oils as antibacterial delivery system for periodontitis treatment. Materials Today: Proceedings. 2021;47:3546-53.

162.   Senarat S, Lwin WW, Mahadlek J, Phaechamud T. Doxycycline hyclate-loaded in situ forming gels composed from bleached shellac, Ethocel, and Eudragit RS for periodontal pocket delivery. Saudi Pharmaceutical Journal. 2021;29(3):252-63.

163.   Patra JK, Das G, Fraceto LF, Campos EVR, Rodriguez-Torres MdP, Acosta-Torres LS, et al. Nano based drug delivery systems: recent developments and future prospects. Journal of Nanobiotechnology. 2018;16(1):71.

164.   Huang J, Deng Y, Ren J, Chen G, Wang G, Wang F, et al. Novel in situ forming hydrogel based on xanthan and chitosan re-gelifying in liquids for local drug delivery. Carbohydrate Polymers. 2018;186.

165.   Sun B, Zhang M, Shen J, He Z, Fatehi P, Ni Y. Applications of cellulose-based materials in sustained drug delivery systems. Current Medicinal Chemistry. 2019;26(14):2485-501.

166.   Atanasov AG, Waltenberger B, Pferschy-Wenzig E-M, Linderd T, Wawroscha C, Uhrine P, et al. Discovery and resupply of pharmacologically active plant-derived natural products: A review. Biotechnology Advance. 2015;33(8):1582-614.

167.   Utreja P, Jain S, Tiwary AK. Novel drug delivery systems for sustained and targeted delivery of anti- cancer drugs: current status and future prospects. Current Drug Delivery. 2010;7(2):152-61.

168.	Garg T, Rath G, Goyal AK. Biomaterials-based nanofiber scaffold: targeted and controlled carrier for cell and drug delivery. Journal of Drug Targeting. 2015;23(3):202-21.

169.	Liu H, Gough CR, Deng Q, Gu Z, Wang F, Hu X. Recent advances in electrospun sustainable composites for biomedical, environmental, energy, and packaging applications. International Journal of Molecular Sciences. 2020;21(11).

170.	Zahedi E, Esmaeili A, Eslahi N, Shokrgozar MA, Simchi A. Fabrication and characterization of core-shell electrospun fibrous mats containing medicinal herbs for wound healing and skin tissue engineering. Marine Drugs. 2019;17:27.

171.	Mutlu G, Calamak S, Ulubayram K, Guven E. Curcumin-loaded electrospun PHBV nanofibers as potential wound-dressing material. Journal of Drug Delivery Science and Technology. 2018;43:185-93.

172.	Moradkhannejhad L, Abdouss M, Nikfarjam N, Shahriari MH, Heidary V. The effect of molecular weight and content of PEG on *in vitro* drug release of electrospun curcumin loaded PLA/PEG nanofibers. Journal of Drug Delivery Science and Technology. 2020;56:101554.

173.	Aung WW, Krongrawa W, Limmatvapirat S, Kulpicheswanich P, Okonogi S, Limmatvapirat C. Fabrication and optimization of electrospun shellac fibers loaded with *Senna alata* leaf extract. Polymers (Basel). 2024;16(2).

174.	Şener AG, Altay AS, Altay F. Effect of voltage on morphology of electrospun nanofibers. 2011. p. I-324.

175.	Chinatangkul N, Pengon S, Piriyaprasarth S, Limmatvapirat C, Limmatvapirat S. Development of electrospun shellac and hydroxypropyl cellulose blended nanofibers for drug carrier application. Key Engineering Materials. 2020;859:239-43.

176.	Motamedi AS, Bagheri-Khoulenjani S, Mirzadeh H, Hajiesmaeilbaigi F, Shokrgozar MA. Effect of electrospinning parameters on morphological properties of PVDF nanofibrous scaffolds. Prog Biomater. 2017;6(3):113-23.

177.	Ozaytekin I. The effect of carboxylic acid group on conductivity of the aromatic polyazomethines and char composites. Polymer Composites. 2014;35(2):372-80.

178.	Sriyanti I, Edikresnha D, Rahma A, Munir MM, Rachmawati H, Khairurrijal K. Mangosteen pericarp extract embedded in electrospun PVP nanofiber mats:

physicochemical properties and release mechanism of α-mangostin. International Journal of Nanomedicine. 2018;13:4927-41.

179.   Böncü TE, Ozdemir N. Effects of drug concentration and PLGA addition on the properties of electrospun ampicillin trihydrate-loaded PLA nanofibers. Beilstein Journal of Nanotechnology. 2022;13:245-54.

180.   Rramaswamy R, Mani G, Venkatachalam S, Venkata RY, Lavanya JS, Choi EY. Tetrahydro curcumin loaded PCL-PEG electrospun transdermal nanofiber patch: Preparation, characterization, and *in vitro* diffusion evaluations. Journal of Drug Delivery Science and Technology. 2018;44:342-8.

181.   Jirofti N, Golandi M, Movaffagh J, Ahmadi FS, Kalalinia F. Improvement of the wound-healing process by curcumin-loaded chitosan/collagen blend electrospun nanofibers: *in vitro* and *in vivo* studies. ACS Biomaterials Science & Engineering. 2021;7(8):3886-97.

182.   Saengsod S, Limmatvapirat S, Luangtana-anan M. Optimum condition of conventional bleaching process for bleached shellac. Journal of Food Process Engineering. 2019;42(8).

183.   Yan G, Cao Z, Devine D, Penning M, Gately NM. Physical properties of shellac material used for hot melt extrusion with potential application in the pharmaceutical industry. Polymers (Basel). 2021;13(21).

184.   Adiana MA, Mazura MP. Study on *Senna alata* and its different extracts by Fourier transform infrared spectroscopy and two-dimensional correlation infrared spectroscopy. Journal of Molecular Structure. 2011;991(1-3):84-91.

185.   Vannuruswamy G, Rathna GVN, Gadgil BST, Gadad AP. Blends of shellac as nanofiber formulations for wound healing. Journal of Bioactive and Compatible Polymers. 2015;30(5):472-89.

186.   Ariyanta HA, Roji F, Apriandanu DOB. Electrochemical activity of glassy carbon electrode modified with ZnO nanoparticles prepared via *Senna alata* L. leaf extract towards antiretroviral drug. Micro and Nano Systems Letters. 2022;10(1):1-7.

187.   Mondal A, Sohel MA, Mohammed AP, Anu AS, Thomas S, SenGupta A. Crystallization study of shellac investigated by differential scanning calorimetry. Polymer Bulletin. 2019;77(10):5127-43.

188.   Sun X-Z, Williams GR, Hou X-X, Zhu L-M. Electrospun curcumin-loaded fibers with potential biomedical applications. Carbohydrate Polymers. 2013;94(1):147-53.

189.   Yang Y, Chen W, MenglongWang, Shen J, Tang Z, Qin Y, et al. Engineered shellac beads-on-the-string fibers using triaxial electrospinning for improved colon-targeted drug delivery. Polymers (Basel). 2023;15(10).

190.   Wei Z, Liu E, Li H, Wei Z, lv Z. Release characteristics of different diameter ultrafine fibers as antibacterial materials. Journal of Innovative Optical Health Sciences. 2021;14(02):1-10.

191.   Farag Y, Leopold CS. Physicochemical properties of various shellac types. Dissolution Technologies. 2009;16 (2):33-9.

192.   Farag Y, Leopold CS. Development of shellac-coated sustained release pellet formulations. European Journal of Pharmaceutical Sciences. 2011;42(4):400-5.

193.   Zhang Y, Huo M, Zhou J, Zou A, Li W, Yao C, et al. DDSolver: an add-in program for modeling and comparison of drug dissolution profiles. American Association of Pharmaceutical Scientists Journal. 2010;12(3):263-71.

194.   Hosseini SM, Abdouss M, Mazinani S, Soltanabadi A, Kalaee M. Modified nanofiber containing chitosan and graphene oxide-magnetite nanoparticles as effective materials for smart wound dressing. Composites Part B: Engineering. 2022;231.

195.   Ekenna IC, Abali SO. Comparison of the use of kinetic model plots and DD Solver software to evaluate the drug release from griseofulvin tablets. Journal of Drug Delivery and Therapeutics. 2022;12(2-S):5-13.

VITA

NAME   Wah Wah Aung

INSTITUTIONS   Bachelor of Pharmacy (B. Pharm), University of
ATTENDED   Pharmacy, Yangon, Myanmar
Master of Pharmacy (M. Pharm), University of Pharmacy, Yangon, Myanmar
Ph. D (Pharmaceutical Engineering), Faculty of Pharmacy, Silpakorn university, Thailand
Home address: Kyaukpadaung Township, Mandalay region, Myanmar
Working place: Department of Traditional Medicine, Ministry of Health, Nay Pyi Taw, Myanmar

PUBLICATION   1) Wah Wah Aung, Wantanwa Krongrawa, Juthaporn Ponphaiboon, Pattranit Kulpicheswanich, and Chutima Limmatvapirat. Yields, Phytochemicals, and Biological Activities of Different Solvent Extracts of Senna alata Leaves. Key Engineering Materials 2022; 914: 135-140.
2) Aung, W.W.; Krongrawa, W.; Limmatvapirat, S.; Kulpicheswanich, P.; Okonogi, S.; Limmatvapirat, C. Fabrication and Optimization of Electrospun Shellac Fibers Loaded with Senna alata Leaf Extract. Polymers 2024, 16, 183. https://doi.org/10.3390/polym16020183

Poster Presentations:
1. Yields, Phytochemicals, and Biological Activities of Different Solvent Extracts of Senna alata Leaves. Silpakorn International Conference on Total Art and Science 2021, Silpakorn University, Virtual conference, Nov 4-5, 2021.
2. Optimization of Ultrasonic-assisted Extraction Conditions for Achieving Rhein-rich Extract from Senna alata Leaves using Box-Behnken Design. 5th international Conference and Exhibition on Pharmaceutical Sciences and Technology 2022, Faculty of Pharmacy, Thammasat University, Virtual conference, June 23-24, 2022.